DOT/FAA/TC-21/25

Federal Aviation Administration
William J. Hughes Technical Center
Aviation Research Division
Atlantic City International Airport
New Jersey 08405

Assessment of Emerging Metallic Structures Technologies through Test and Analysis of Fuselage Structure: Panel 1

Feb 05, 2021

Final report

U.S. Department of Transportation
Federal Aviation Administration

NOTICE

This report is available at the Federal Aviation Administration William J. Hughes Technical Center's Full-Text Technical Reports page: actlibrary.tc.faa.gov in Adobe Acrobat portable document format (PDF).

Form DOT F 1700.7 (8-72) Reproduction of completed page authorized

1. Report No.	2. Government Accession No.	3. Recipient's Catalog No.
DOT/FAA/TC-21/25		

4. Title and Subtitle	5. Report Date
Assessment of Emerging Metallic Structures Technologies through Test and Analysis of Fuselage Structure: Test Panel 1	February 2021
	6. Performing Organization Code: ANG-E281
7. Author(s): Yongzhe Tian, Dave Stanley, John Bakuckas Jr., Mike Kulak, Erin Fulton	8. Performing Organization Report No.
9. Performing Organization Name and Address: William J. Hughes Technical Center, Federal Aviation Administration, Aviation Research Division, Structures and Materials Section, Atlantic City International Airport, NJ 08405	10. Work Unit No. (TRAIS)
	11. Contract or Grant No.
12. Sponsoring Agency Name and Address: U.S. Department of Transportation, Federal Aviation Administration, FAA Transport Airplane Directorate, Airframe/Cabin Safety, ANM-115, 1601 Lind Avenue SW, Renton, WA 98057	13. Type of Report and Period Covered: Final Report
	14. Sponsoring Agency Code

15Supplementary Notes

16. Abstract

In partnership with Arconic and Embraer, the Federal Aviation Administration (FAA) is assessing emerging metallic structures technologies (EMST) using the FAA's Full-Scale Aircraft Structural Test Evaluation and Research (FASTER) facility. In this collaborative effort, full-scale fuselage panel test data will be obtained to assess the effect of EMST fuselage concepts on damage tolerance performance as compared to the current baseline aluminum fuselage structures located on the crown of a typical single-aisle aircraft forward of the wing. Several technologies will be considered in the scope of the project, including advanced aluminum–lithium alloys, selective reinforcement using fiber metal laminates, and advanced joining processes, such as friction stir welding. Data from this study will be used to verify improved weight and structural safety performance of EMST and to assess the adequacy of existing airworthiness standards and guidance needed for the implementation of arising technologies and their impact on future designs. Results from the first baseline panel test are summarized in this technical note and will be compared to future tests on advanced panels containing varying EMST to assess the damage-tolerance performance.

17. Key Words	18. Distribution Statement
FASTER, Advanced Technologies, Damage Tolerance, Residual Strength, Finite Element Modeling, Aircraft Fuselage Structure	This document is available to the U.S. public through the National Technical Information Service (NTIS), Springfield, Virginia 22161. This document is also available from the Federal Aviation Administration William J. Hughes Technical Center at actlibrary.tc.faa.gov.

19. Security Classif. (of this report)	20. Security Classif. (of this page)	21. No. of Pages	22. Price
Unclassified	Unclassified	78	

Contents

Figures

Tables

Acronyms

Acronym	Definition
DIC	Digital Image Correlation
EMST	Emerging Metallic Structures Technologies
FAA	Federal Aviation Administration
FASTER	Full-Scale Aircraft Structure Test Evaluation and Research
FCG	Fatigue Crack Growth
FEA	Finite Element Analysis
FEM	Finite Element Modeling
SHM	Structural Health Monitoring
SRM	Structural Repair Manual

Executive summary

In partnership with Arconic and Embraer, the Federal Aviation Administration (FAA) is assessing emerging metallic structures technologies (EMST) using the FAA's Full-Scale Aircraft Structural Test Evaluation and Research (FASTER) facility. In this collaborative effort, full-scale fuselage panel test data will be obtained to assess the effect of EMST concepts on damage tolerance performance of the current baseline aluminum fuselage structures, which are located on the crown of a typical single-aisle aircraft forward of the wing. Several technologies were considered in the scope of the project, including advanced aluminum-lithium alloys, selective reinforcement using fiber metal laminates, and advanced joining processes, such as friction stir welding. Data from this study will be used to verify improved weight and structural safety performance of EMST and to assess the adequacy of existing airworthiness standards and guidance needed for the implementation of arising technologies and their impact on future designs.

Results from the first baseline panel test are summarized in this technical note. A phased approach was undertaken for Panel 1 to study three scenarios simulating damage that represents cracks in the structure: (1) a two-bay crack-like notch in the skin along the circumferential direction, with central stringer severed; (2) a crack-like notch along a mill-line parallel to stringer, located near the edge of the milled section of a skin bay; and (3) a two-bay crack-like notch in the longitudinal direction, with the central frame severed.

The results will be compared to future tests on advanced panels containing varying EMST to assess the damage-tolerance performance.

1 Introduction

The aircraft industry is striving to both improve performance and reduce costs in fabrication, operations, and maintenance by introducing advanced materials in conjunction with innovative manufacturing and production technologies. In light of the structural material decision made for the B787 and A350 airframe, and increasing competition from composite materials, the aluminum industry has made significant advancements over the past decade in developing new lightweight alloys and product forms, improved structural concepts, and manufacturing processes aimed at being competitive with composite materials in terms of manufacturing cost and performance. Collectively, these advances fall under the umbrella classification of emerging metallic structures technologies (EMST). Substantial investments have been made to demonstrate the potential to design and build durable and damage-tolerant fuselage and wing structures using EMST, including advanced alloys (Prasad et al., 2014; Stonaker et al., 2015), bonding and joining methods (Bertoni et al., 2014; Chavez, 2017; Kok et al., 2011; Schmidt, 2005), and metallic-composite hybrids (Bertoni et al., 2014; Beumler, 2014; Chavez, 2017; Heinimann et al., 2007; Schmidt, 2005; Silva et al., 2017).

However, the introduction of a new material or concept in the aerospace industry can be quite challenging. A significant amount of test data at the coupon, substructure, and full-scale level is needed to fully vet and properly assess a new technology and understand potential certification and continued airworthiness issues. This includes the assessment of existing regulations and guidance materials to determine if the FAA needs to revise them or create new safety standards or guidance materials. For these reasons, regulators and industry ideally should work together in preparation for the application and certification of EMST.

In recognizing these challenges, the Federal Aviation Administration (FAA), Arconic, and Embraer are collaborating in a research effort to evaluate EMST for fuselage applications through full-scale testing and analysis. The goal is to assess and verify that the EMST have an improved durability and damage tolerance compared with the current baseline aluminum fuselage located on the crown of a typical single-aisle aircraft forward of the wing spar. Several EMST are being considered, including integral frames, friction stir welded skin joints, new metallic alloys, bonded stringers, and selective reinforcement using fiber metal laminates. Fuselage panels with various EMST will be designed, fabricated, and tested in this multi-year effort, as shown, for example, in Figure 1. Panels will be tested using the FAAs Full-Scale Aircraft Structural Test Evaluation and Research (FASTER) facility, which was designed for testing fuselage panels and is capable of simulating aircraft service load conditions through

synchronous application of mechanical and environmental load conditions (Tian and Bakuckas, 2019), Figure 2.

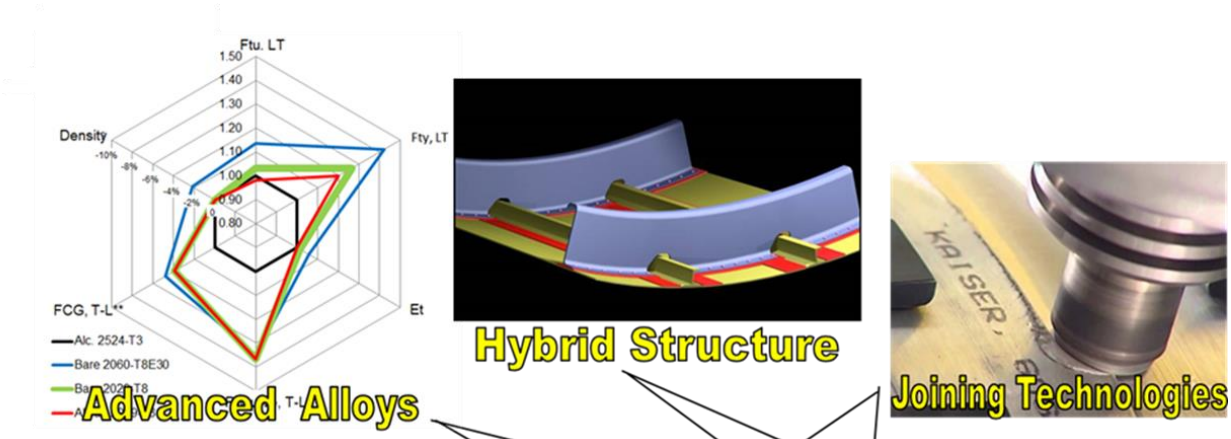

		1 Baseline	2 Advanced Density Reduction	3 Advanced Materials	4 Advanced Materials, FSW	5 FSW and Bonded Stringers
Component	Skin	2524-T3 sheet	2060 - T8 Al-Li sheet	2029-T8 sheet	2029-T8 sheet, FSW	2060 Al-Li sheet, FSW joint and bonded FML straps
	Stringer	7150 extrusions, riveted	2055 or 2099 Al-Li extrusions, riveted	2055 or 2099 Al-Li extrusions, riveted	2055 or 2099 Al-Li extrusions, FSW	2055 or 2099 Al-Li extrusions, bonded
	Frame	7075-T62 - shear tied, extruded, riveted	2055 or 2099 Al-Li integral extrusions, riveted	2055 or 2099 Al-Li integral extrusions, riveted	2055 or 2099 Al-Li integral extrusions, FSW	2055 or 2099 Al-Li integral extrusions, riveted

Figure 1. Potential EMST test matrix

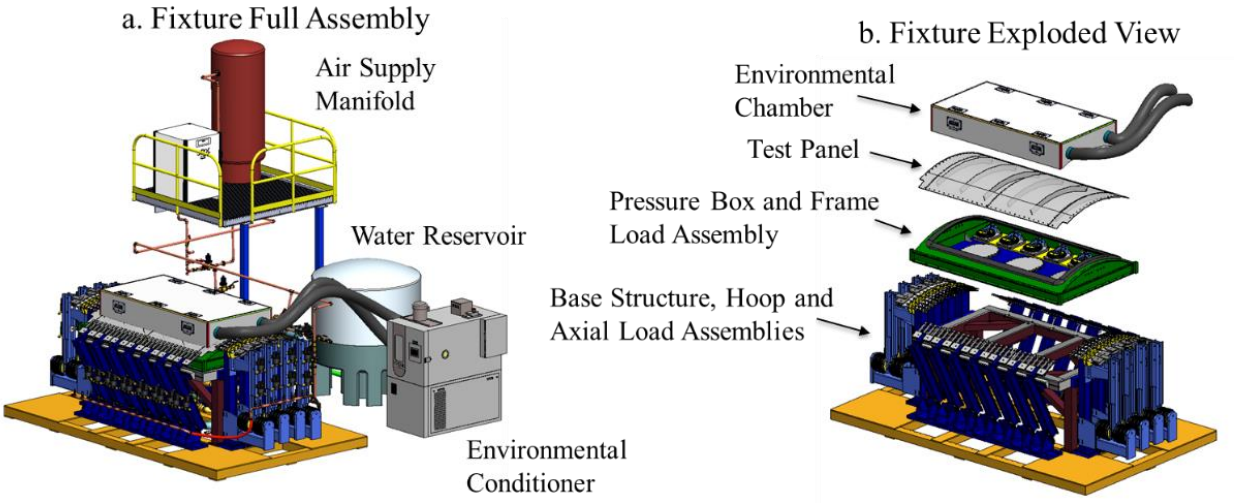

Figure 2. FAA FASTER fixture assembly and major components

A phased approach will be undertaken to study several damage scenarios, including: (1) a two-bay skin notch, along the circumferential direction, with central stringer severed; (2) a mill-line notch parallel to stringer, located near the edge of the milled section of a skin bay; and (3) a two-bay skin notch, along the longitudinal direction, with the central frame severed. For each damage scenario phase, strain surveys will first be conducted and compared to finite element predictions to verify proper load and panel alignment. The panels will then be subjected to fatigue crack growth (FCG) testing using an equivalent constant-amplitude load sequence determined through coupon-level tests that represent the complex load history of a fuselage panel located on the crown of the aircraft, forward of the wing (Kulak et. al, 2019 and Stonaker et. al., 2019). To demonstrate potential improvements in operational usage when considering aircraft equipped with EMST, an elevated fuselage pressure differential was used in the load sequence, which is approximately 15% higher than that used in a typical single-aisle transport category aircraft, such as the B737 and A320. The final stage of testing will be a residual strength test to limit load conditions identified in 14 CFR 25.571. Data from this program will be used to demonstrate the improvement in damage tolerance and structural safety potential of EMST and to assess the adequacy of existing regulations when considering EMST.

This report documents results from tests conducted on the first baseline panel, consisting of 2524-T3 skin and conventional 7000-series aluminum substructure assembled through riveting. The baseline panel was subjected to three phases of testing and accumulated over 84,000 simulated flights over a 10-month period. During all phases of testing, crack growth was monitored and recorded using high-magnification cameras, several nondestructive inspection methods, strain gages, and a digital image correlation (DIC) system. For each phase, prior damage was repaired. Results from the baseline panel tests are summarized below and will be compared with advanced panels containing varying EMST to assess the damage tolerance performance:

- **Phase 1**: A two-bay crack-like notch in the circumferential direction having a total length (tip-to-tip) of 1.3 in. was machined in the skin with the central stringer severed. The panel was then fatigue tested under simulated flight load conditions for 33,600 cycles in which slow and stable crack growth occurred to a final total length of 11.3 in. During the subsequent test conducted up to approximately 2.5 g (g-force) axial limit load, local stable tearing extension occurred from each crack-tip.
- **Phase 2**: A crack-like notch along a mill-line having a total length of 6.0 in. was machined in the skin mid-bay and parallel to a stringer and then subjected to 7,500

fatigue cycles. The crack extended about 2.0 in. from each notch-tip and displayed intermittent periods of slow-to-no crack growth because of crack binding.

- **Phase 3**: A two-bay crack-like notch in the longitudinal direction having a total length of 1.5 in. was machined in the skin with the central frame severed and then fatigue tested to 43,600 cycles. During the fatigue test, the crack extended across two frame bays to a final length of 16 in. Afterwards, a residual strength test was conducted during which the panel failed at an applied pressure of 17 psi. Approximately 1.0 in. of stable tearing was observed from each crack tip prior to failure of the panel.

2 Experimental procedure

Testing for this program was conducted using the FAA's FASTER facility. A description of the test panel, test phases, applied loads, inspection, and monitoring methods are outlined in this chapter.

2.1 Target application and panel description

The target aircraft considered in this study is a typical single-aisle airplane, such as the B737 or A320. The location of the fuselage panel is assumed to be the crown just forward of the wing, where the major modes of loading are pressurization and vertical bending due to flight and landing loads. LMI Aerospace was contracted by Arconic to fabricate the baseline panel using standard aerospace manufacturing practices, including but not limited to forming, chemical milling, surface treatment, and joining technologies. The baseline test article, Panel 1, was fabricated per drawings provided in Appendix A.

The final panel dimensions were 125 in. × 76 in. with a radius of 74 in., as shown in Figure 3. The skin material was 2524-T3 with a pocketed construction, where the skin thickness was 0.059 in. in the mid-bay regions and 0.065 in. in the pad-up regions under the frames and stringers. Note that the panel was designed to have pocket skin thickness of 0.055 in. with a build tolerance of 0.005 in. and was discovered later to have an average of 0.059 in. The impact of thickness difference is addressed by Kulak (2019). The substructure included eight stringers made from 7150-T77511 extruded in a Z-section with a 7 in. spacing and six 7075-T62 frames connected using 7075-T62 shear ties with a 20 in. spacing. A two-piece floating Z-section frame and L-section shear tie construction was used. Reinforcing doublers were installed along the outer perimeter of the skin and to the frame ends for load attachment points of the fixture. Holes of 0.5 in. diameter were drilled along the reinforced doubler edge of the panel for load introductions in the axial and hoop directions. Loads were also introduced into each frame. The

major panel dimensions are listed in Table 1. The materials used for the major components are listed in Table 2.

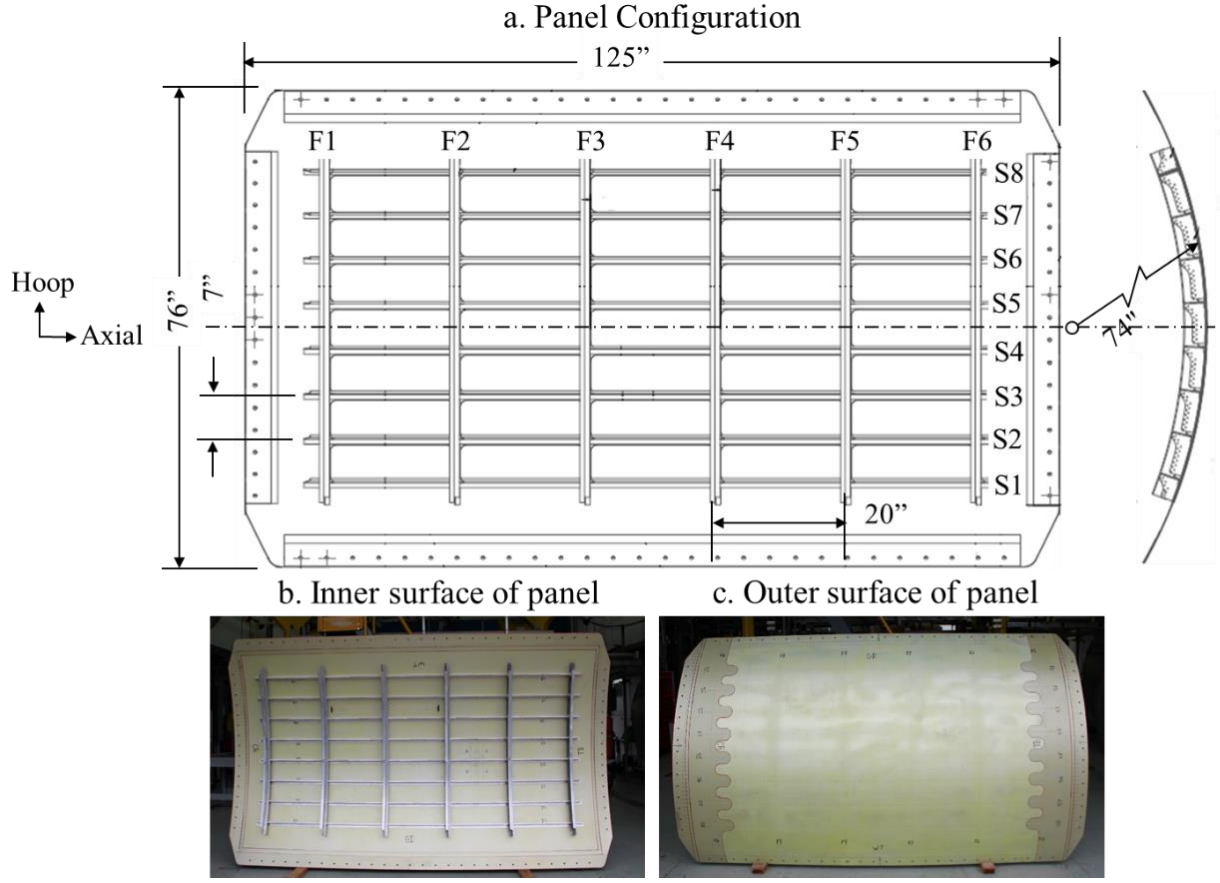

Figure 3. Baseline panel configuration and views of the internal and external surface

Table 1. Panel 1 dimensions

Panel length	125 in.
Panel width	76 in.
Panel radius	74 in.
Panel skin thickness, pad-up	0.065 in.
Panel skin thickness, mid-bay	0.059 in.
Number of frames	6
Number of stringers	8
Frame spacing	20 in.
Stringer spacing	7.0 in.

Table 2. Component materials used to fabricate Panel 1

Component	**Material**
Skin	2524-T3 sheet
Stringer	7150-T7511 extrusions, riveted
Frame	Extrusions O or F temper, stretch formed and heat treated to T62 temperature
Shear ties	7075-T62 sheet

2.2 Test phases and damage scenarios

A phased approach was undertaken to study the three damage scenarios summarized as follows.

Phase 1: Initial damage consisted of a crack-like notch having a length of 1.3 in. in the circumferential direction spanning two skin bays between frames F2 and F3, with the central stringer S4 severed (see Figure 4a). Strain surveys were conducted to ensure proper load introduction. The panel was then fatigue tested under loads representing pressure, flight maneuver and gust accelerations, and landing loads in the forward crown section of a single-aisle aircraft. Fatigue testing was conducted until the crack extended to a final total length of 11.3 in. Afterwards, a limit load test was conducted, during which the panel was subjected to approximately 2.5 g axial load while holding the pressure constant under operational conditions. The panel was then repaired for follow-on phases (Appendix B).

Phase 2: To study crack turning phenomena, the initial damage consisted of a crack-like notch along a mill-line having a total length of 6.0 in. in the skin parallel to stringer S2 midway between frames F4 and F5, as shown in Figure 4b. Strain surveys were conducted to ensure proper load introduction and to verify no effects from the repair made in Phase 1. The panel was then fatigue tested, simulating pressure-only flight-load conditions to monitor the direction and rate of crack growth. Afterwards, the panel was repaired for follow-on phases (Appendix B).

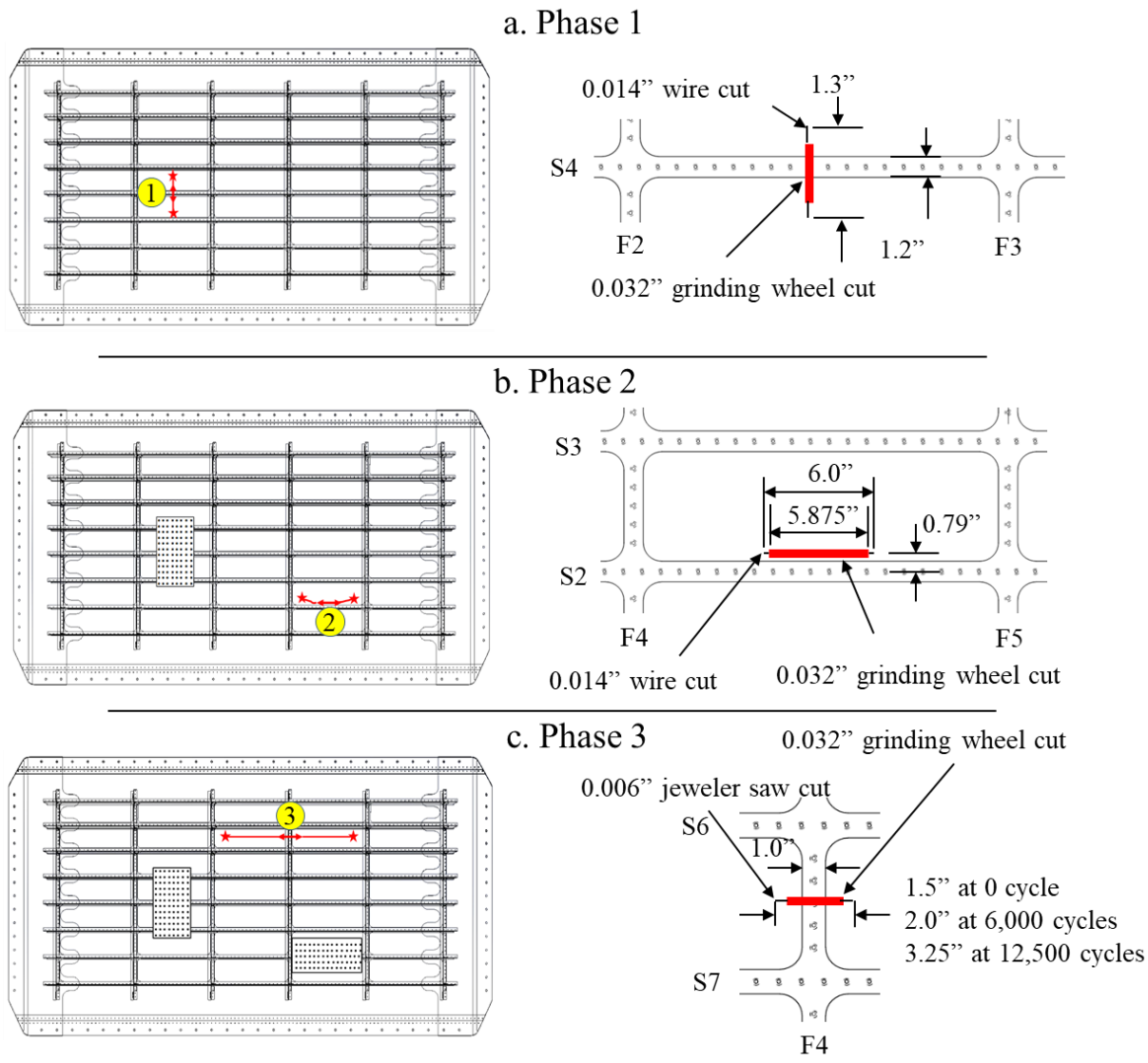

Figure 4. Initial damage scenarios used in the three test phases

Phase 3: Initial damage consisted of a two-bay longitudinal crack-like notch between stringers S6 and S7, with the central frame/shear tie F4 severed, as shown in Figure 4c. Three notch lengths at the same location were used, having lengths of 1.5, 2.0 and 3.25 in. and inserted at 0, 6000, and 12,500 fatigue cycles, respectively, due to crack binding issues as discussed in section 4.3. Initial strain surveys were conducted to ensure proper load introduction and to verify no effects from the repairs made in Phases 1 and 2. The panel was then fatigue tested, simulating pressure-only operational conditions, until the crack extended to a final length of approximately 16 in. A residual strength test was finally conducted to failure, measuring the load-carrying capacity of the panel.

2.3 Inspection and monitoring methods

During all phases of testing, several nondestructive inspection methods were used to monitor and record the formation and growth of cracks. Visual inspections were made on the inner and outer surfaces of the skin using high-magnification cameras that could be remotely controlled during the test. High-frequency eddy current was used on the outer surface of the skin. Along with these inspection methods, the baseline panel was instrumented with 200 strain gages and digital image correlation (DIC) systems to monitor strains throughout the tests, as summarized in Appendices C and D, respectively. In addition, a commercial piezoelectric-based structural health monitoring system was used to collect data and to assess its capabilities to monitor FCG, highlighted in Appendix E.

2.4 Applied mechanical loads

The loads on the crown of the fuselage forward of the wing are primarily due to pressure and bending from flight and landing loads. An elevated fuselage pressure of 9.9 psi was used as the operational condition for an aircraft equipped with EMST. It was shown by Steadman (2007), and assumed in this study, that flight loads measured in typical single-aisle aircraft, such as the B727 and B737, resemble the mini-TWIST spectrum (Lowack et. al., 1979) if the acceleration excursions are reduced by a factor of 2.0. Using a hierarchical finite element approach (Kulak et al., 2019), hoop and axial stresses applied to a panel located on the crown of an aircraft were determined, as shown in Figure 5a. Hoop stresses were assumed to be due to pressurize cycles only, and axial stresses were assumed to be due to pressure, flight, and landing loads, as shown schematically in Figure 5b.

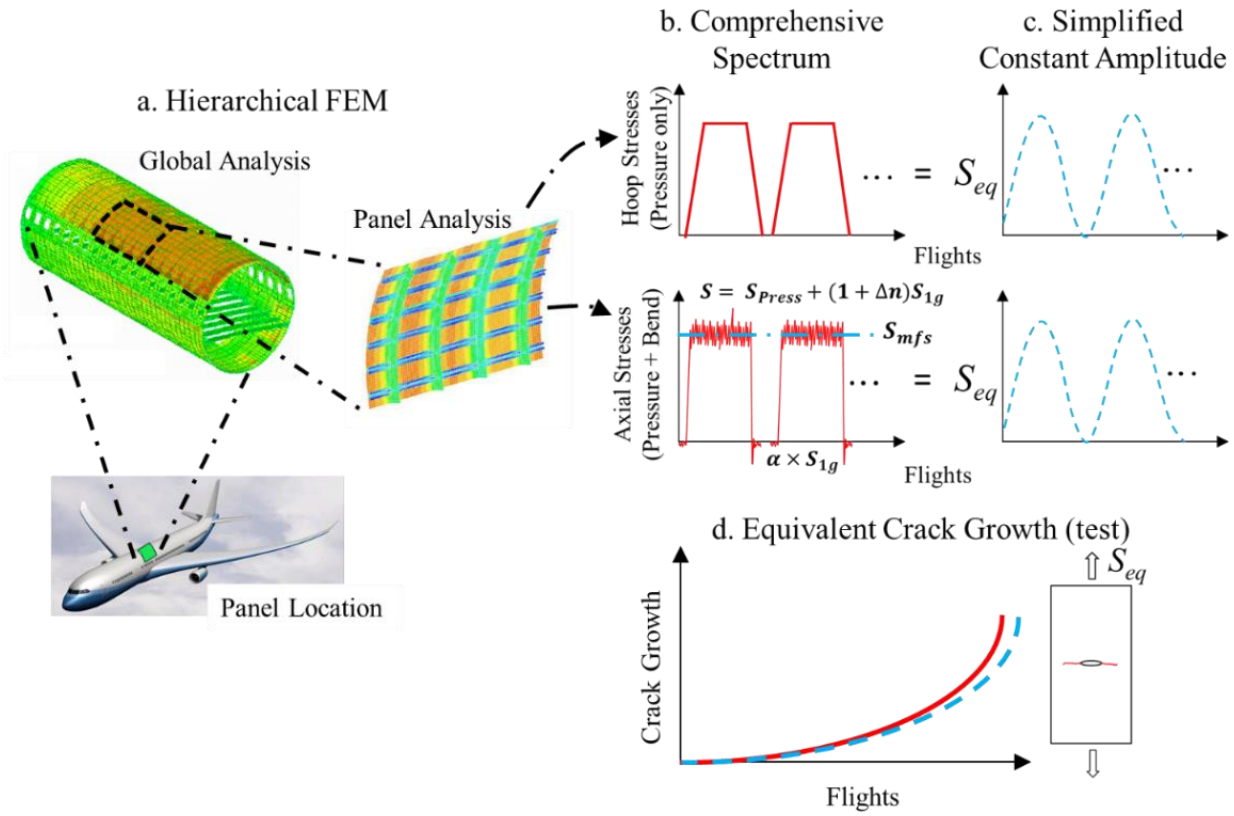

Figure 5. Determination of equivalent constant-amplitude loads used in full-scale test

The axial stresses during flight and landing are given by:

$$S_F = S_{Press} + (1 + \Delta n)S_{1g} \quad (1)$$

respectively, where S_{Press} is the stress due to pressure, S_{1g} is the bending stress under 1 g, S_{mfs} is the mean flight stress, and Δn is the incremental load factor from the 50% Mini-TWIST spectrum. Finite element analyses were conducted to calculate the pressure and bending stresses (Kulak et al., 2019).

Though the FASTER fixture is capable of executing complex variable-amplitude spectrum loading that represents fuselage down-bending loads, it is not practical to run a full-scale fatigue test program under such conditions. Instead, an equivalency approach was used to determine a constant-amplitude load applied in the axial direction, designated as S_{eq}, used in the panel test as shown in Figure 5c. This equivalent constant-amplitude load would provide an equivalent crack growth as the complex flight loads, as shown in Figure 5d. This was done experimentally using M(T) specimens, as described by Stonaker et al. (2019).

The approximate applied stresses used in each test phase are shown in Table 3. Strain surveys were conducted at 75% of the fatigue loads. Fatigue loading was conducted using $R = 0.05$ and a frequency of 0.03 Hz. All testing was done under lab ambient conditions.

Table 3. Summary of applied stresses

Phase	**Test Type**	**Pressure (psi)**	**Axial Stress**		
			S_{eq} (ksi)	**S_{Press} (ksi)**	**S_{1g} (ksi)**
1	Strain Survey	7.425	9.20	3.93	5.06
	Fatigue	9.9	12.30	5.24	6.75
	Limit Load	9.9	22.12	5.24	6.75
2	Strain Survey	7.425	3.93	3.93	0
	Fatigue	9.9	5.24	5.24	0
3	Strain Survey	7.425	3.93	3.93	0
	Fatigue	9.9	5.24	5.24	0
	Residual Strength	17	9.00	9.00	0

3 Finite element analysis

Finite element analysis (FEA) for this program was conducted by Arconic. As shown in Figure 6, a hierarchical approach using global and panel models provided:

- actuator loads for the FASTER fixture to provide stresses in the test section that match stresses in the global model of the idealized fuselage;
- pre-test predictions of the stress and strain fields;
- crack drive force (stress-intensity factor) used in the equivalent constant-amplitude stress testing, fatigue crack growth analysis, and residual strength calculations; and
- other fracture parameters, including δ_5 for comparison of stable tearing measurements.

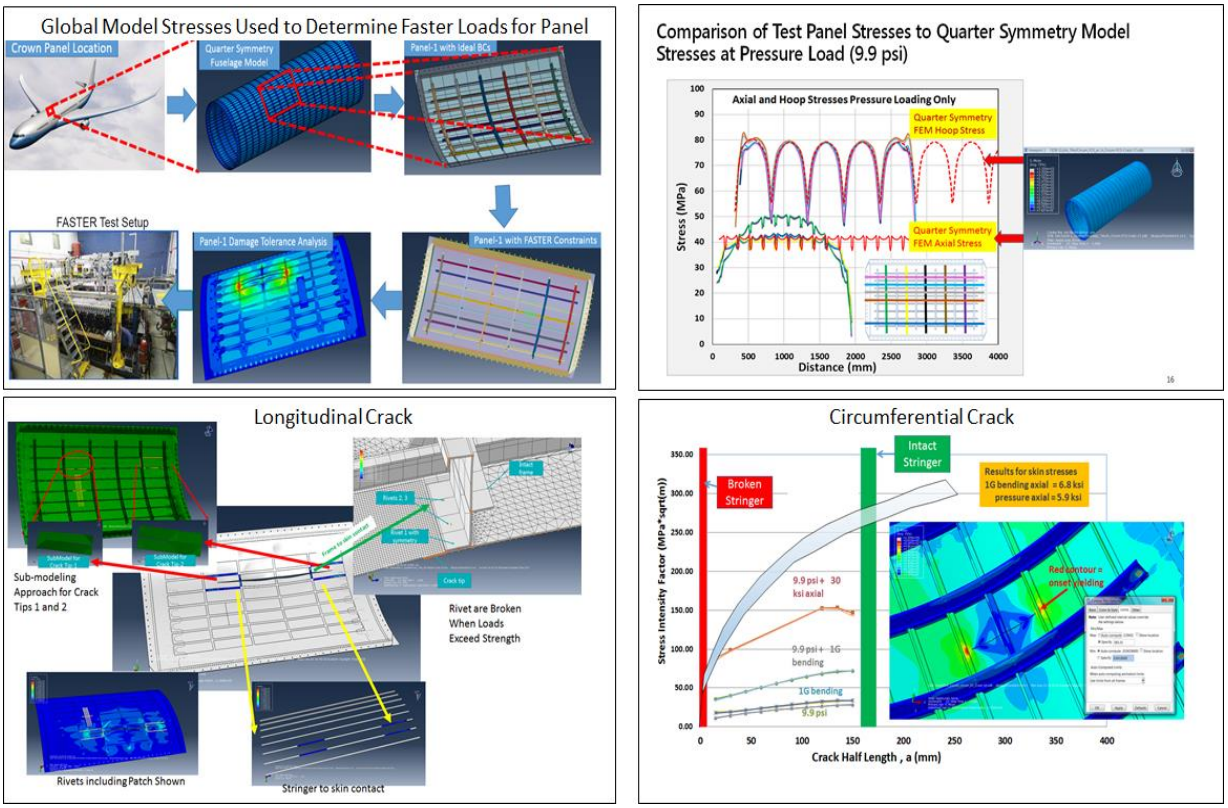

Figure 6. Hierarchical FEA approach used in program

The quarter symmetry finite element model, *Qsymm*, of a fuselage was used to develop stress and crack drive forces (stress-intensity factors) for various conditions of pressure and bending. These target results were then used as reference to determine the FASTER fixture actuator loads for all three phases and two residual strength testing phases. This approach was used because the configuration of the panel, the thick reinforcement doublers along the parameter of the panel, the frame and stringer termination within the panel, and the load paths into the frame, stringer, and skin are different from the Qsymm model. The FASTER fixture actuator loads were determined so that the test panel model had the same crack drive force as well as measured strain gage data as Qsymm model. It was also shown that by matching the stresses in the undamaged panel model, the differences of crack drive forces are within ±5% with respect to those in the baseline Qsymm model. Therefore, it is not necessary to change the actuator loads at different crack length, and the FASTER actuator loads were kept the same during the crack growth testing at each phase. Details of the analysis approaches used in this program are provided by Kulak at al. (2019).

The actuator loads for each phase are shown in Figure 7, Figure 8, and Figure 9.

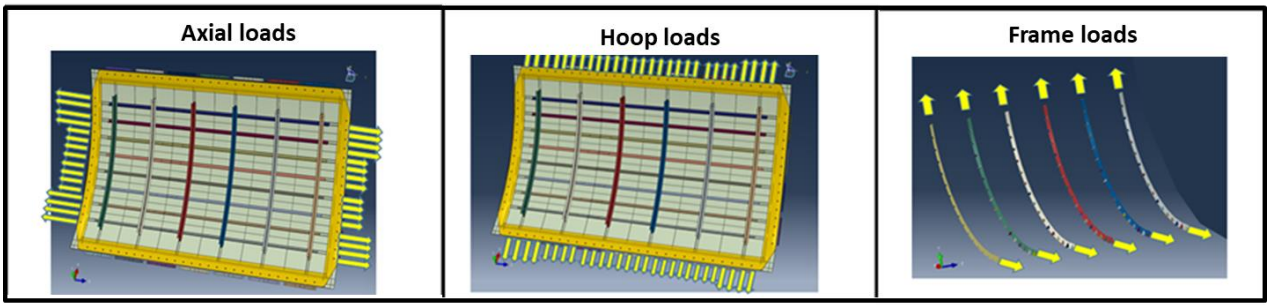

Skin Axial Actuator Load Arm Number	Applied Load (lbf)
1-4	20,270
5-8	12,715
9-12	12,715
13-16	20,270

Skin Hoop Actuator Load Arm Number	Applied Load (lbf)
1-4	10,675
5-8	9,946
9-12	9,716
13-16	9,625
17-20	9,716
21-24	9,946
25-28	10,675

Frame Number	Applied Load (lbf)
1	1,783
2	2,420
3	2,433
4	2,433
5	2,420
6	1,783

Figure 7. FASTER actuator loads for Phase 1 fatigue test

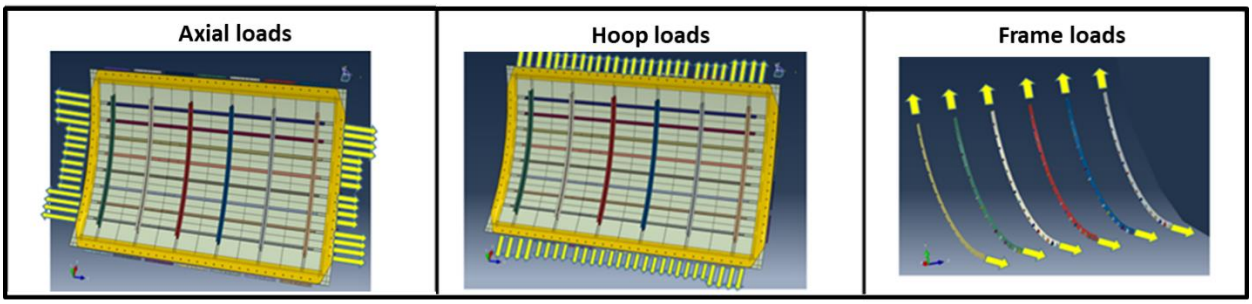

Skin Axial Actuator Load Arm Number	Applied Load (lbf)
1-4	35,767
5-8	22,435
9-12	22,435
13-16	35,767

Skin Hoop Loaders	Applied Load (lbf)
1-4	10,675
5-8	9,946
9-12	9,716
13-16	9,625
17-20	9,716
21-24	9,946
25-28	10,675

Frame-Y	Applied Load (lbf)
1	1,783
2	2,420
3	2,433
4	2,433
5	2,420
6	1,783

Figure 8. FASTER actuator loads for Phase 1 limit load test

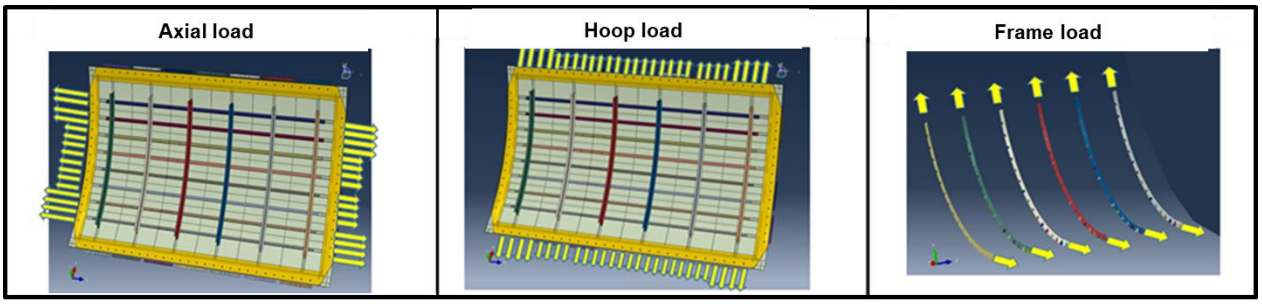

Skin Axial Actuator Load Arm Number	Applied Load (lbf)
1-4	9,231
5-8	5,790
9-12	5,790
13-16	9,231

Skin Hoop Actuator Load Arm Number	Applied Load (lbf)
1-4	10,675
5-8	9,946
9-12	9,716
13-16	9,625
17-20	9,716
21-24	9,946
25-28	10,675

Frame Number	Applied Load (lbf)
1	1,783
2	2,420
3	2,433
4	2,433
5	2,420
6	1,783

Figure 9. FASTER fixture actuator loads for Phase 2 and Phase 3 fatigue test, pressure only

4 Results and discussion

Tests and analyses were performed to determine the fatigue and damage-tolerance performance of the baseline fuselage panel, which was constructed using conventional materials and fabrication processes. The results from this panel will be used for comparison to future test results from testing of advanced fuselage panels with varying EMST. Representative results focus on the baseline panel test for each of the three phases.

4.1 Phase 1: two-bay circumferential notch with central stringer severed

4.1.1 Initial Strain Survey

A central crack-like notch was machined in the skin above the severed stringer S4, which is 1.30 in. total length and 0.032 in. wide. The notch was centered about the removed fastener, having the geometry shown in Figure 10. Initial strain surveys were conducted to verify proper load introduction to the baseline panel and validate the FEA model. Representative results shown in Figure 11 reveal that axial strains measured at gages near the original notch-tip were in agreement with FEA results.

4.1.2 Fatigue Test

The panel was then fatigue tested under simulated flight load conditions for 33,600 cycles, during which the skin crack extended across two stringer bays to a final length of approximately 11 in., as shown in Figure 12 and Figure 13. In general, slow and stable crack growth was observed during the fatigue test. The crack surface morphology had distinct transition points where, on the left side, the surfaces changed from V (valley) to S (slant) fracture and on the right side transitioned from a +45° to a -45° slant fracture. Results indicate that crack-growth rates changed at these transition points similar to those observed in coupon tests conducted on M(t) specimens (Stonaker et al., 2019).

Strain surveys were conducted during the fatigue test at 1,000-cycle intervals up to 19,000 cycles, and 2,000-cycle intervals afterward. The far-field axial strains in the mid-bay regions remained relatively constant throughout the fatigue test. Slight strain redistribution was evident after 28,000 cycles due to the crack extension, as shown in Figure 14. Strains increased in gages 7 and 10 as the crack grew closer to those gages. In addition, strains in gage 8 reduced due to crack shielding.

Local to the crack, strain redistribution was more significant on internal local skin and stringer gages, as shown in Figure 15 and Figure 16, respectively. The magnitude of strain increased as the crack tip approached the gages. As the crack grew past the gages, strains in the skin subsequently reduced. The excellent correlation with FEM analysis further confirmed strain redistribution with crack growth as shown in Figure 17. Local notch-tip strains on the inner surface of the skin were measured using chain gage consisting of 10 miniature strain gages spaced at 0.04 in. to monitor the initial 0.45 in. of crack extension up to 10,000 cycles, as shown in Figure 18. As shown, skin strain increased as the crack extended. This was also evident from full-field notch-tip strains measured on the outer surface of the skin using DIC, Figure 19. Representative results show the increase in size of high-strain region near the tip of the crack as it grew.

During the fatigue test, the frame end at F5 failed unexpectedly at 19,800 cycles. The test was stopped and the panel was removed from the fixture to repair all frame ends, as shown in Appendix F. The strain survey was conducted after repairing the frame ends, and confirmed there is no noticeable difference due to the repairs.

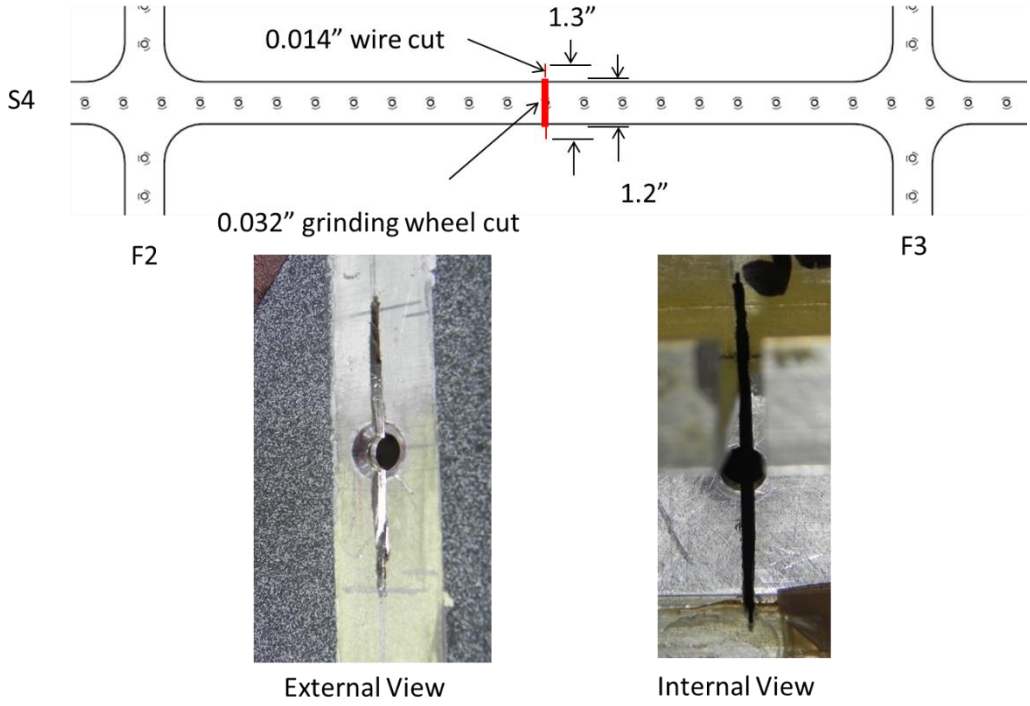

Figure 10. Configure of Phase 1 damage scenario

4.1.3 Limit Load Test

Afterwards, the panel was subjected to approximately 2.5 g of axial load in a limit load test holding the pressure constant at 9.9 psi. Strain gages located on the inner and outer flanges of the stringer ahead of the fatigue crack revealed that the stresses were below the yield strength of the stringer material (see Figure 21). In addition, limited stable tearing extension and crack-tip plasticity was observed from each crack tip, as shown in Figure 21 using DIC measurements. The intact stringers ahead of the crack were effective in containing the damage.

The panel was then repaired for follow-on phases, as shown in Appendix B. The strain survey was conducted to ensure there is no effect of repair on Phase 2 test bay, as shown in Figure 22.

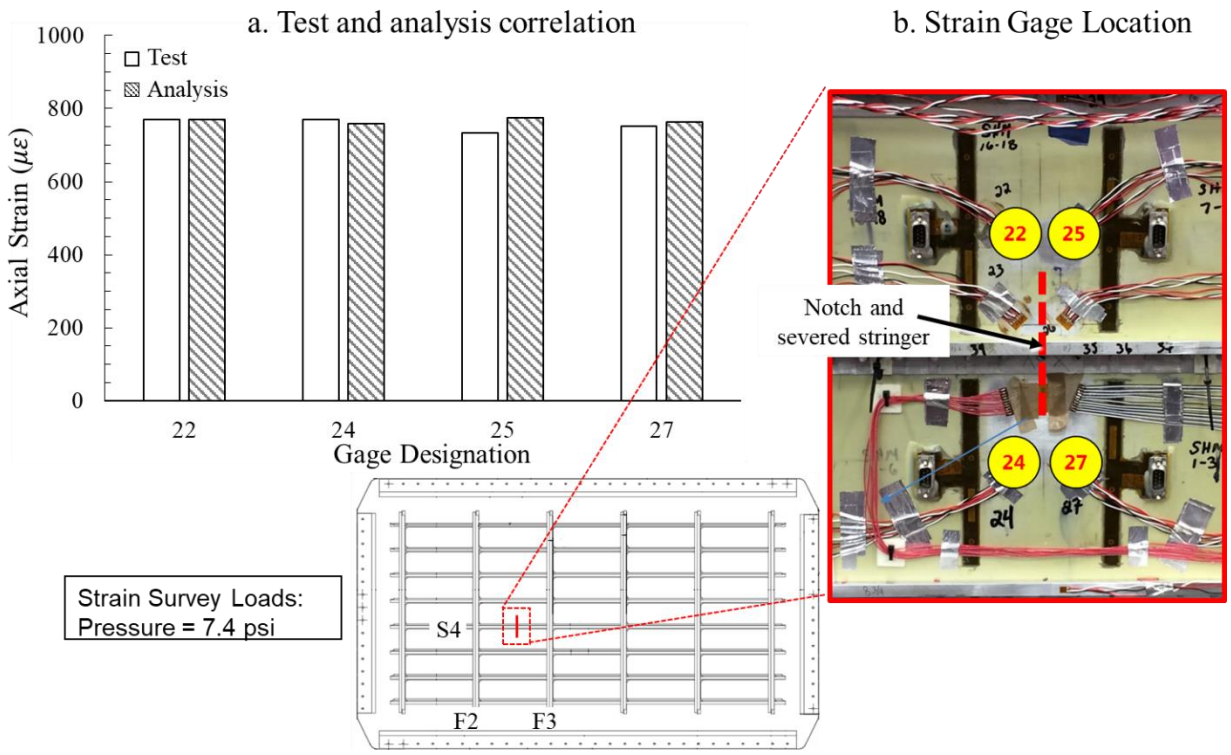

Figure 11. Phase 1 strain survey results verify FEA and applied loads

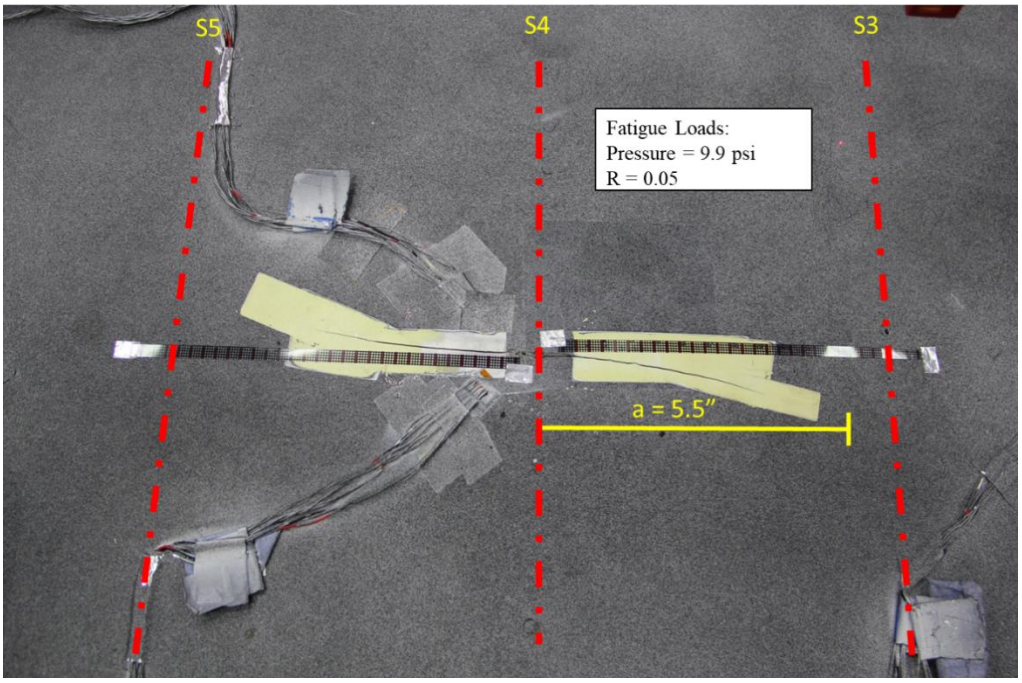

Figure 12. Picture of Phase 1 fatigue crack growth at 33,600 cycles

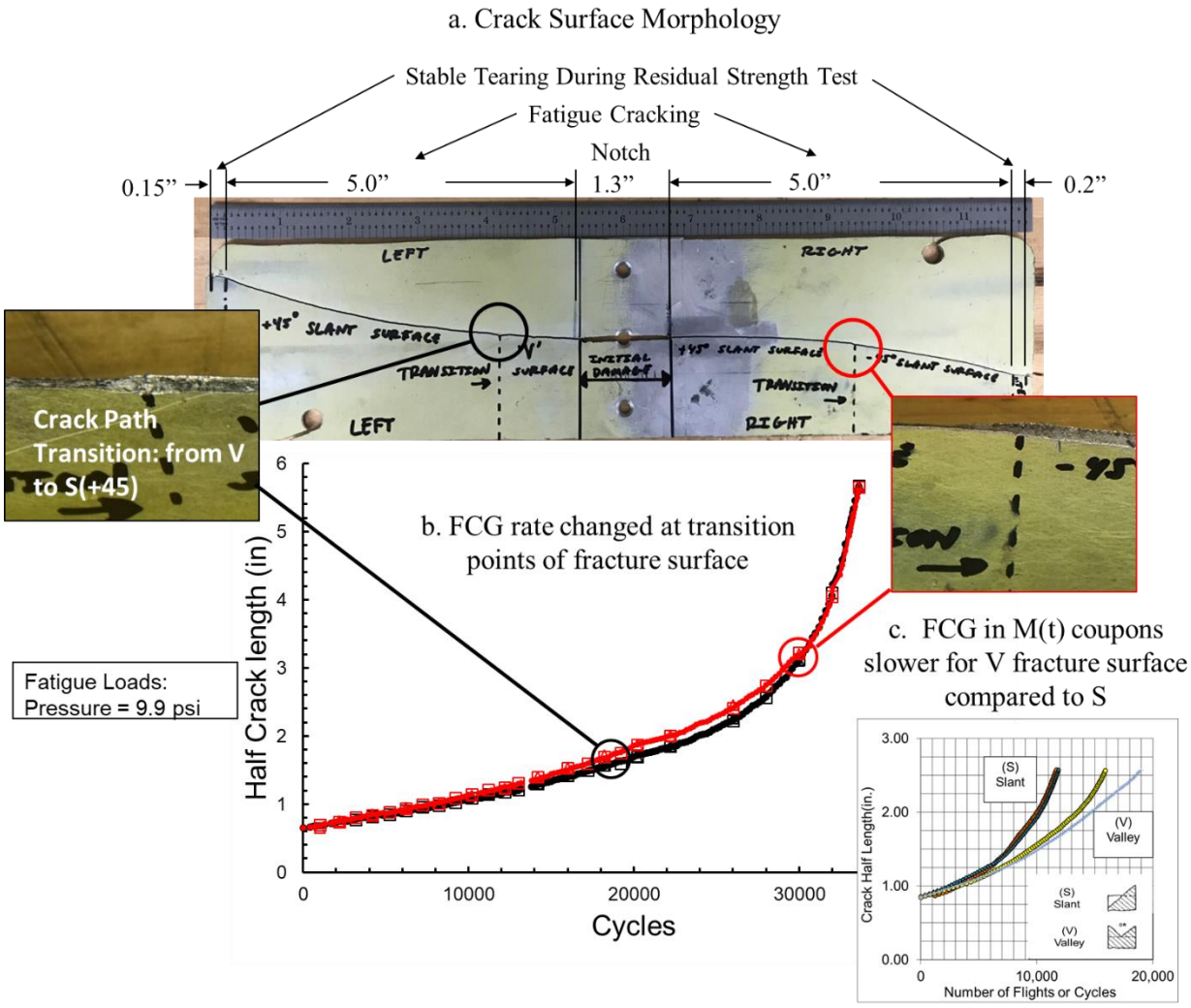

Figure 13. Phase 1 transition points of fracture surface morphology where FCG rates change

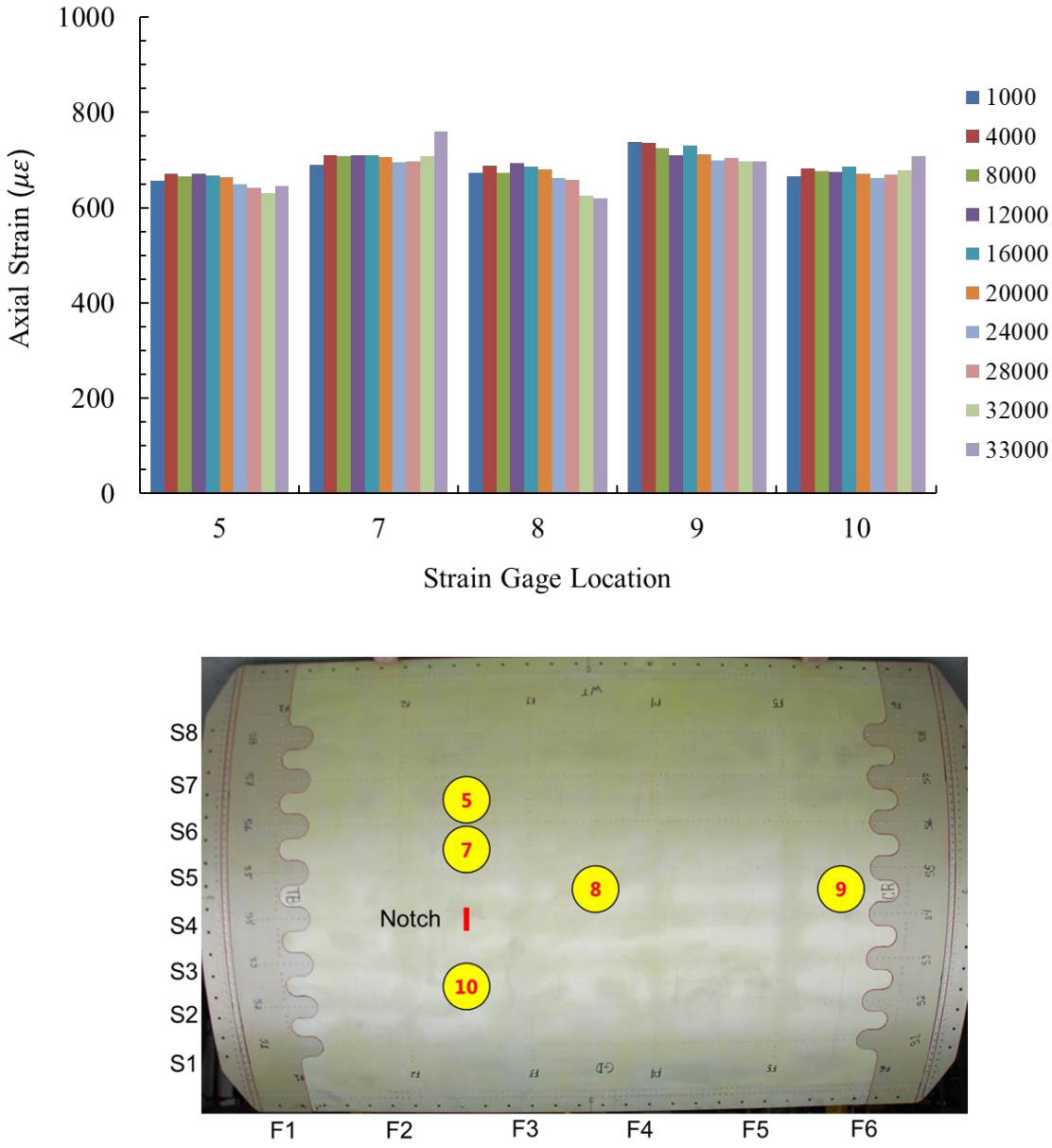

Figure 14. Far-field axial strain distribution measured in skin mid-bay regions during the fatigue test

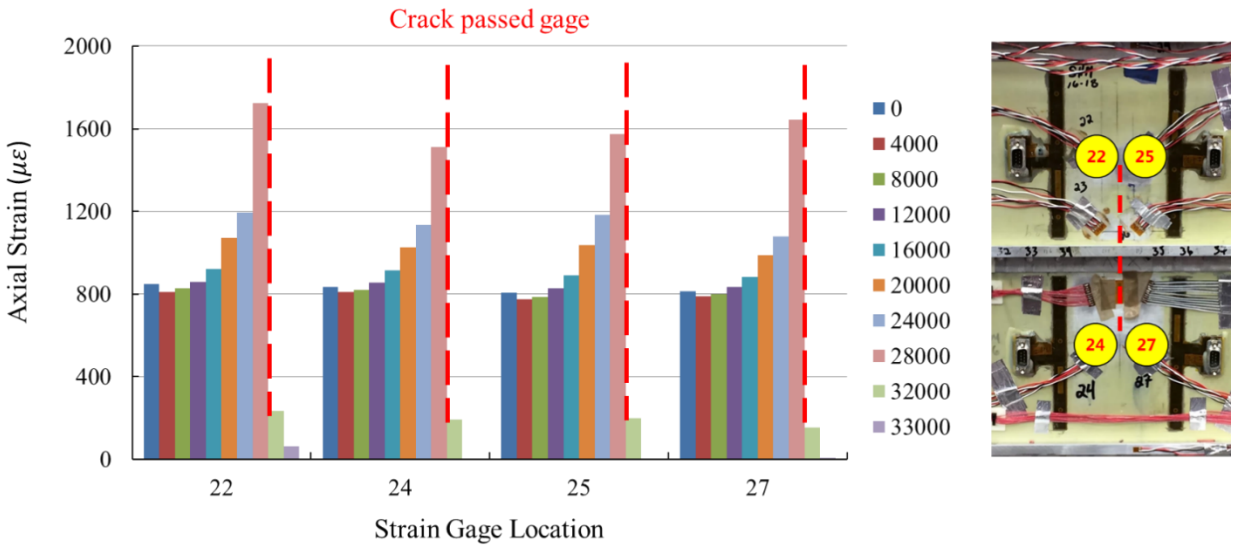

Figure 15. Representative strain survey results for Phase 1 internal skin rosette gages

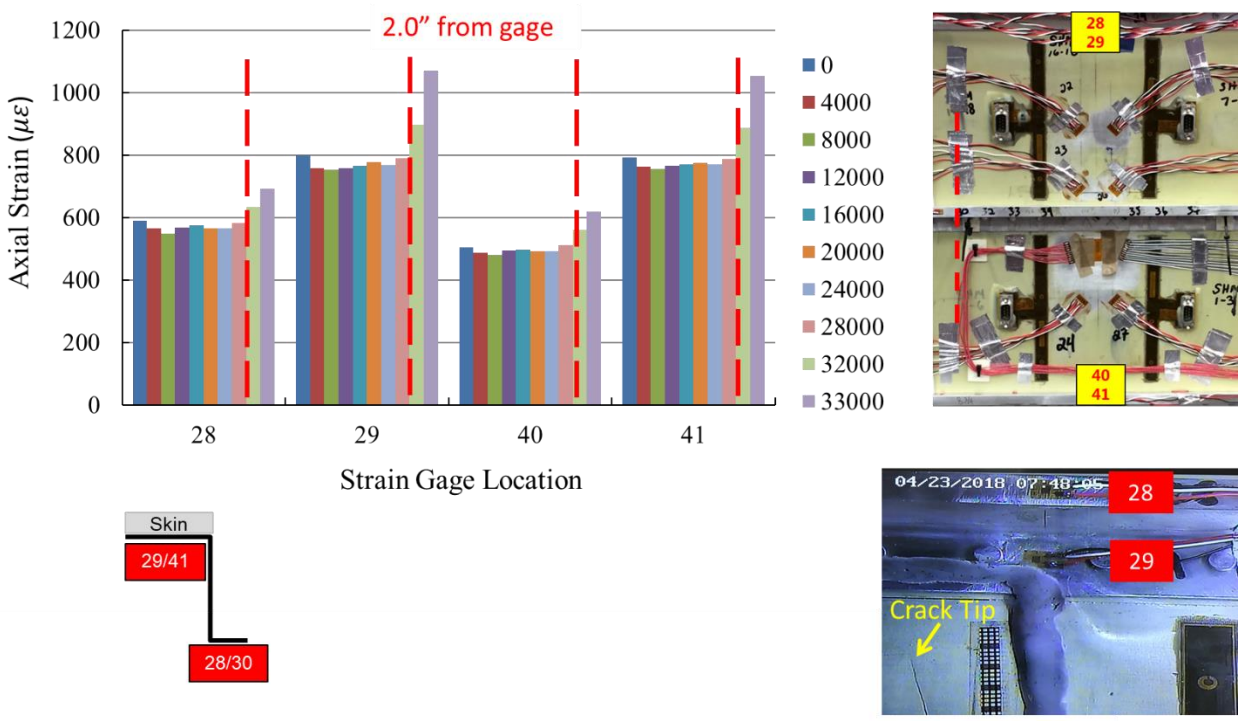

Figure 16. Representative strain survey results for Phase 1 stringer gages

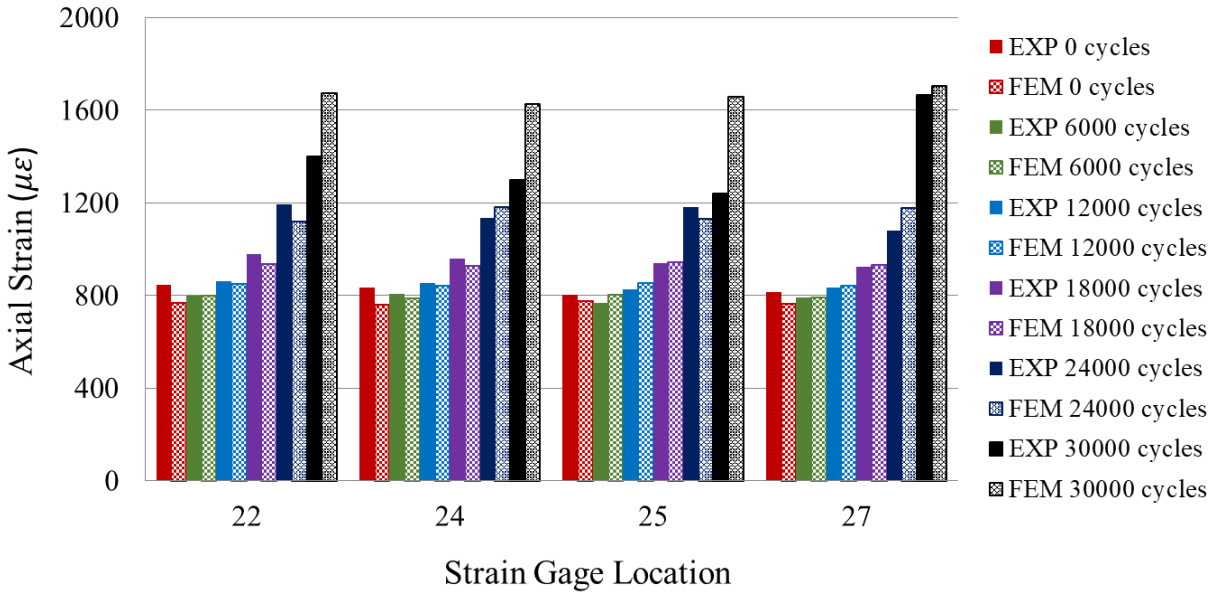

Figure 17. Correlation between the test and FEM analysis

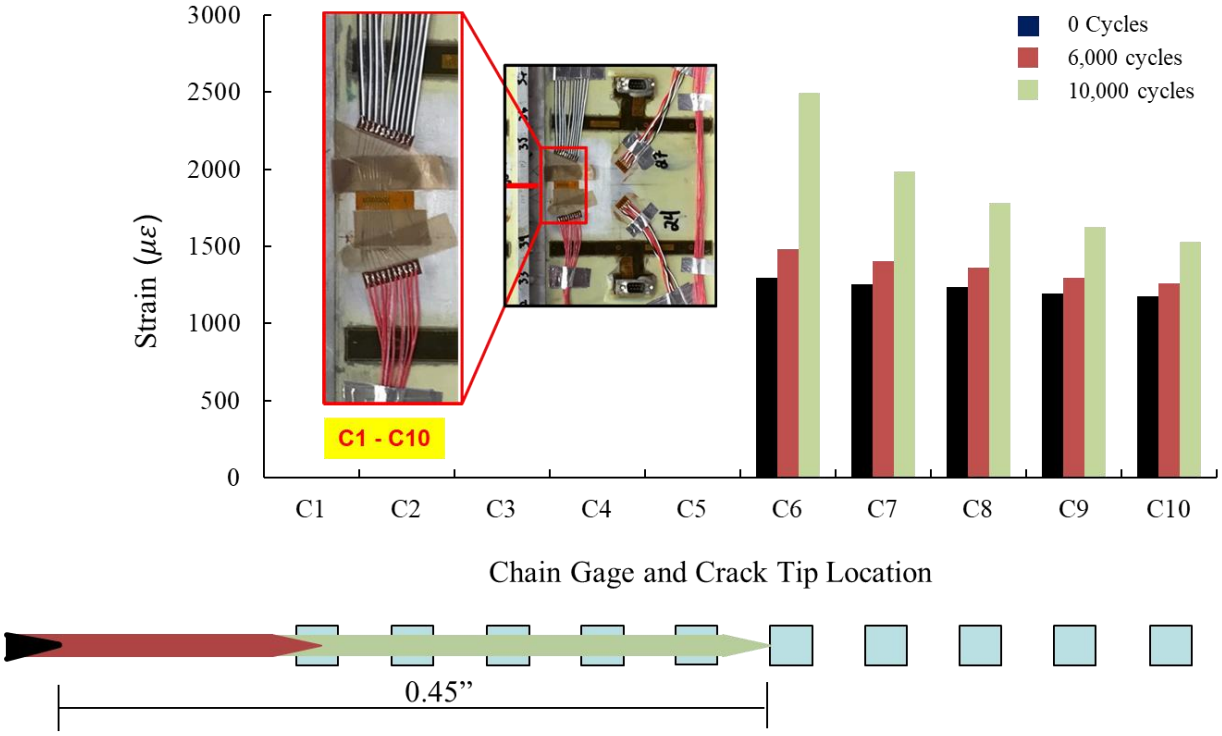

Figure 18. Chain gage data up to 10,000 cycles and 0.45 in. fatigue crack extension

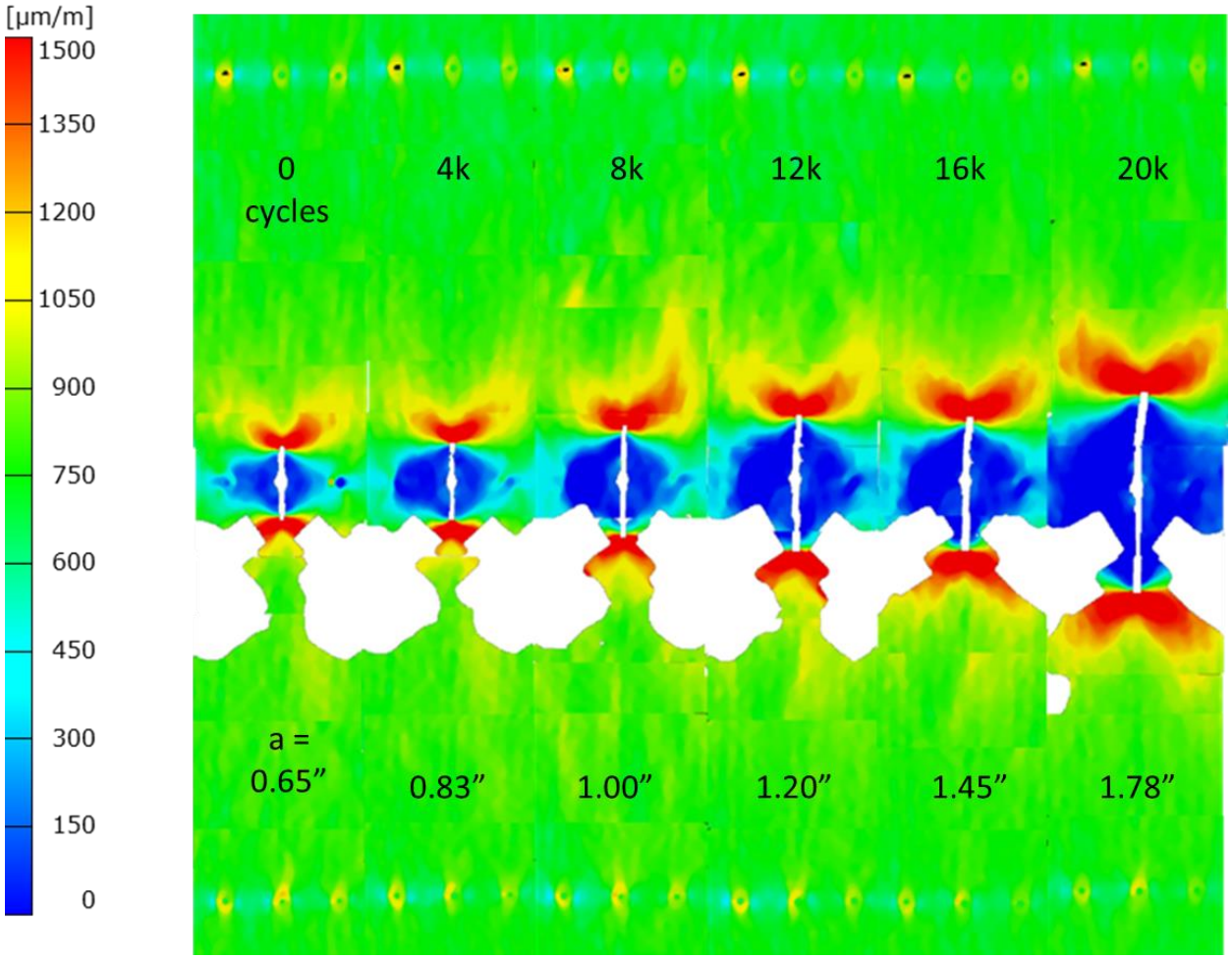

Figure 19. Narrow field of view ARAMIS data at different cycles

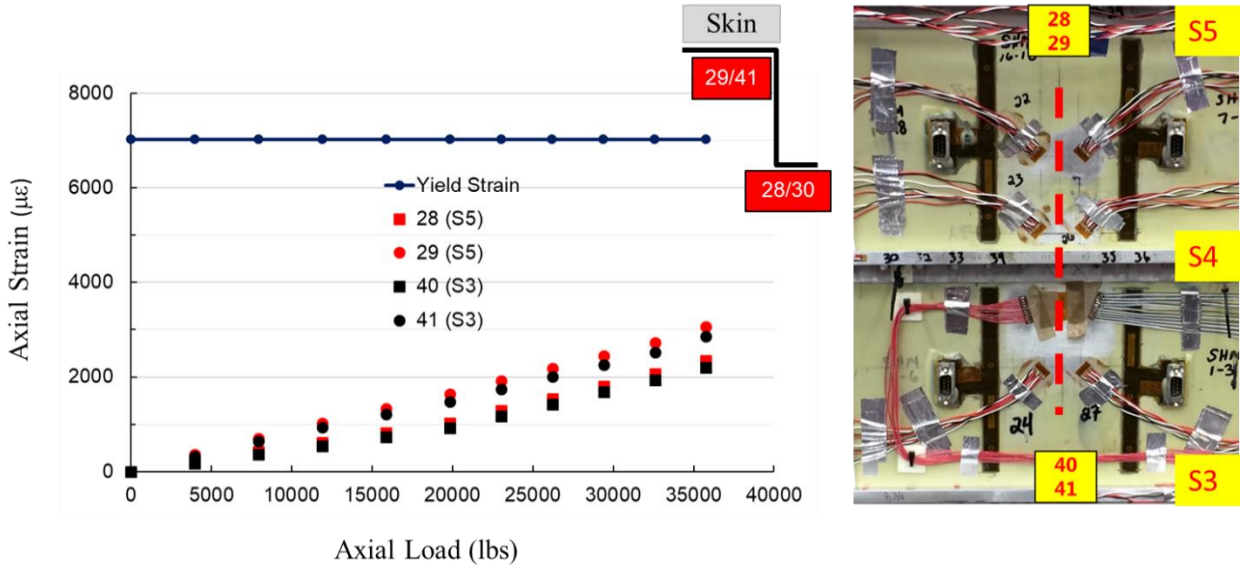

Figure 20. The result of stringer gages during the circumferential direction limit load test

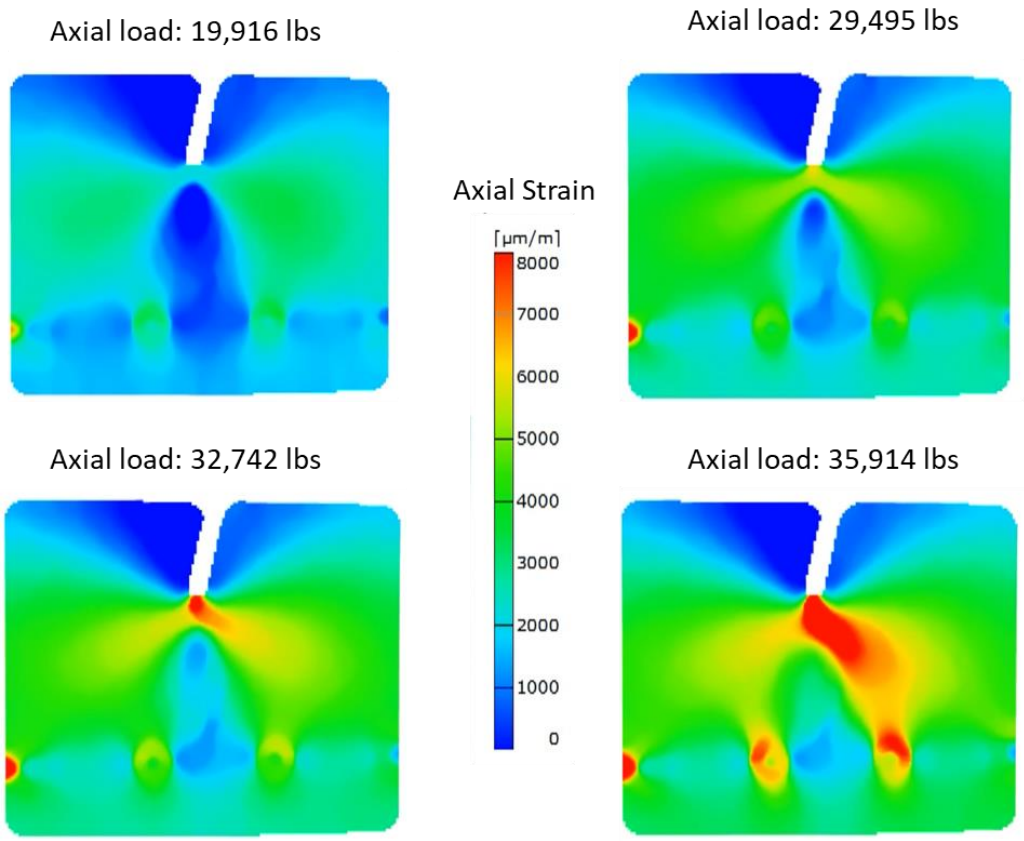

Figure 21. ARAMIS result during the circumferential direction limit load test

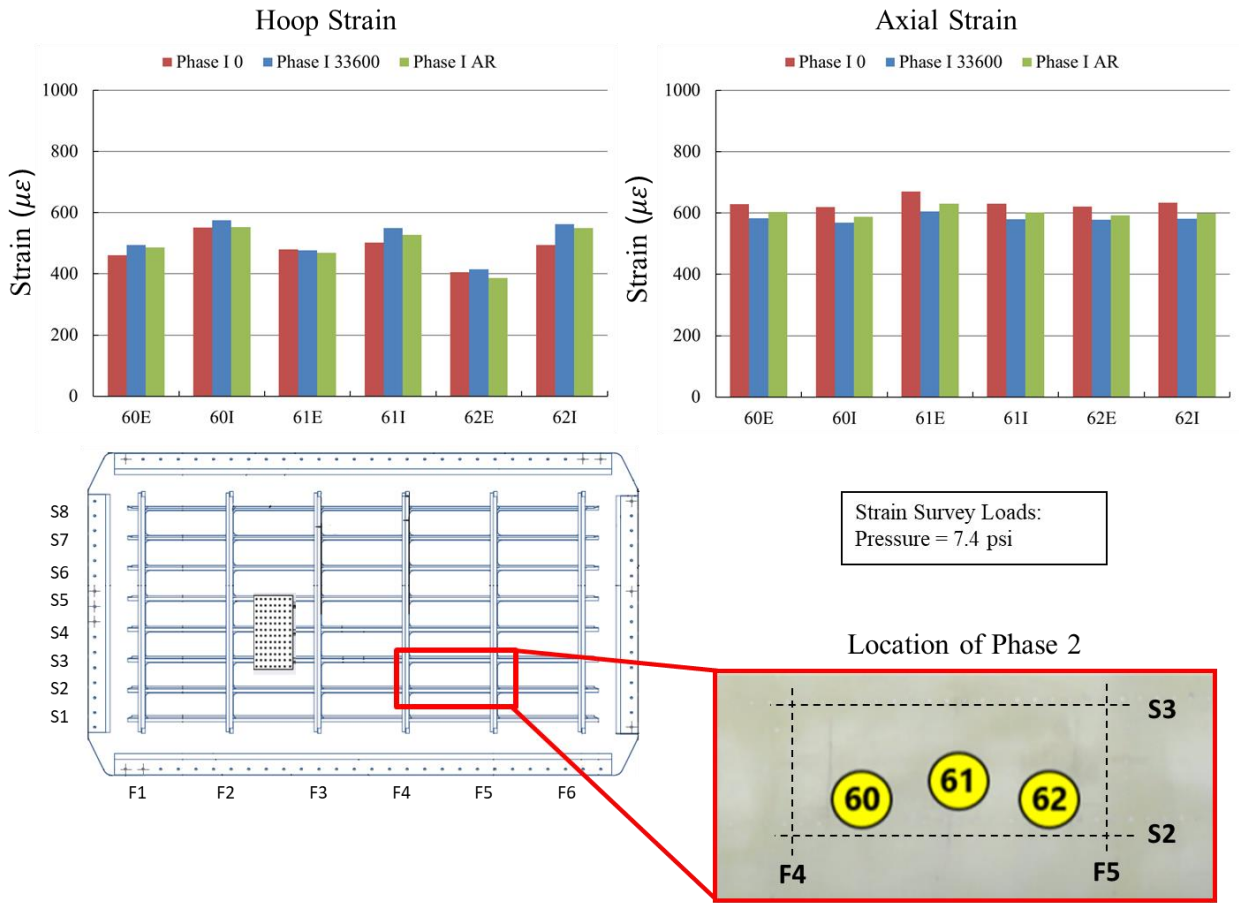

Figure 22. Strain survey after Phase 1 crack repair

4.2 Phase 2: mid-bay mill-line notch parallel to stringer

The crack scenario for Phase 2 is shown in Figure 23. A crack-like notch, located in mid-bay between frame F4 and F5, was machined in the skin parallel to stringer S2. The notch along the longitudinal direction was 6.0 in. long and 0.032 in. wide.

In this phase, the panel was fatigue tested under pressure load conditions for 7,500 cycles, in which the crack extended approximately 1.97 in. from each notch-tip. Representative results are shown in Figure 24. In general, natural cracks developed at 18° and 15° angles from the left and right notch-tips, respectively, which agreed with FEA predictions, as shown in Figure 24a. The initial crack growth increased steadily and correlated with analysis up to approximately 1,000 cycles, where crack extension reduced precipitously, as shown in Figure 24b. Subsequently, the fatigue behavior displayed additional slow/no growth intervals at 4,500 and 6,000 cycles, at which the crack wake surfaces were notched with 0.014 in. diamond wire, leaving the natural

crack-tip (see Figure 25c). Results from DIC revealed crack binding where the highest tensile strains were measured in the wake of the crack during slow/no crack growth interval, as shown in Figure 25. After notching the crack wake, the high-tensile strain region transitioned back to the crack-tip (see Figure 25d).

Upon completing the fatigue test, the panel was repaired for the final phase of testing, as shown in Appendix B. A strain survey conducted revealed that there was no effect of the repair on Phase 3 test bay, as shown in Figure 26.

During the fatigue test, a frame end failed unexpectedly at approximately 4,500 cycles due to deficient tab end installation (incorrect 1000-series rivet types were used and structural adhesive was not applied between doublers). The test was stopped, and the panel was removed from the fixture to repair all frame ends, as shown in Appendix C. The strain survey was conducted after repairing the frame ends, and it confirmed there was no noticeable difference in panel strain distribution due to the repairs.

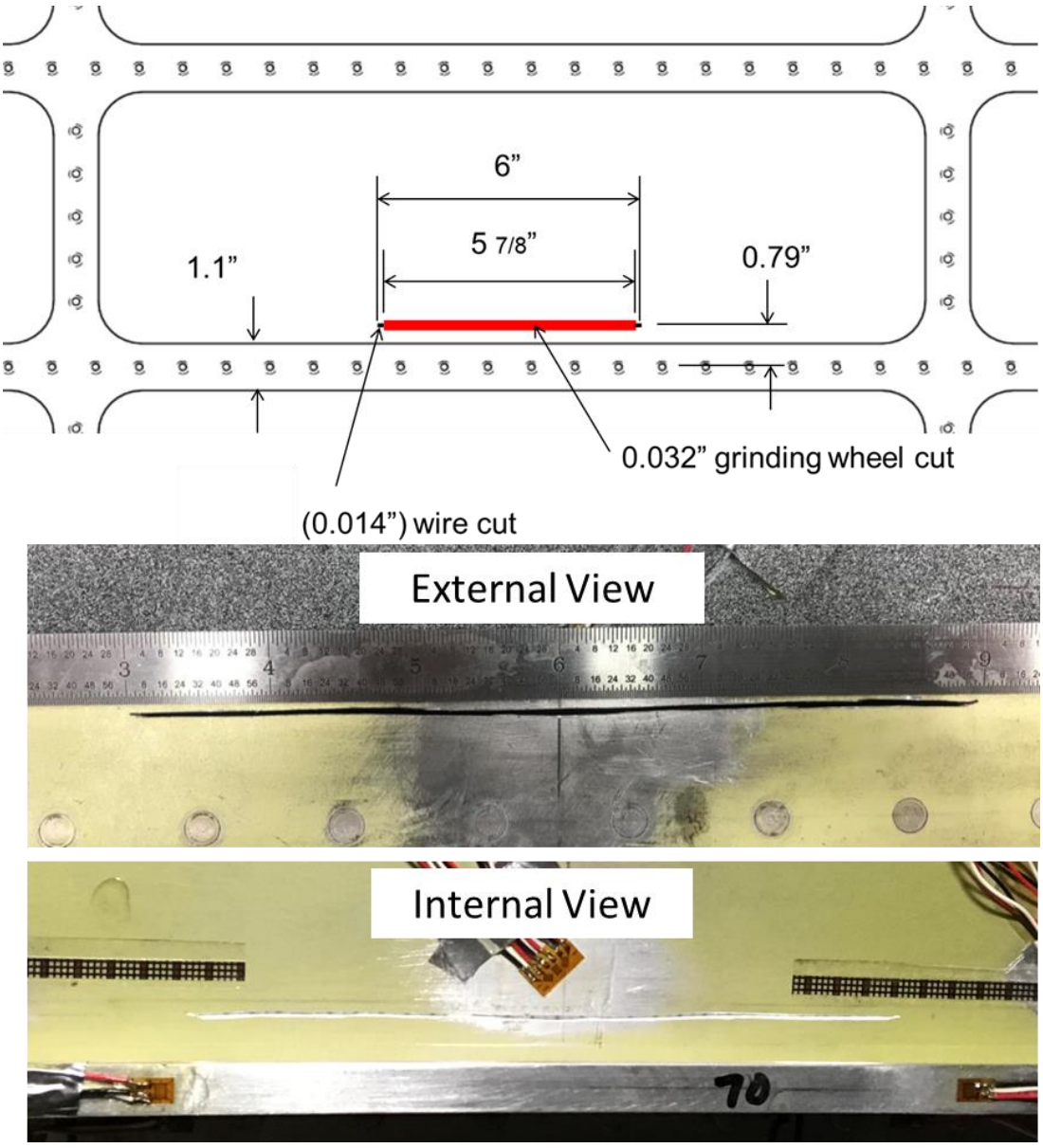

Figure 23. Configuration of Phase 2 damage scenario

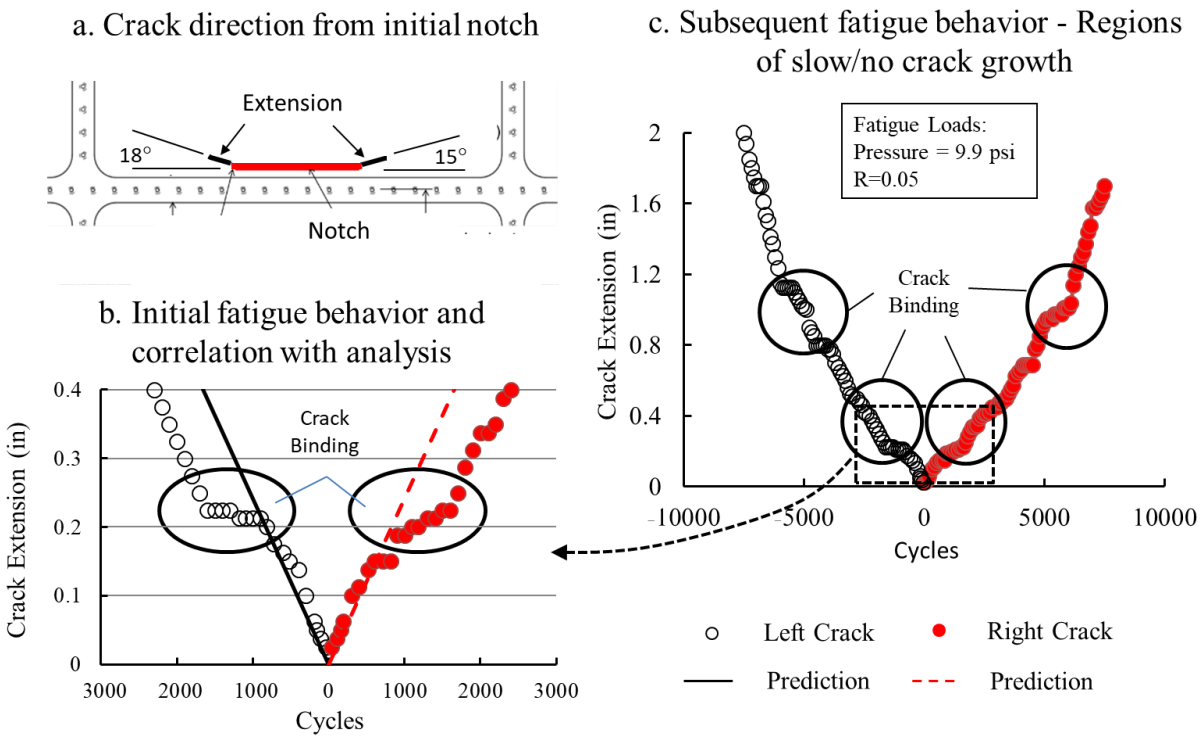

Figure 24. Phase 2 FCG results revealed regions of slow/no growth due to crack binding

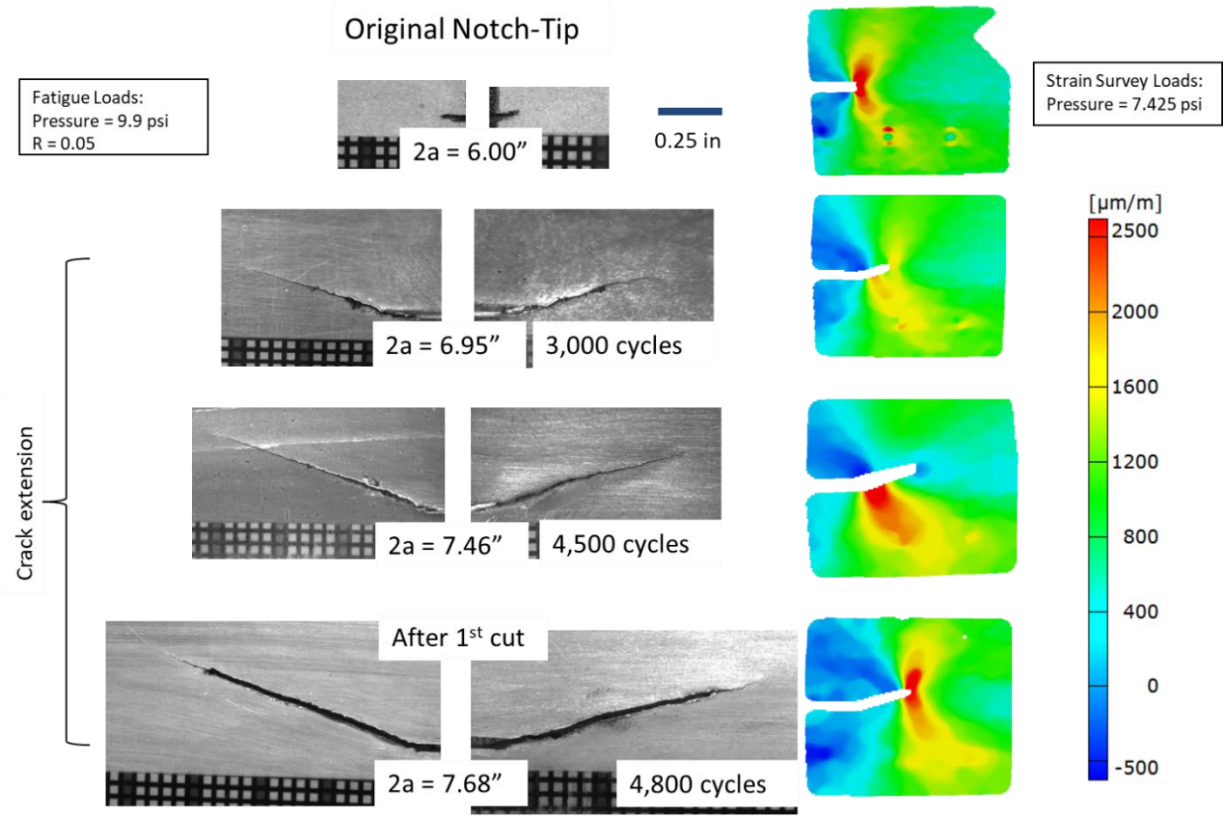

Figure 25. Phase 2 FCG results reveal high strains in the crack wake due to binding

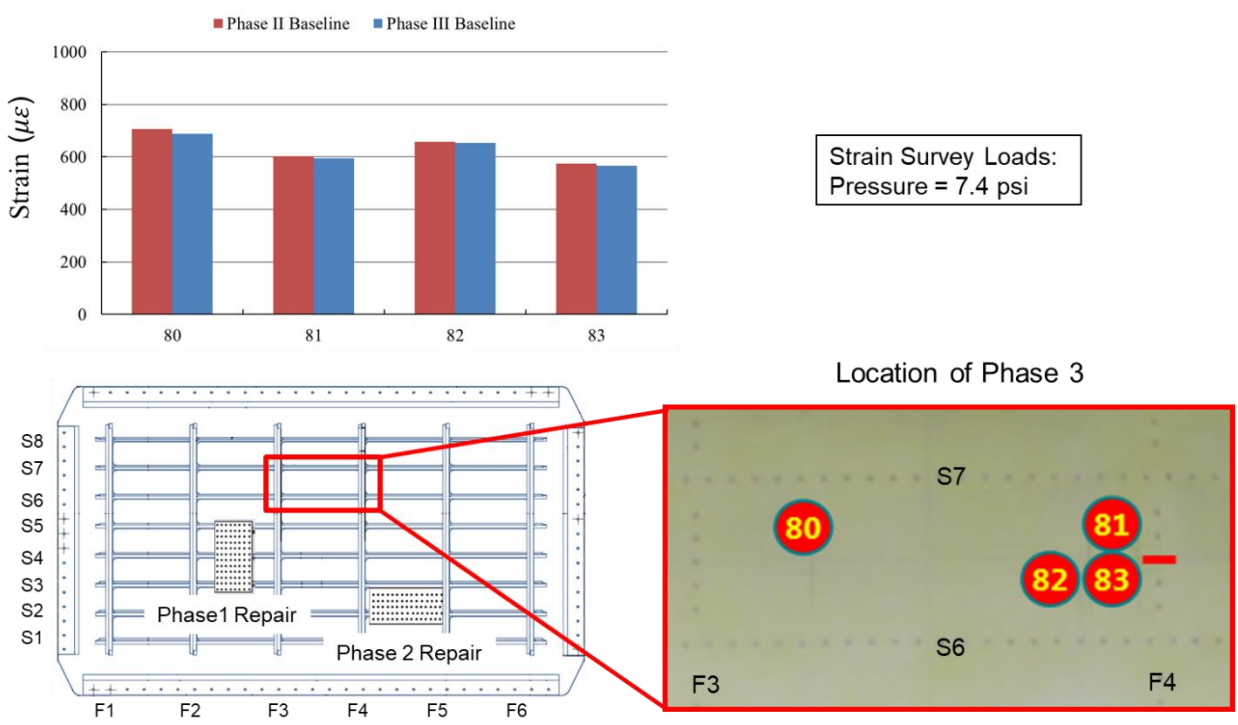

Figure 26. Strain survey conducted after Phase 2 crack repair

4.3 Phase 3: two-bay longitudinal notch with central frame severed

The longitudinal damage scenario for Phase 3 is shown in Figure 27. The frame F4 rivet at the mid-frame location between stringers S6 and S7 was removed, and frame F4 was severed at this location. Damage was simulated by machining a 1.5-in.–long notch in the skin above the severed F4 frame.

For this final phase, the panel was fatigue tested under pressure load conditions for 43,600 cycles, during which the skin crack extended across two frame bays to a final total length of approximately 16 in. Representative results are shown in Figure 28. The crack growth was quite slow in the initial stages of fatigue testing from the initial total notch length of 1.5 in. Consequently, the notch was extended twice to lengths of 2.0 in. and 3.25 in. after 6,000 cycles and 12,500 cycles, respectively. Local effects from the severed frame-end suppressed crack growth and caused binding for the shorter notch lengths (less than 3.25 in.).

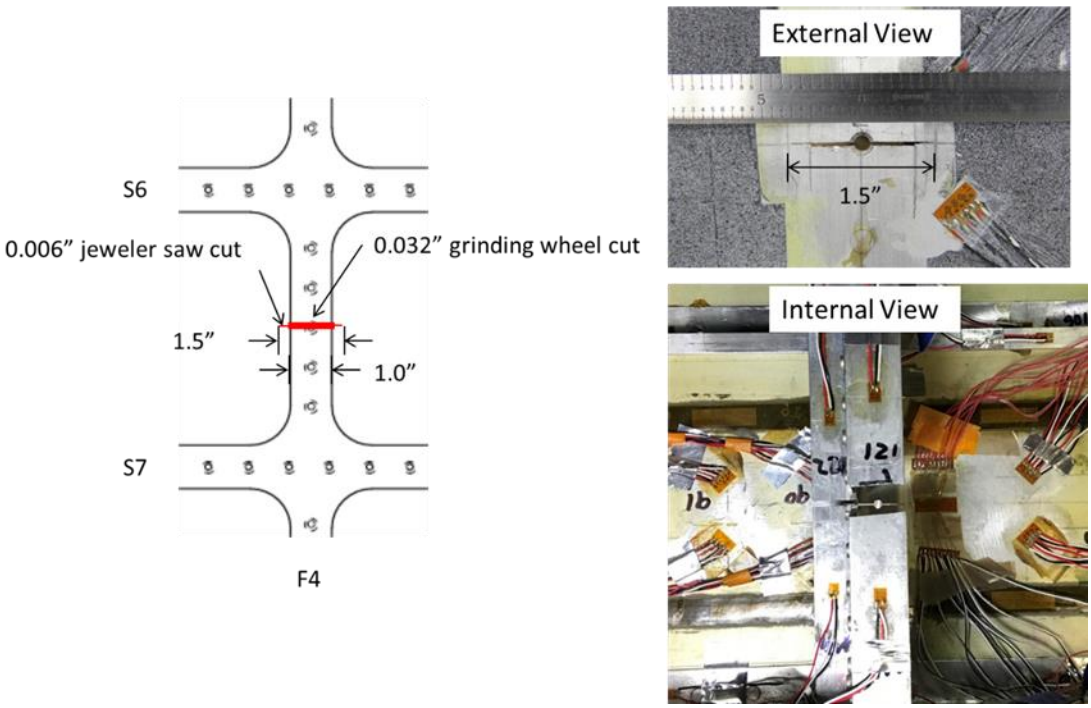

Figure 27. Configuration of Phase 3 damage scenario

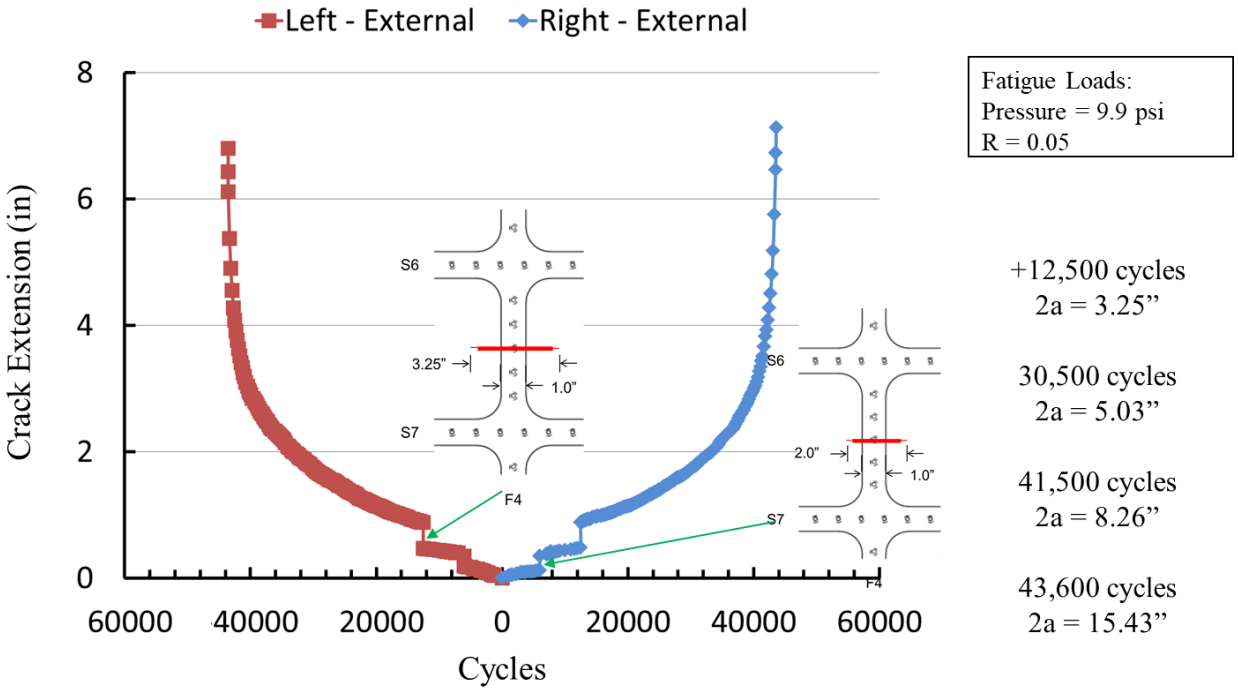

Figure 28. Slow FCG for short crack lengths due to local effects of severed frame and binding

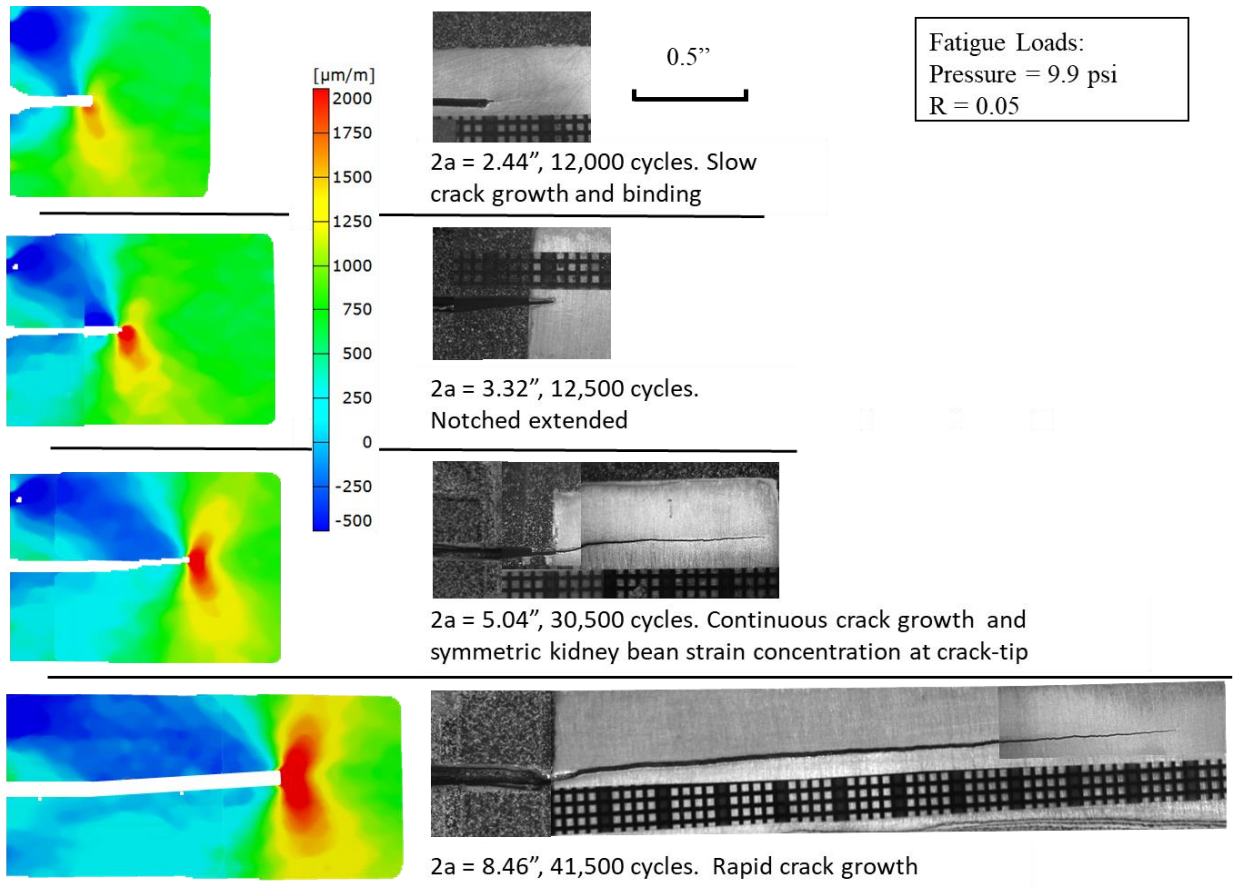

Figure 29. Phase 2 FCG results reveal high strains in the crack wake due to binding

DIC results shown in Figure 29 revealed dispersed and asymmetric crack-tip strains for the shorter cracks, which transitioned to the classical kidney bean strain field as the crack-tip extended from the central severed frame. Subsequent to the second notch inserted at 12,500 cycles, the fatigue crack growth was symmetric, stable, and continuous, as shown in Figure 28. After approximately 41,500 cycles, rapid, but stable, crack extension was observed.

A residual strength test was then conducted under pressure loading applied quasi-statically. Representative results are shown in Figure 30. Both the crack extension and fracture parameter, δ_5, were measured as a function of applied pressure (see Figure 30a). As shown, initial crack extension was measured at an applied pressure of 11 psi. Approximately 1.02 in. of stable tearing was observed from each crack tip prior to reaching the maximum applied pressure of 17 psi, as shown in Figure 30b. Unstable tearing then occurred, resulting in failure of the panel (see Figure 30c). Extensive damage occurred to the panel where the skin crack extended to a total length of 77 inches and severed two intact frames, as shown in Figure 30d. The pressure at failure exceeded the residual strength damage tolerance requirements in Title 14, Code of Federal Regulations 25.571.

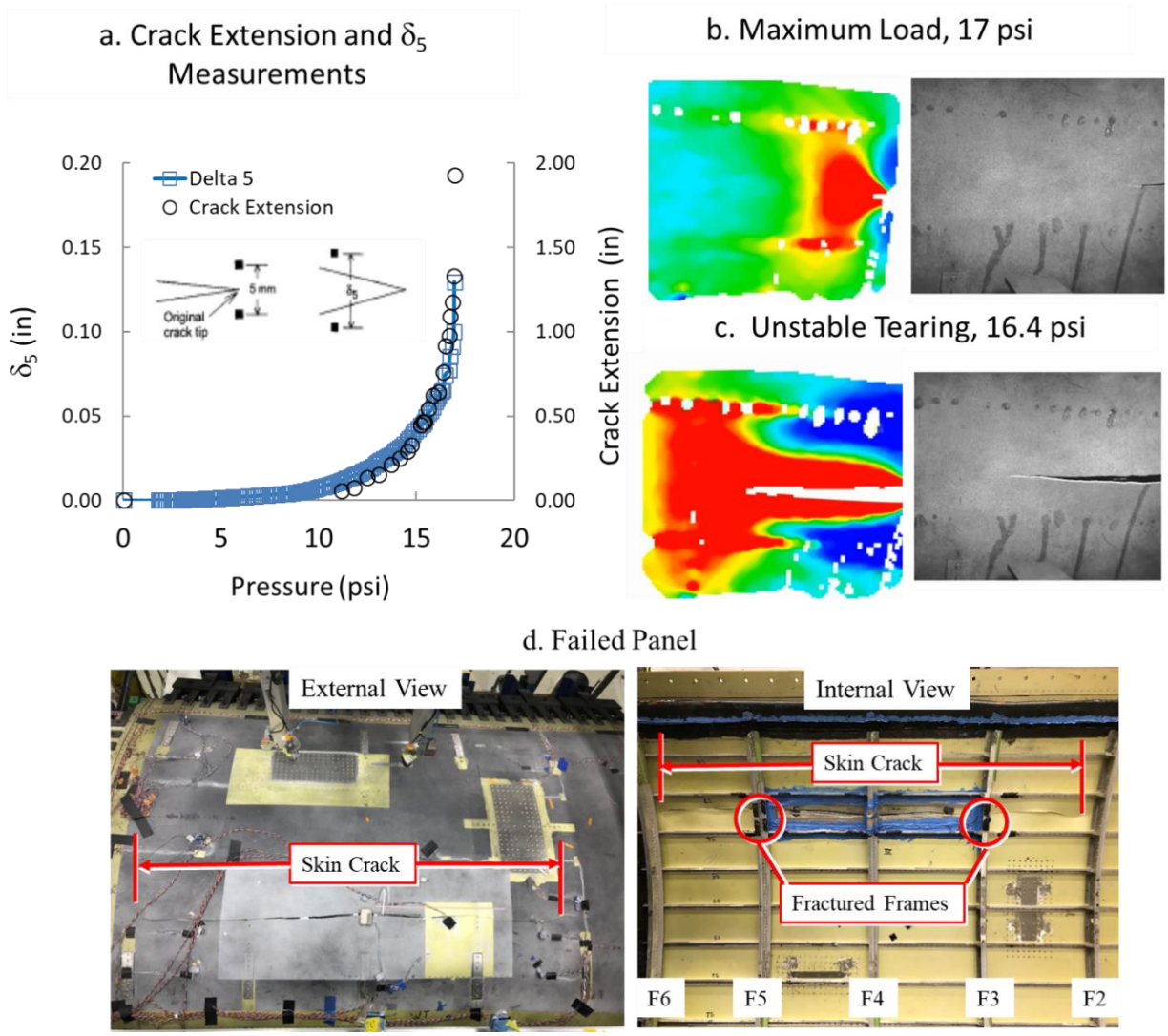

Figure 30. Measurements of crack extension, δ_5, progressive tearing, and final state of failure

5 Summary

In a collaborative effort, the FAA, Arconic, and Embraer are assessing emerging metallic structures technologies (EMST) for fuselage applications through full-scale test and analysis. Several technologies were considered, including advanced aluminum-lithium alloys, selective reinforcement using fiber metal laminates, and advanced joining processes, such as friction stir welding. Data from this study will be used to verify potential improved damage tolerance performance that EMST offer compared to the current fuselage structure constructed with conventional materials and fabrication processes. Recent efforts focused on the baseline panel, consisting of 2524-T3 skin and 7000-series aluminum substructure assembled through riveting.

The baseline panel was subjected to several phases of testing and accumulated more than 84,000 simulated flights during a 10-month period.

Results from the first baseline panel test will be compared to future tests on advanced panels containing varying EMST. Results and other major findings include:

- **Phase 1**: A two-bay circumferential crack-like notch having a total length of 1.3 in. was machined in the skin with the central stringer severed. The panel was then subjected to 33,600 fatigue cycles, during which slow and stable crack growth occurred to a final length of 11.3 in. Afterwards, a limit load test was conducted in which the panel was subjected to approximately 2.5 g axial load under a constant operational pressure level. Limited stable tearing extension was observed from each crack-tip.
- **Phase 2**: A crack-like notch along a mill-line having a total length 6 in. was machined in the skin mid-bay and parallel to a stringer. During subsequent fatigue test to 7,500 cycles, the crack extended approximately 2.0 in. from each notch-tip, displaying intermittent periods of slow-to-no growth due to crack binding.
- **Phase 3**: A two-bay longitudinal crack-like notch was machined in the skin having a total length of 1.5 in. with the central frame severed. After 43,600 cycles of fatigue testing, the skin crack extended approximately to a total length of 16 in. During the subsequent residual strength test, approximately 1 in. of stable tearing was observed from each crack tip prior to failure of the panel at 17 psi pressure. This pressure exceeded the residual strength damage tolerance requirements defined in Title 14, Code of Federal Regulations 25.571.

6 References

Bertoni, M., Fernandez, F., Miyazaki, M. (2014). Fuselage Technology Demonstrator. *Proceedings of AeroMat 2014*, June 16–19, 2014, Orlando, FL.

Beumler, T. (2014). Development of Thin-Walled FML-Structures. *Proceedings of AeroMat 2014*, June 16–19, 2014, Orlando, FL.

Chaves, C. (2017). A Review of Aeronautical Fatigue Investigations in Brazil. *Proceedings of the 35th ICAF Conference*, June 5–6, 2017, Nagoya, Japan.

Eberl, F., Smith, P., Laye1, J., Fernandez, F., Nunes, D., Cruz, M., Miyazaki, M., Aleixo, G., Sanchez, R., and Garcia, J. (2015). Manufacturing of a Novel Upper Wing Cover

Demonstrator Using Friction Stir Welding. *Proceedings of AeroMat 2015*, May 11–14, 2015, Long Beach, CA.

Heinimann, M., Kulak, M., Bucci, R., James, M., Wilson, G., Brockenbrough, J., Zonker, H., and Sklyut, H. (2007). Validations of Advanced Metallic Hybrid Concepts with Improved Damage Tolerance Capabilities for Next Generation Lower Wing and Fuselage Applications. *Proceedings of the 24th ICAF Symposium*, May 16–18, 2007, Naples, Italy.

Kok, L., Poston, K., Moore, G. (2011). Bombardier Aerospace FSW Demonstrator. *Proceedings of the 26th ICAF Symposium*, June 1–3, 2011, Montreal, Canada.

Kulak, M. and Chang, P., Sklyut, H. and Heinimann, M. (2019/2020?). *Design, Analysis and Test Development of Full-Scale Fuselage Test Panels to Assess Emerging Metallic Structures Technologies. DOT/FAA/TC-TNxx/x.*

Lowak, H., de Jonge, J., Franz, T., and Schutz, D. (1979). *MINITWIST—A shortened version of TWIST.* NLR *Report No. TB-146.*

Prasad, N., Gokhale, A., Wanhill, R. (Eds.) (2014). *Aluminum-Lithium Alloys, Processing, Properties and Applications.* Elsevier.

Schmidt, H. (2005). Damage Tolerance Technology For Current and Future Aircraft Structure. *Proceedings of the 23rd ICAF Symposium*, June 8–10, 2005, Hamburg, Germany.

Silva, D., Cruz, M., Mendonca, W., Brandao, F., Sakata, A., Silva, G., and Kulak, M. (2017). Manufacturing of a Fiber Metal Laminate Lower Wing Cover Demonstrator. *Proceedings of AeroMat 2017*, April 10–12, 2017, Charleston, SC.

Steadman, D. (2007). Destructive Evaluation and Extended Fatigue Testing of Retired Transport Aircraft, Volume 5: Data Analysis Report. DOT/FAA/AR-07/22, V5.

Stonaker, K., Bakuckas, Won, I., and Freisthler, M. (2015). Material Characterization of Aluminum Lithium Alloys Used in Aerospace Applications. *Proceedings of the 28th ICAF Symposium*, June 3–5, 2015, Helsinki, Finland.

Stonaker, K., Bakuckas, J., Stanley, D., Kulak, M., Chang, P., and Freisthler, M. (2019). Assessment of Fatigue Behavior of Advanced Aluminum Alloys Under Complex Variable Amplitude Loading. *Proceedings of the 30th ICAF Symposium*, June 5–7, 2019, Krakow, Poland.

Tian, Y., and Bakuckas, J. (2019). Full-Scale Aircraft Structural Test Evaluation and Research (FASTER) Fixture—Capabilities Description and User Manual. DOT/FAA/TC-TN19/6.

A Panel 1 geometry

The skin, frame, and stringer geometry described in this Appendix were selected from a crown location 28 ft forward of the wing centerline. At this location, the panel geometry was equally critical for crack growth circumferentially and longitudinally, and the same geometry would be relevant for axial and longitudinal loading.

The materials in the baseline Panel 1 are described in Table 2. The geometry was determined using the sizing methods using the materials in Table 2.

The overall panel design is shown in Figure 31. To accommodate the FASTER setup, a panel radius of 74 in. was chosen. It should be noted that the actual single-aisle radius is about 78 in. The small effect of the lower radius on geometry and stresses is discussed in Kulak (2019). The panel length is approximately 125 in. and the length of the panel arc is 76.5 in. with a vertical projection of 73.2 in.

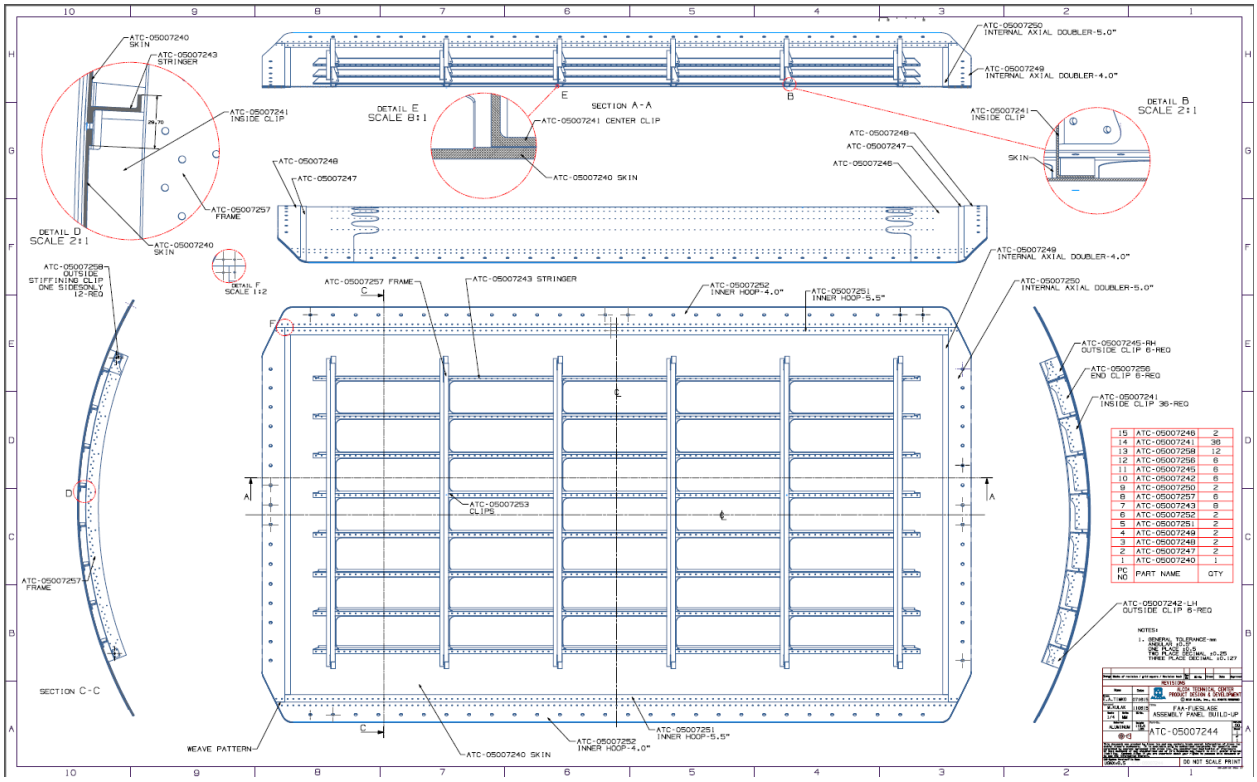

Figure 31. Panel 1 overall dimensions

The Panel 1 test panel represents a single-aisle construction using current technology. The engineering drawings for Panel 1 construction are included below.

Fuselage Skin Sheets

The fuselage skin for the baseline Panel 1 utilized 2524-T3 sheet, which has superior crack-growth and toughness properties compared to 2024-T3. The skin was supplied in a gage of 0.09 in. and was clad on both sides. The final skin thickness in the stringer and frame attachment landings was 0.063 in., and the skin was pocketed to 0.055 in. (see Figure 32). The rivets on the airflow side of the fuselage panels for the skins, stiffeners, and frames were the 100-degree countersunk fastener NAS1097AD-5, which has a 5/32-in. diameter (AD = 2117-T4 rivet). For the shear-tie-to-frame, shear-tie-to-stringer, and the stringer clips in Concept #2, the universal head rivet MS20470AD-5 (5/32-in. diameter, 2117-T4) was used.

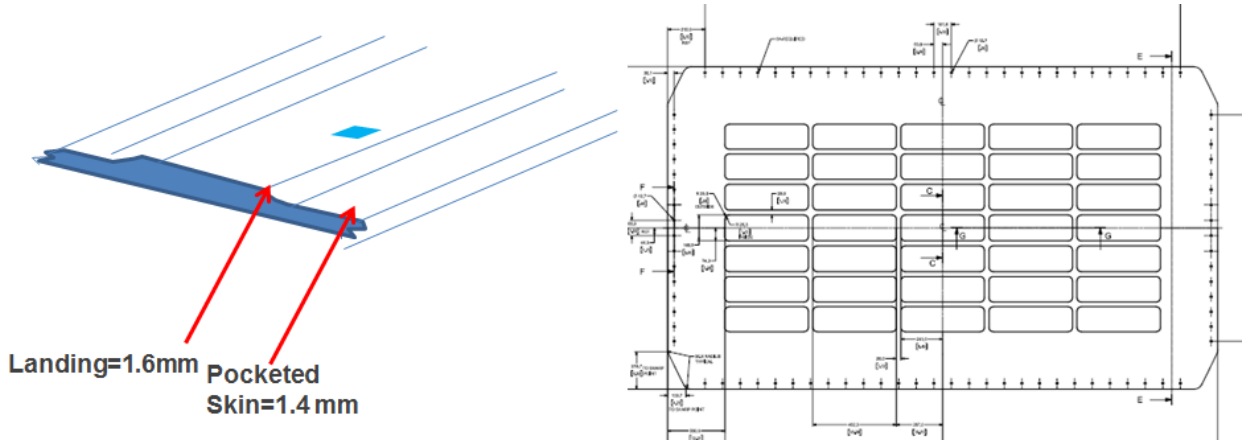

Figure 32. Pocketed skin

Panel 1 Load Introduction Doublers and Bonding to Skins

For panel doublers, a higher-strength 7xxx sheet, like 7075, was used (non-clad). The edge doublers package on both the inside and outside of the fuselage panel were roll formed to curvature. The doubler package was prepared for bonding to the skins.

The doublers were bonded to the skin, either using an oven-cured epoxy like FM73 or a cold bonding adhesive. In addition, countersunk Huck bolt or Lock bolt fasteners were used to secure all edge doublers.

After chemical milling, the panel underwent the appropriate surface treatment procedure—in stringer frame landings and pocketed regions—to protect the panel against corrosion and allow for sealant to be used under the frame and stringer areas, which are riveted to the skin. After chemical milling, the pocketed regions were anodized and primed.

Shear Tie

The frame system for Panel 1 utilized a two-piece construction, where the Z-shaped extruded frame is attached to the skin via a shear tie (see Figure 34). The shear tie is fastened to the skin and the Z-shaped 7150-T7511 stress-relieved stiffener. The shear tie used 7075 sheet supplied in a low-strength O or F temper appropriate to hydroforming operation. LMI designed the hydroforming tools and created the three types of shear tie geometries (two are the partial shear ties at both ends of the frame). The shear tie was aged to the final temper of 7075-T62. The shear ties were anodized and primed before being attached to the frames. A sealant was used between the shear tie and frame connection.

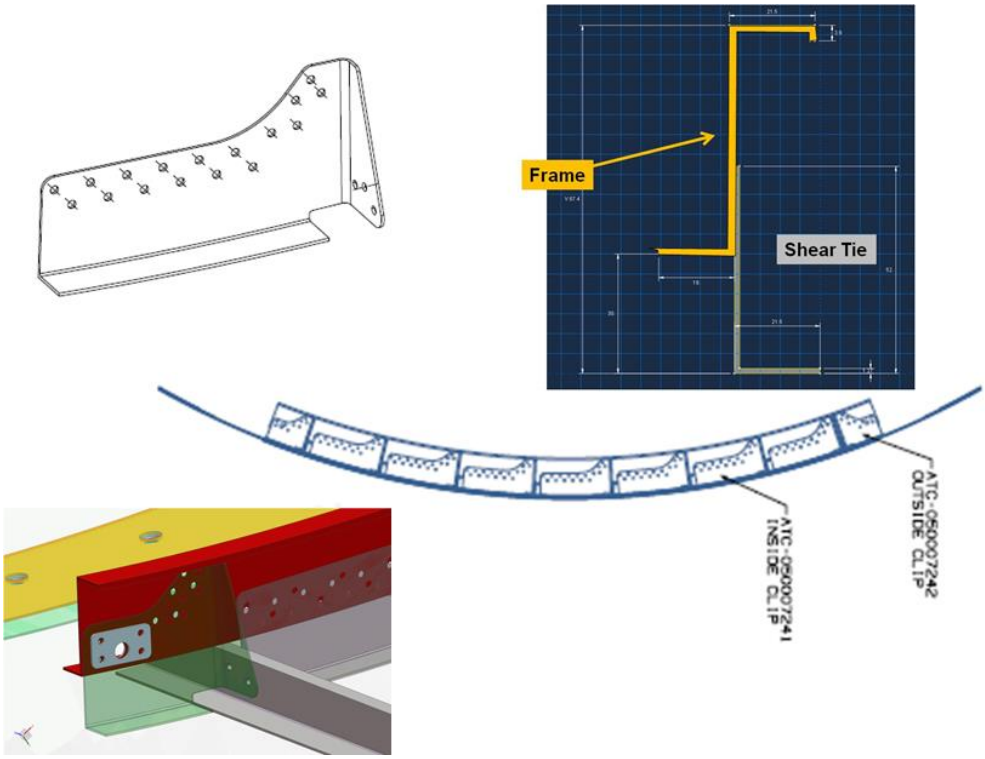

Figure 33. Shear tie

Frame

The frame was riveted to the shear tie using the previously identified fasteners. The frame was made of a high-strength 7075 extrusion alloy and was supplied in a temper appropriate to the stretch-forming operation (O or F temper). The frame was stretch formed to a constant radius reflecting the offset from the skin radius. After stretch forming, the frame was aged to the final temper of 7075-T62. The frame was anodized and primed before being attached to the shear ties.

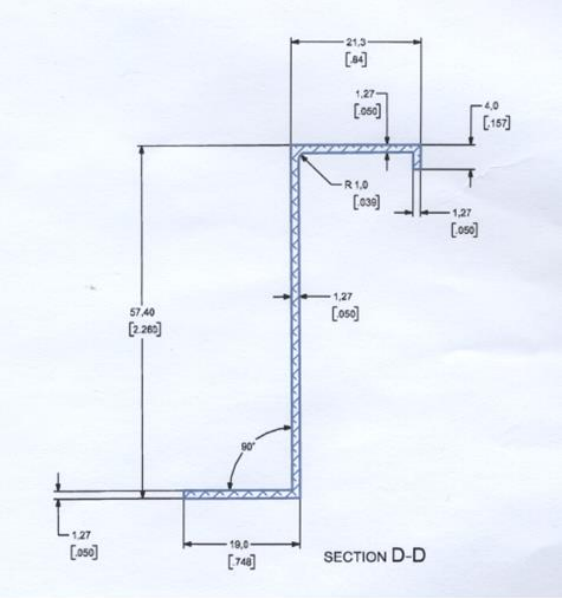

Extruded Frame which is Connected to Skin with a Sheet Metal Shear Tie

Figure 34. Frame

Stringer

The stringers were made of 7150-T7511 stress-relieved extrusions and provided in final temper. The Z cross-section was extruded with attach flanges of a radius to match the 74-inch-radius curve of the panel. The stringers were anodized and primed before being attached to the skins.

Loading and doublers

The test panel was loaded through the skin by actuators axially and in the hoop direction. The frames were also loaded in the hoop direction at each frame end by individual actuators. The test panel was loaded internally by pressure. There was an additional small source of loading in the FASTER setup from the radial links at the frame ends, which restrain the panel from moving in the radial direction and thus react some of the pressure load. Note that in the FASTER test fixture, the panel pressure, axial/hoop/frame actuator loads, and radial link loads are in static equilibrium. The only displacement restraint on the panel is due to the radial links at each edge of the frame.

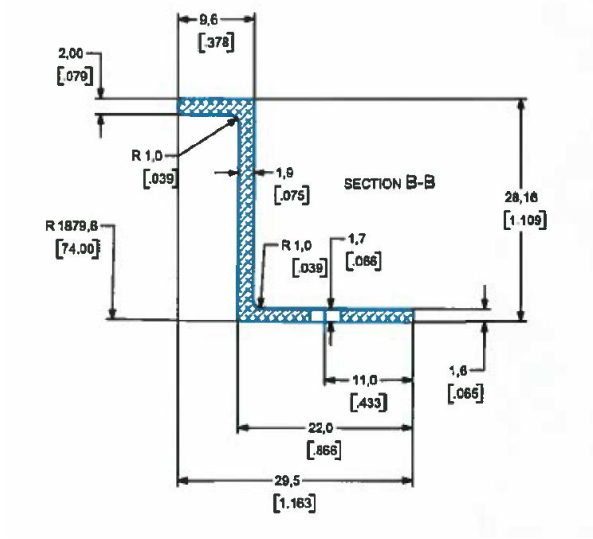

Figure 35. Stringer

The test panel utilized heavy skin doublers (see Figure 36 to Figure 37) around the panel edges to introduce the large point loads to be applied to the skin in both the axial and hoop directions. These doublers were bonded and riveted. The doublers stiffened the panel and created a separate picture-frame-type load which affected the load paths through the panel. Thus, the actuator loads along the panel edges were not the same loads in magnitude or distribution that would be applied along the edge of an idealized, cylindrical, stiffened fuselage symmetry model.

Doubler plates (5 mm; 7150 plate) were used at the frame end load introduction points, as shown in Figure 38.

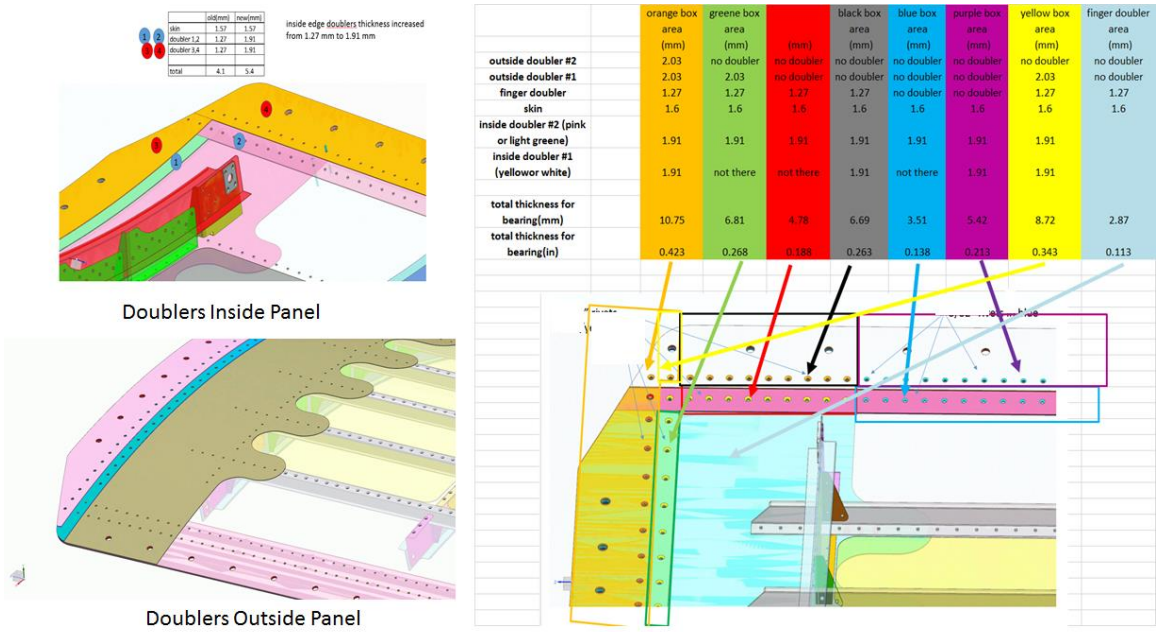

	orange box area (mm)	greene box area (mm)	(mm)	black box area (mm)	blue box area (mm)	purple box area (mm)	yellow box area (mm)	finger doubler area (mm)
outside doubler #2	2.03	no doubler	no doubler	no doubler	no doubler	no doubler	no doubler	no doubler
outside doubler #1	2.03	2.03	no doubler	no doubler	no doubler	no doubler	2.03	no doubler
finger doubler	1.27	1.27	1.27	1.27	no doubler	no doubler	1.27	1.27
skin	1.6	1.6	1.6	1.6	1.6	1.6	1.6	1.6
inside doubler #2 (pink or light greene)	1.91	1.91	1.91	1.91	1.91	1.91	1.91	
inside doubler #1 (yellowor white)	1.91	not there	not there	1.91	not there	1.91	1.91	
total thickness for bearing(mm)	10.75	6.81	4.78	6.69	3.51	5.42	8.72	2.87
total thickness for bearing(in)	0.423	0.268	0.188	0.263	0.138	0.213	0.343	0.113

Figure 36. Description doublers at panel edges

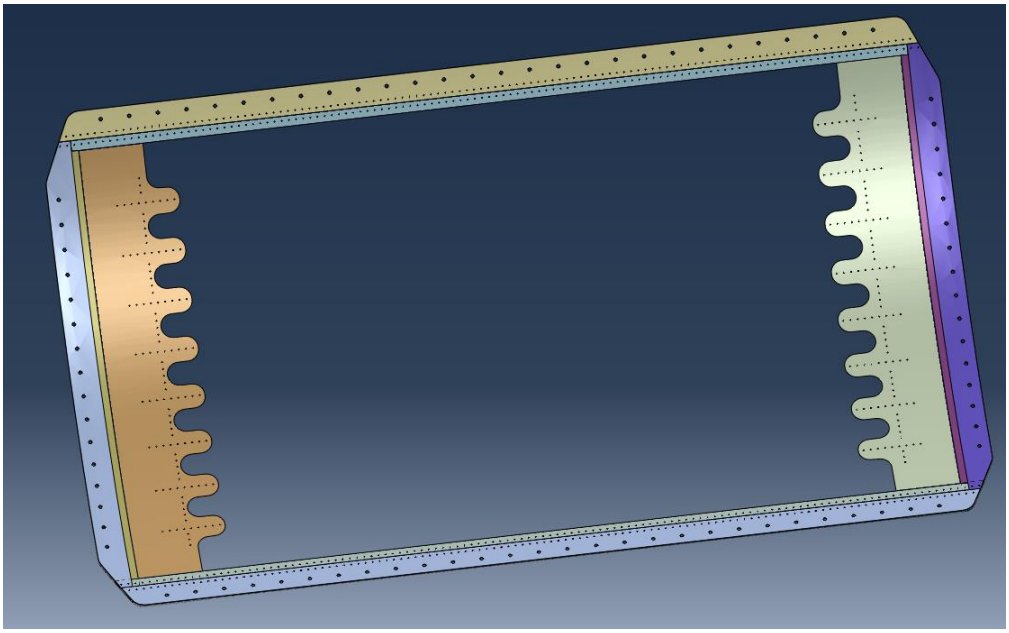

Figure 37. A view of all hoop and axial doublers

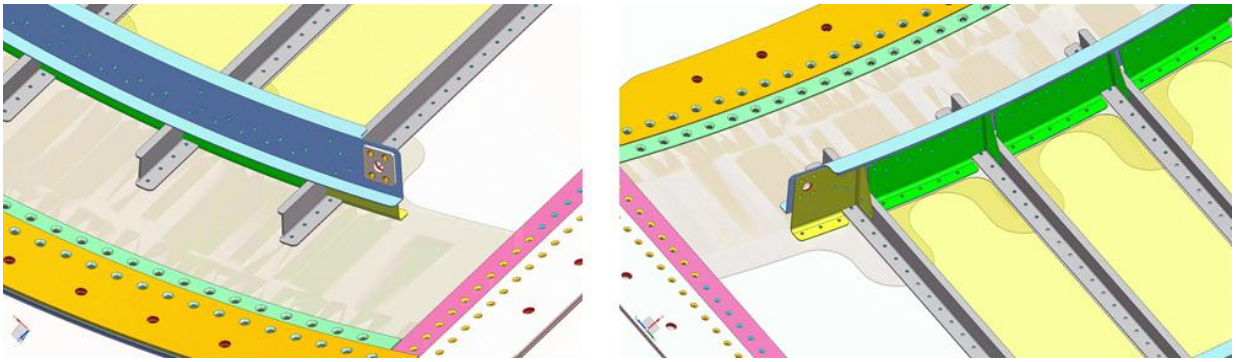

Figure 38. A view of the frame end load introduction doubler

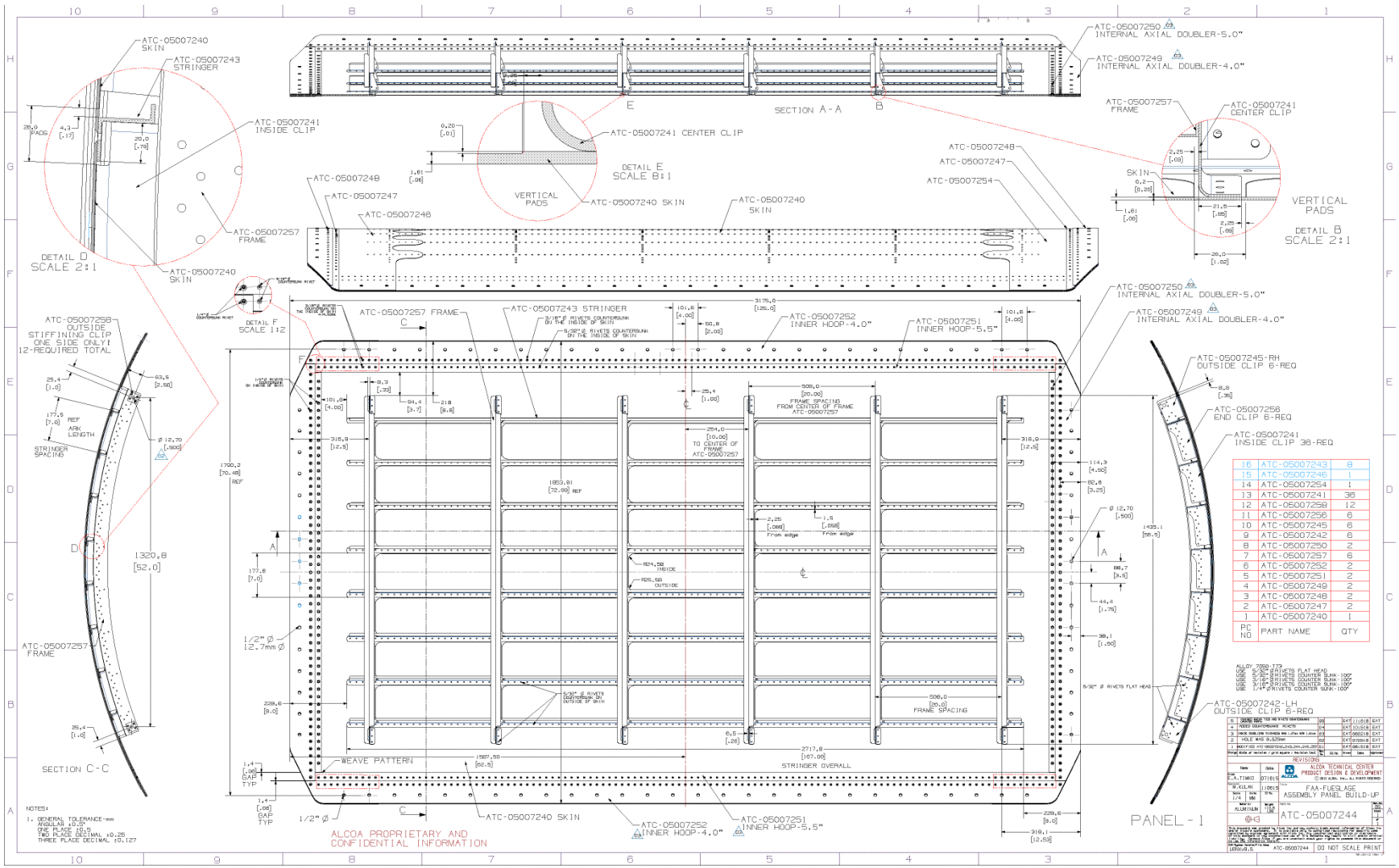

PC NO	PART NAME	QTY
16	ATC-05007243	8
15	ATC-05007246	1
14	ATC-05007254	1
13	ATC-05007241	36
12	ATC-05007258	12
11	ATC-05007256	6
10	ATC-05007245	6
9	ATC-05007242	6
8	ATC-05007250	2
7	ATC-05007257	6
6	ATC-05007252	2
5	ATC-05007251	2
4	ATC-05007249	2
3	ATC-05007248	2
2	ATC-05007247	2
1	ATC-05007240	1

ALLOY 7050-T73
USE 5/32" Ø RIVETS FLAT HEAD
USE 5/32" Ø RIVETS COUNTER SUNK -100°
USE 3/16" Ø RIVETS COUNTER SUNK -100°
USE 3/16" Ø RIVETS COUNTER SUNK -100°
USE 1/4" ØRIVETS COUNTER SUNK -100°

NOTES:
1. GENERAL TOLERANCE-mm
ANGULAR ±0.5°
ONE PLACE ±0.5
TWO PLACE DECIMAL ±0.25
THREE PLACE DECIMAL ±0.127

REVISIONS

ALCOA TECHNICAL CENTER
PRODUCT DESIGN & DEVELOPMENT

FAA-FUSELAGE
ASSEMBLY PANEL BUILD-UP

ATC-05007244

DO NOT SCALE PRINT

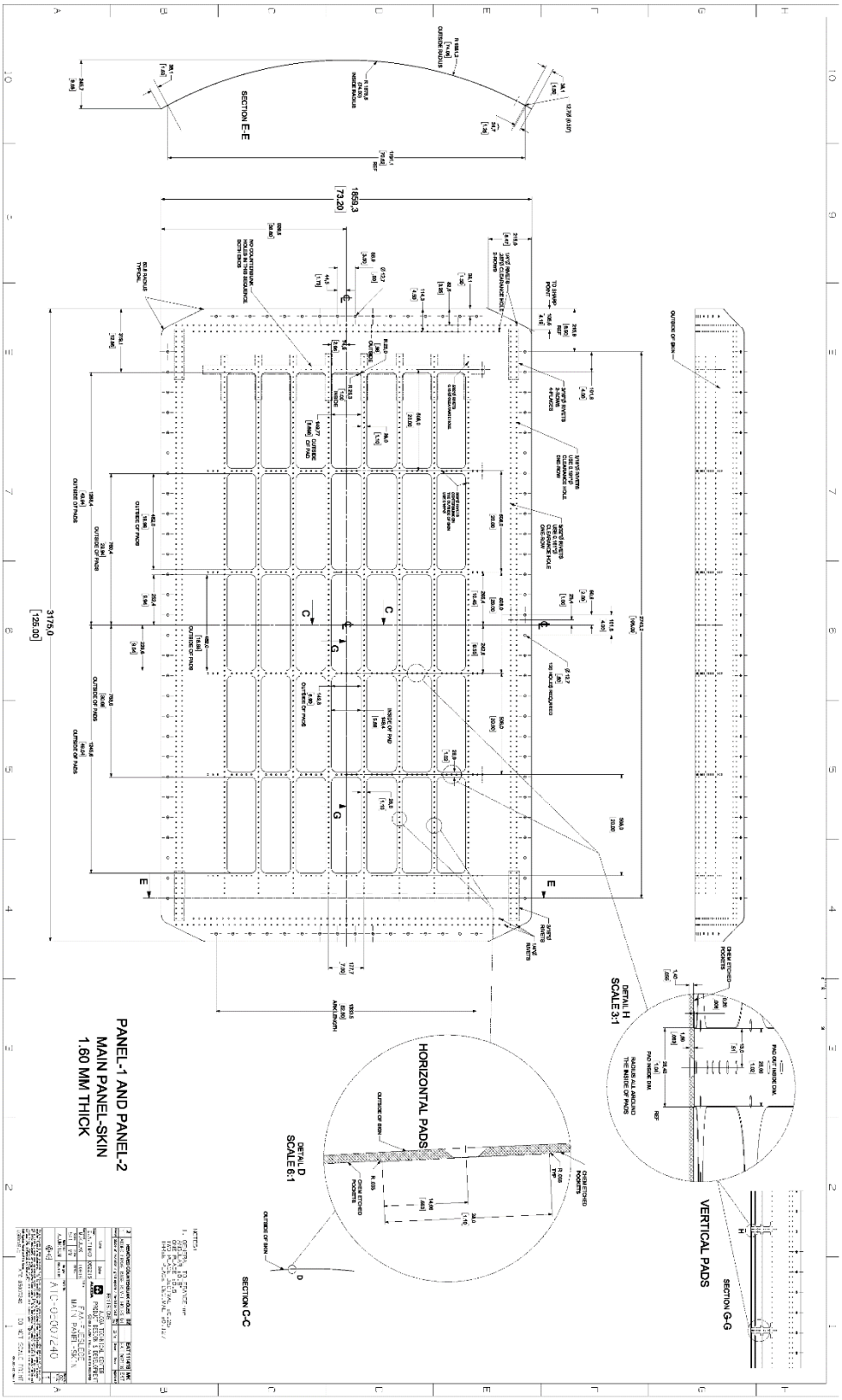
PANEL-1 AND PANEL-2
MAIN PANEL-SKIN
1.60 MM THICK
SECTION E-E
SECTION C-C
SECTION G-G
DETAIL D
SCALE 6:1
DETAIL H
SCALE 3:1
HORIZONTAL PADS
VERTICAL PADS
3175.0
[125.00]
1859.3
[73.20]

+-

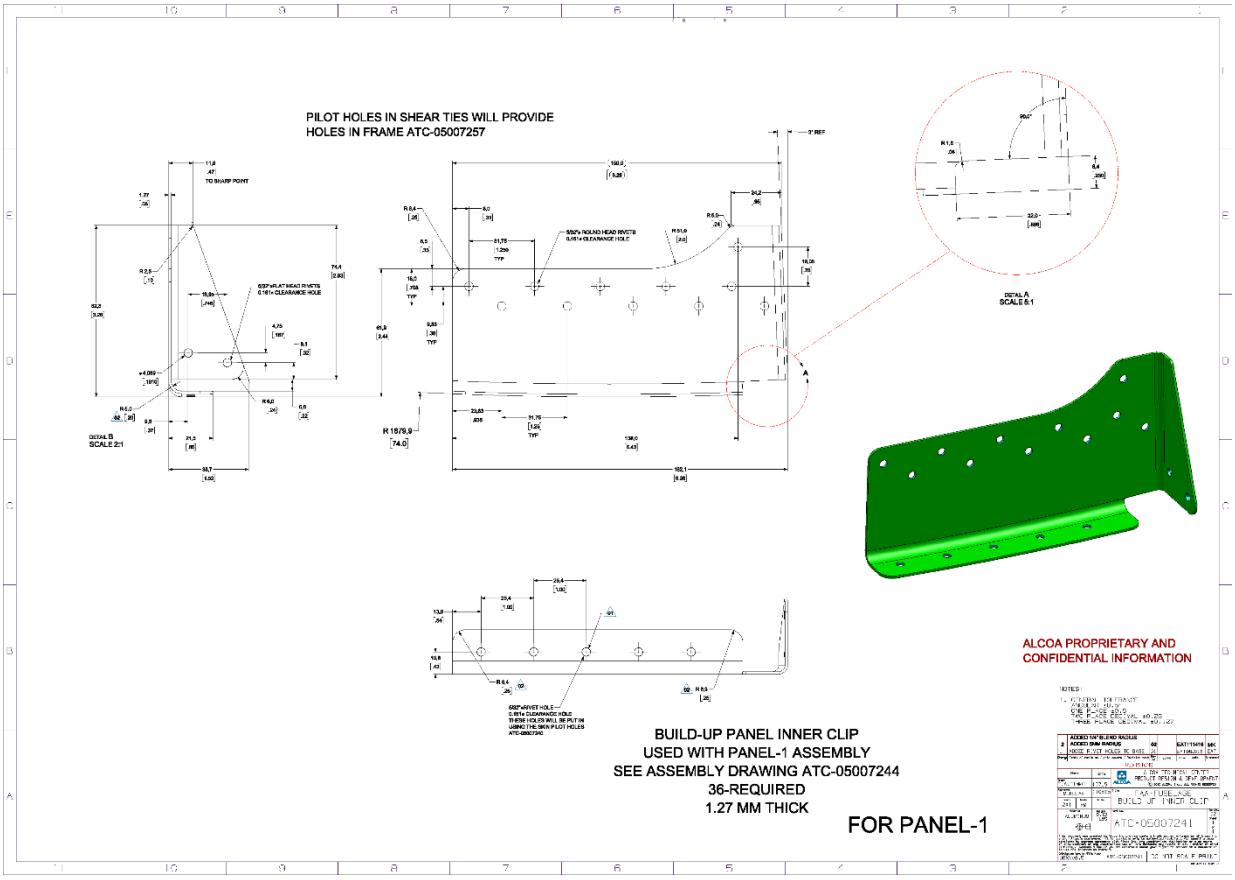
PILOT HOLES IN SHEAR TIES WILL PROVIDE
HOLES IN FRAME ATC-05007257
DETAIL A
SCALE 5:1
DETAIL B
SCALE 2:1
R 15/9.9
74.0
ALCOA PROPRIETARY AND
CONFIDENTIAL INFORMATION
BUILD-UP PANEL INNER CLIP
USED WITH PANEL-1 ASSEMBLY
SEE ASSEMBLY DRAWING ATC-05007244
36-REQUIRED
1.27 MM THICK
FOR PANEL-1
ATC-05007241

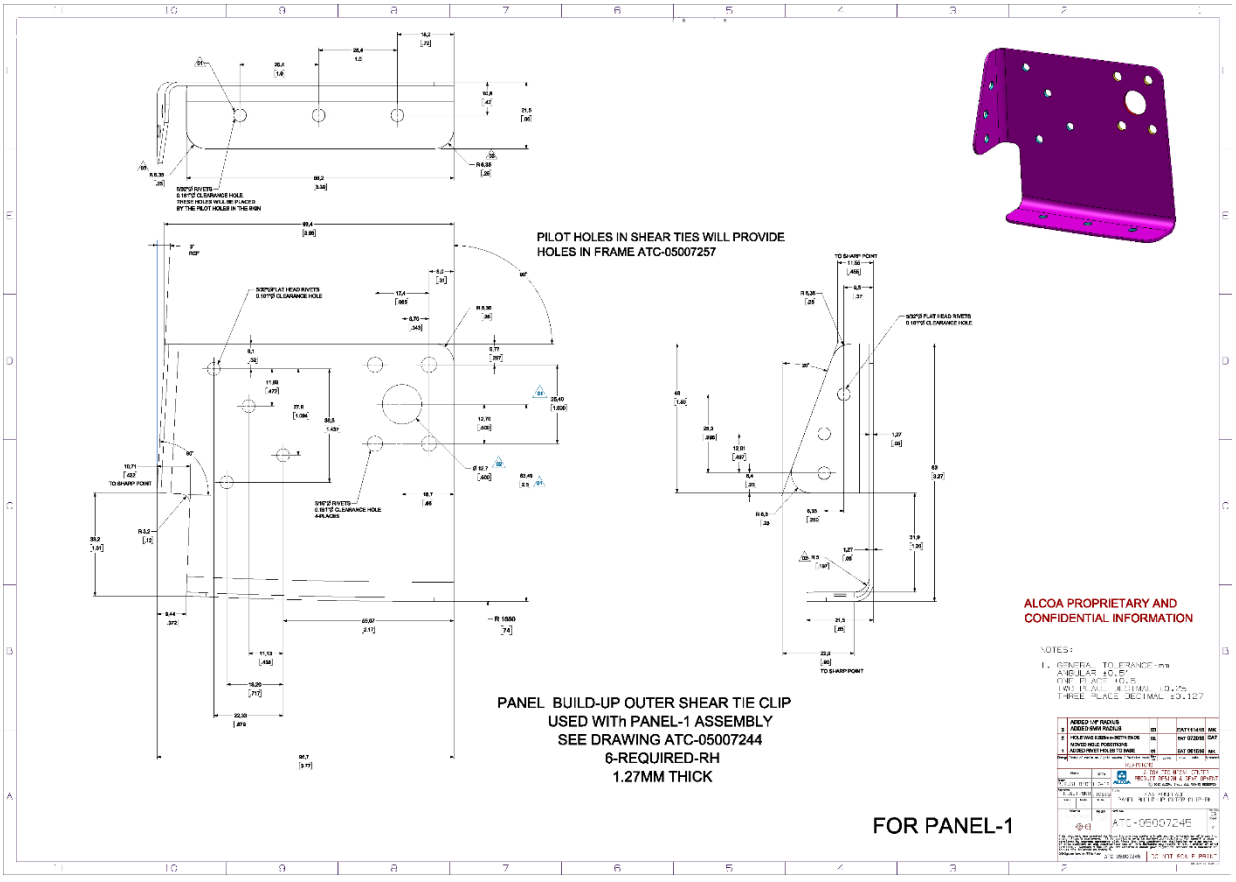
PILOT HOLES IN SHEAR TIES WILL PROVIDE
HOLES IN FRAME ATC-05007257
PANEL BUILD-UP OUTER SHEAR TIE CLIP
USED WITh PANEL-1 ASSEMBLY
SEE DRAWING ATC-05007244
6-REQUIRED-RH
1.27MM THICK
FOR PANEL-1
ALCOA PROPRIETARY AND
CONFIDENTIAL INFORMATION
ATC-05007245

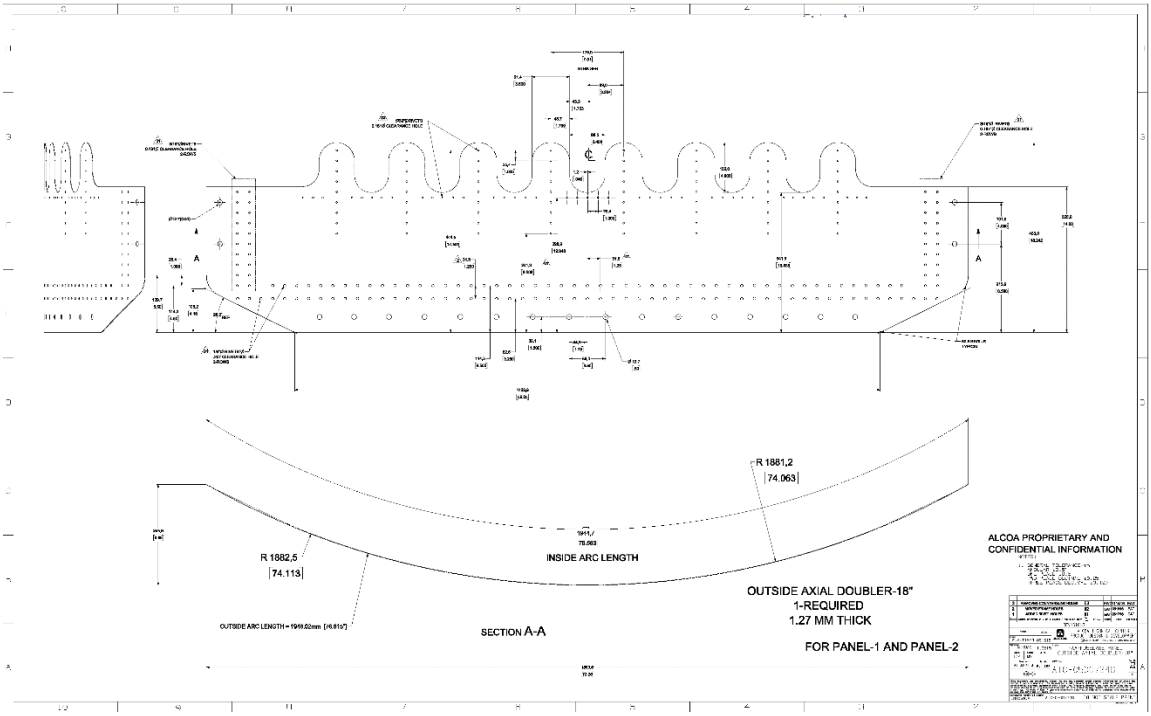
R 1881,2
74.063
INSIDE ARC LENGTH
R 1882,5
74.113
OUTSIDE ARC LENGTH = 1949.82mm [76.8117]
SECTION A-A
OUTSIDE AXIAL DOUBLER-18"
1-REQUIRED
1.27 MM THICK
FOR PANEL-1 AND PANEL-2
ALCOA PROPRIETARY AND
CONFIDENTIAL INFORMATION

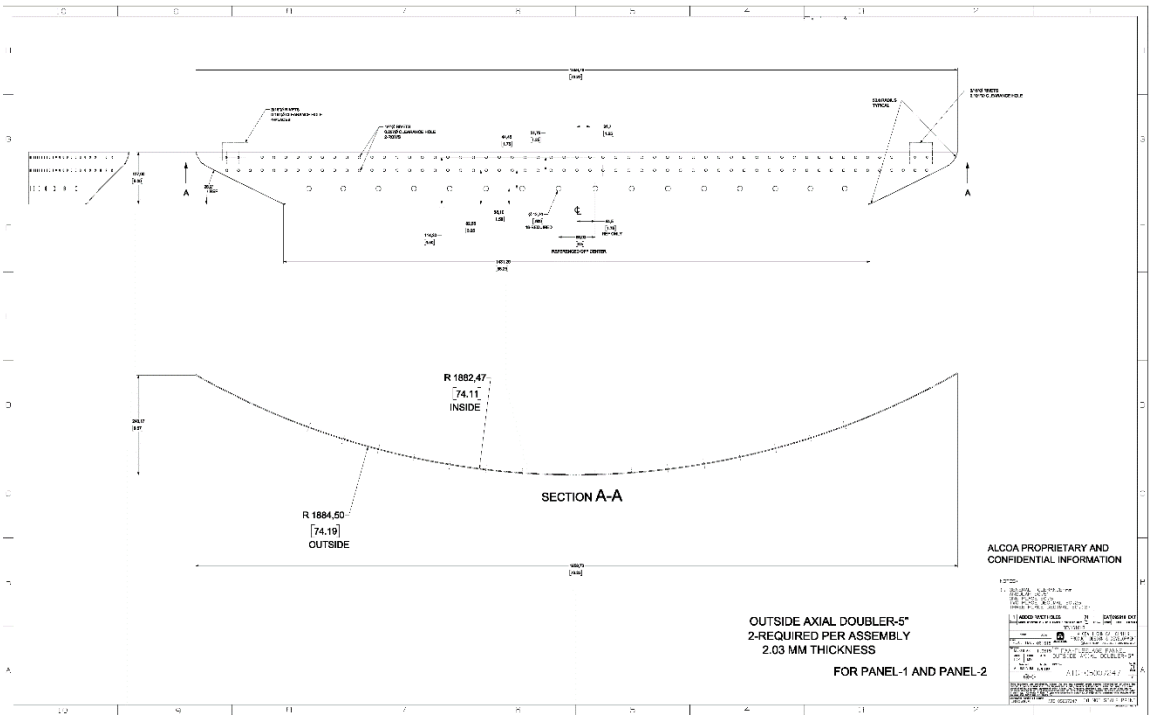
R 1882,47
74,11
INSIDE
SECTION A-A
R 1884,50
74.19
OUTSIDE
ALCOA PROPRIETARY AND
CONFIDENTIAL INFORMATION
OUTSIDE AXIAL DOUBLER-5"
2-REQUIRED PER ASSEMBLY
2.03 MM THICKNESS
FOR PANEL-1 AND PANEL-2

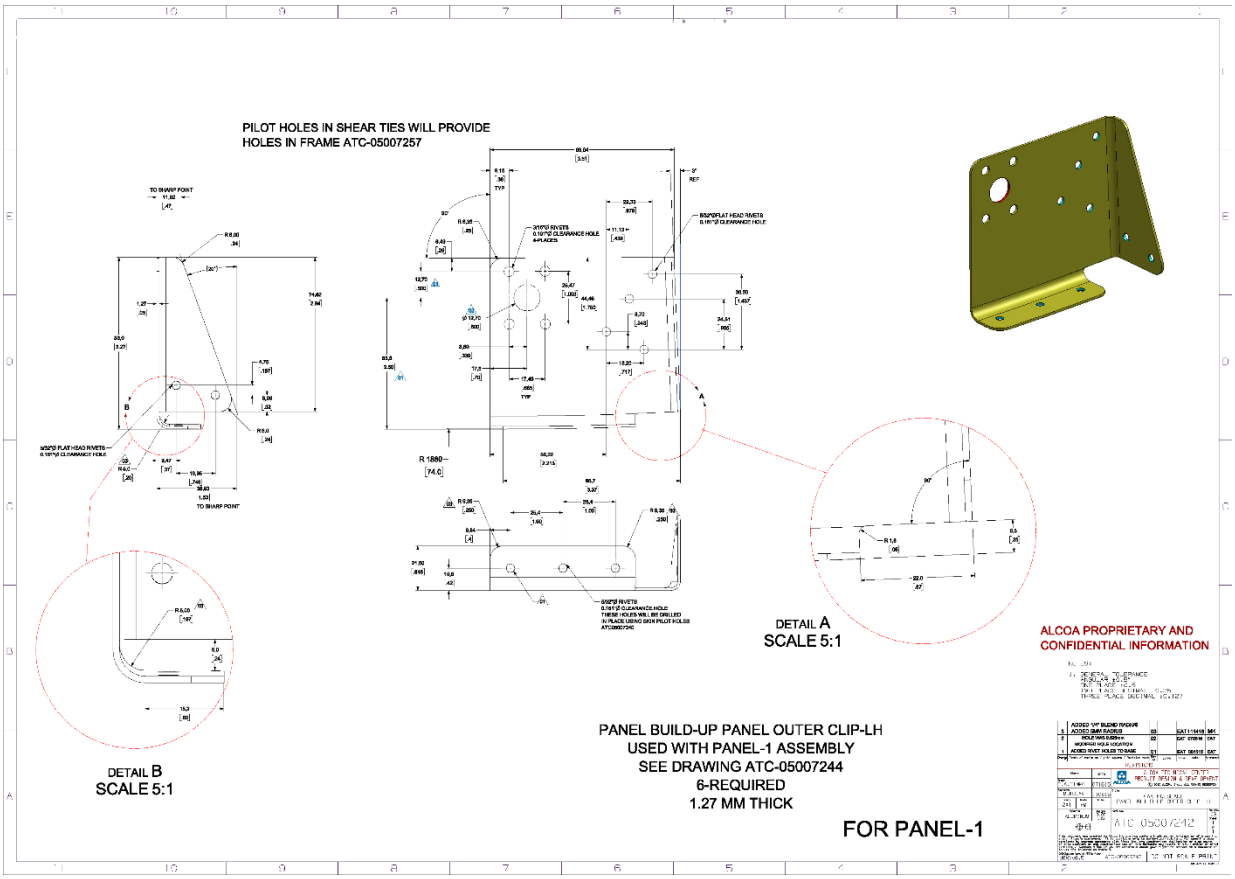
PILOT HOLES IN SHEAR TIES WILL PROVIDE
HOLES IN FRAME ATC-05007257
R 1880
74.0
DETAIL A
SCALE 5:1
DETAIL B
SCALE 5:1
ALCOA PROPRIETARY AND
CONFIDENTIAL INFORMATION
PANEL BUILD-UP PANEL OUTER CLIP-LH
USED WITH PANEL-1 ASSEMBLY
SEE DRAWING ATC-05007244
6-REQUIRED
1.27 MM THICK
FOR PANEL-1

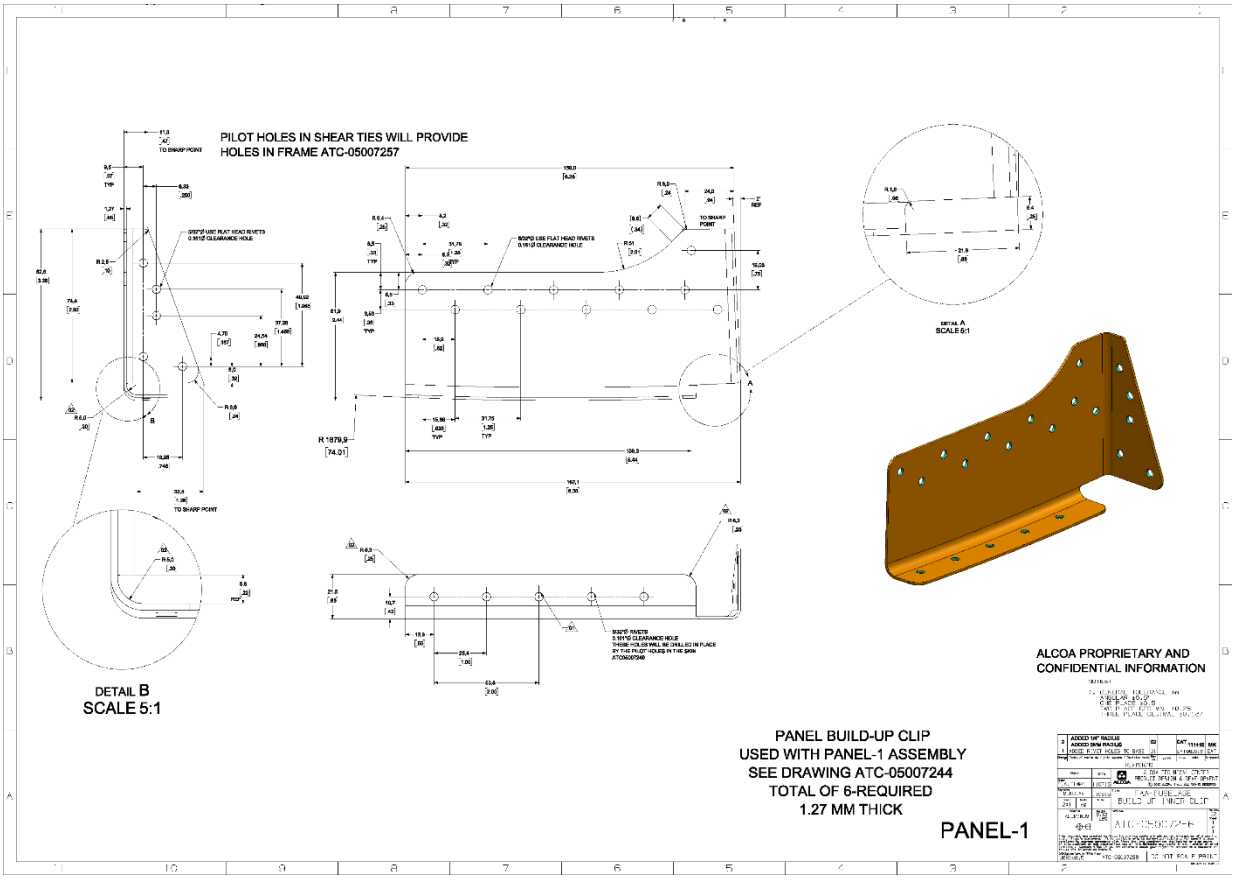
PILOT HOLES IN SHEAR TIES WILL PROVIDE
HOLES IN FRAME ATC-05007257
DETAIL B
SCALE 5:1
DETAIL A
SCALE 5:1
ALCOA PROPRIETARY AND
CONFIDENTIAL INFORMATION
PANEL BUILD-UP CLIP
USED WITH PANEL-1 ASSEMBLY
SEE DRAWING ATC-05007244
TOTAL OF 6-REQUIRED
1.27 MM THICK
PANEL-1

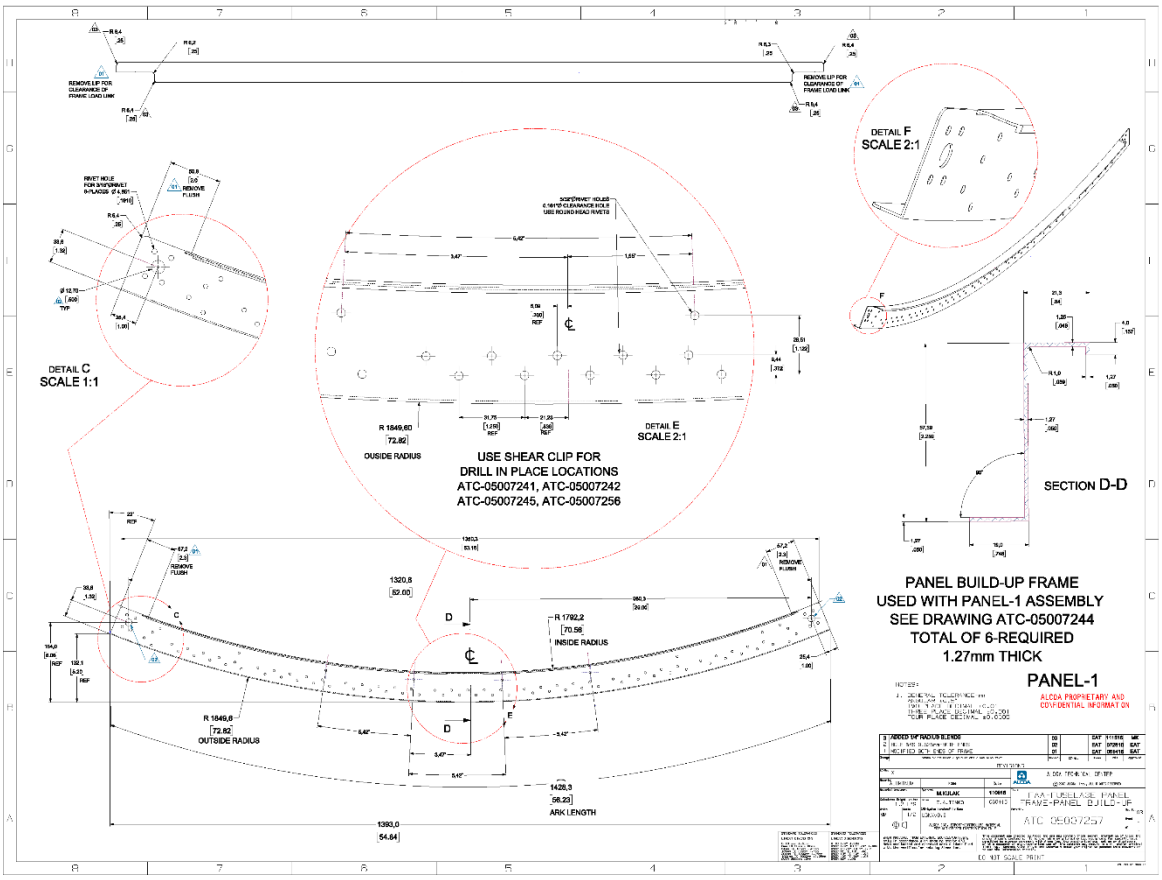
DETAIL C
SCALE 1:1
DETAIL E
SCALE 2:1
DETAIL F
SCALE 2:1
USE SHEAR CLIP FOR
DRILL IN PLACE LOCATIONS
ATC-05007241, ATC-05007242
ATC-05007245, ATC-05007256
SECTION D-D
PANEL BUILD-UP FRAME
USED WITH PANEL-1 ASSEMBLY
SEE DRAWING ATC-05007244
TOTAL OF 6-REQUIRED
1.27mm THICK
PANEL-1
ALCOA PROPRIETARY AND
CONFIDENTIAL INFORMATION
R 1849,60
72.82
OUTSIDE RADIUS
R 1792,2
70.56
INSIDE RADIUS
1428,3
56.23
ARK LENGTH
1393,0
54.84

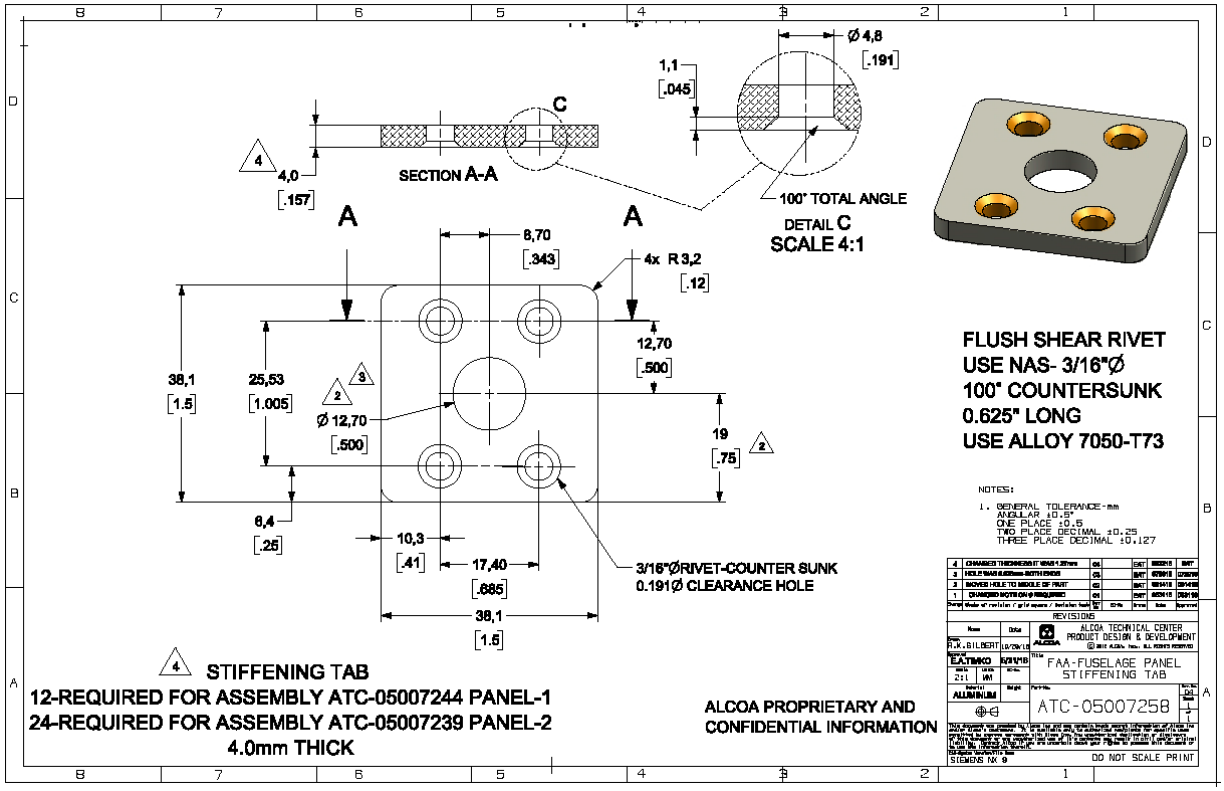
SECTION A-A
DETAIL C
SCALE 4:1
100° TOTAL ANGLE
4,0
.157
Ø 4,8
.191
1,1
.045
8,70
.343
4x R 3,2
.12
12,70
.500
38,1
1.5
25,53
1.005
Ø 12,70
.500
19
.75
6,4
.25
10,3
.41
17,40
.685
38,1
1.5
3/16"ØRIVET-COUNTER SUNK
0.191Ø CLEARANCE HOLE
FLUSH SHEAR RIVET
USE NAS- 3/16"Ø
100° COUNTERSUNK
0.625" LONG
USE ALLOY 7050-T73
NOTES:
1. GENERAL TOLERANCE-mm
ANGULAR ±0.5°
ONE PLACE ±0.5
TWO PLACE DECIMAL ±0.25
THREE PLACE DECIMAL ±0.127
4 STIFFENING TAB
12-REQUIRED FOR ASSEMBLY ATC-05007244 PANEL-1
24-REQUIRED FOR ASSEMBLY ATC-05007239 PANEL-2
4.0mm THICK
ALCOA PROPRIETARY AND
CONFIDENTIAL INFORMATION
ALCOA TECHNICAL CENTER
PRODUCT DESIGN & DEVELOPMENT
FAA-FUSELAGE PANEL
STIFFENING TAB
ATC-05007258
DO NOT SCALE PRINT

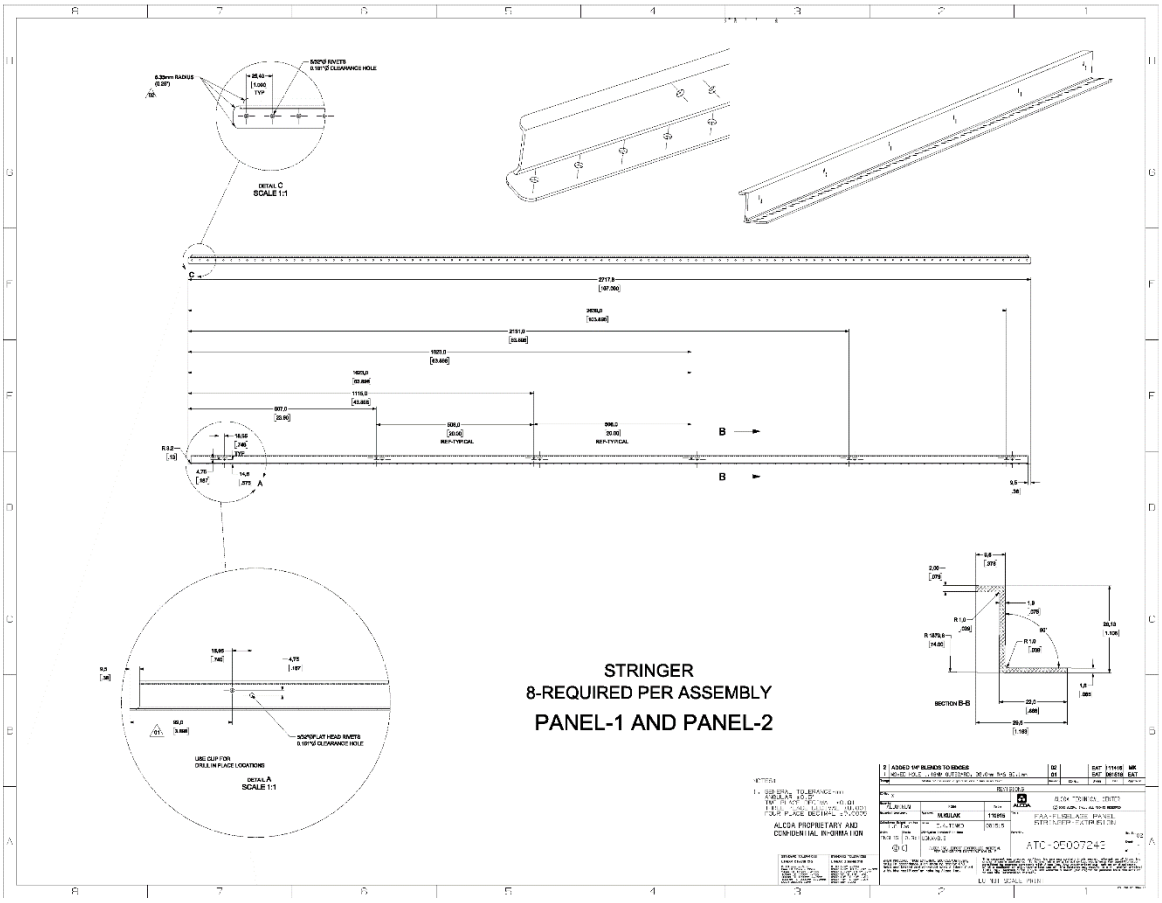
DETAIL C
SCALE 1:1
SECTION B-B
DETAIL A
SCALE 1:1
USE CUP FOR
DRILL IN PLACE LOCATIONS
STRINGER
8-REQUIRED PER ASSEMBLY
PANEL-1 AND PANEL-2
ALCOA PROPRIETARY AND
CONFIDENTIAL INFORMATION
ATC-0E007242

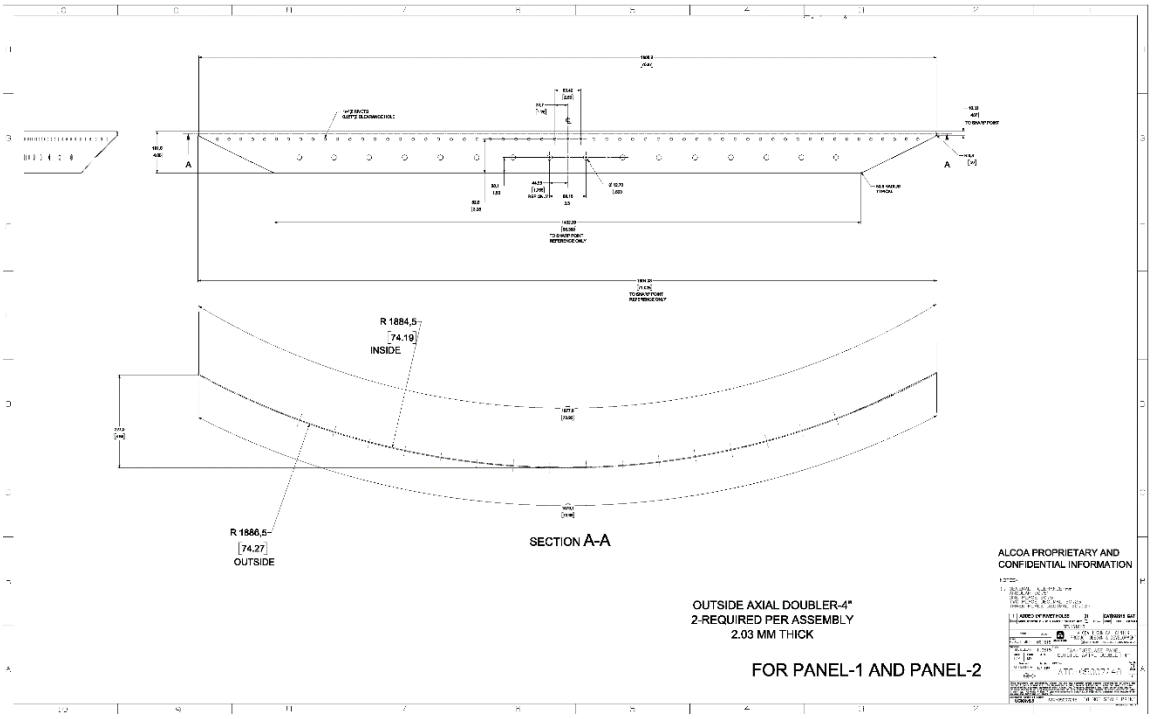
R 1884,5
74.19
INSIDE
R 1886,5
74.27
OUTSIDE
SECTION A-A
OUTSIDE AXIAL DOUBLER-4"
2-REQUIRED PER ASSEMBLY
2.03 MM THICK
FOR PANEL-1 AND PANEL-2
ALCOA PROPRIETARY AND
CONFIDENTIAL INFORMATION

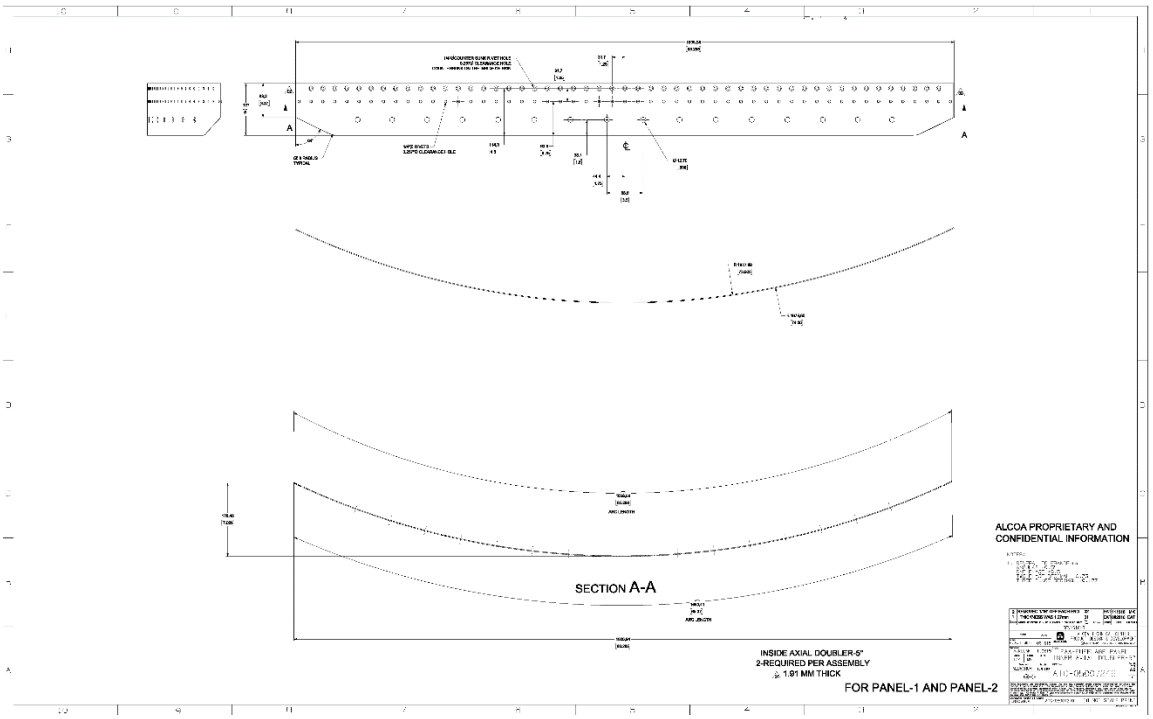
SECTION A-A
ALCOA PROPRIETARY AND
CONFIDENTIAL INFORMATION
INSIDE AXIAL DOUBLER-5"
2-REQUIRED PER ASSEMBLY
@ 1.91 MM THICK
FOR PANEL-1 AND PANEL-2

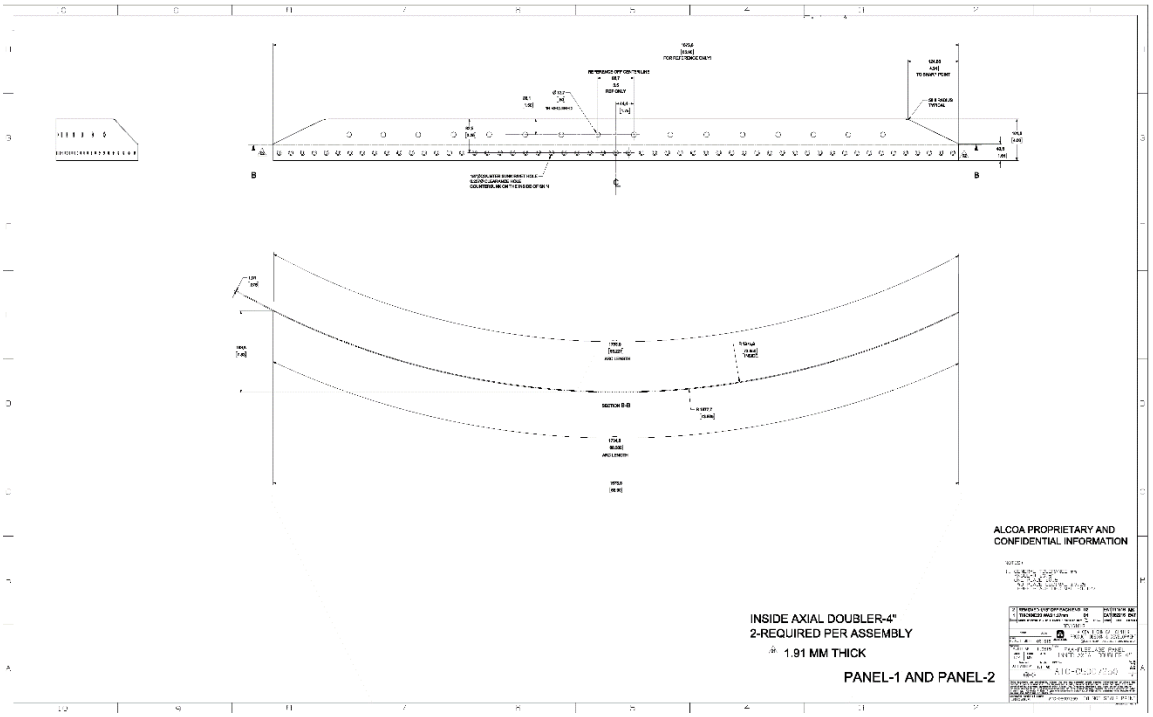
SECTION B-B
ALCOA PROPRIETARY AND
CONFIDENTIAL INFORMATION
INSIDE AXIAL DOUBLER-4"
2-REQUIRED PER ASSEMBLY
@ 1.91 MM THICK
PANEL-1 AND PANEL-2

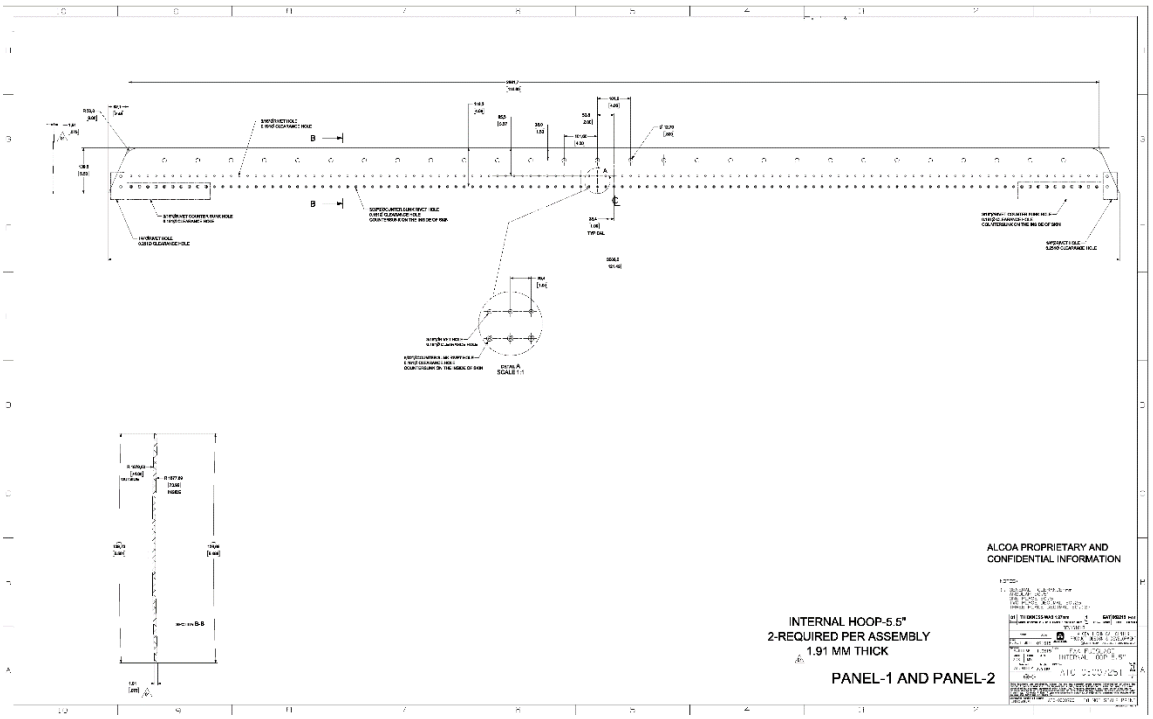

ALCOA PROPRIETARY AND CONFIDENTIAL INFORMATION

INTERNAL HOOP-5.5"
2-REQUIRED PER ASSEMBLY
1.91 MM THICK

PANEL-1 AND PANEL-2

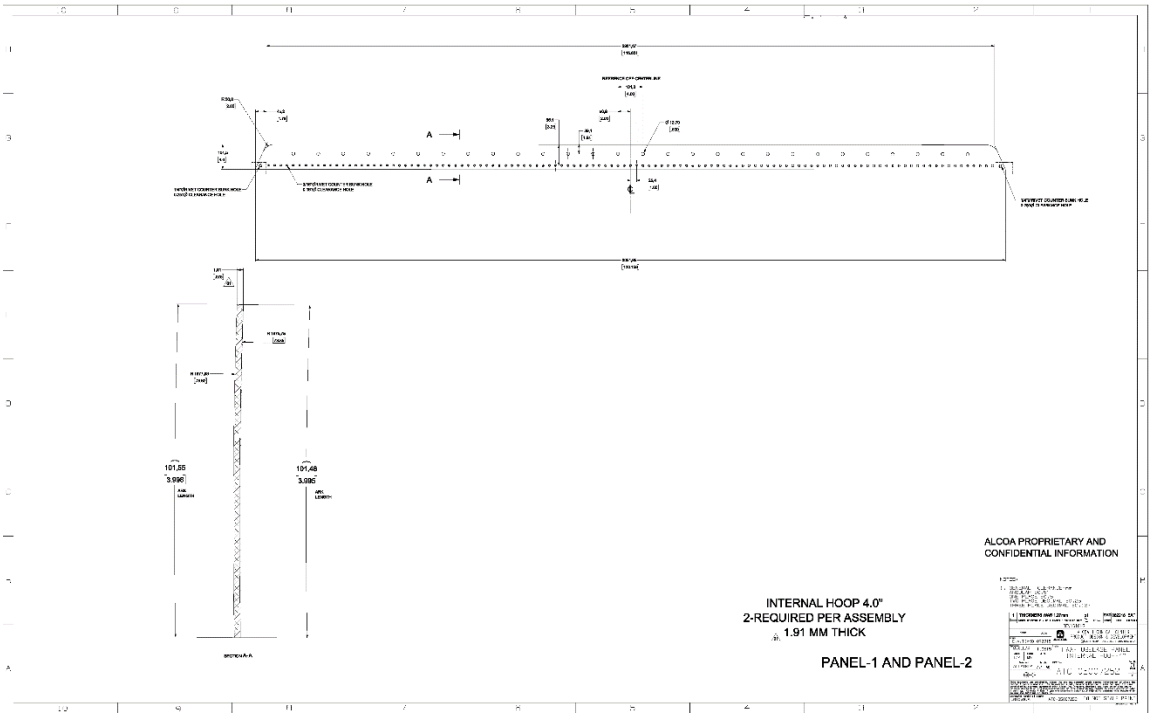

ALCOA PROPRIETARY AND CONFIDENTIAL INFORMATION

INTERNAL HOOP 4.0"
2-REQUIRED PER ASSEMBLY
1.91 MM THICK

PANEL-1 AND PANEL-2

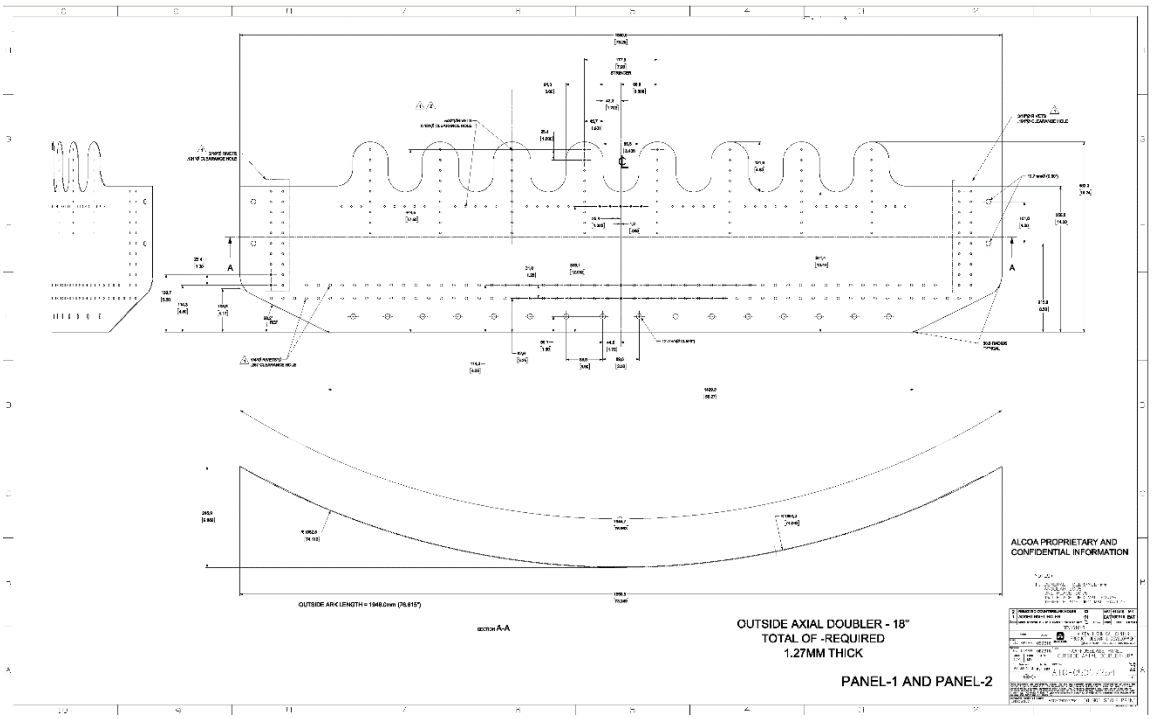
OUTSIDE ARC LENGTH = 1946.0mm (76.615")
SECTION A-A
OUTSIDE AXIAL DOUBLER - 18"
TOTAL OF -REQUIRED
1.27MM THICK
PANEL-1 AND PANEL-2
ALCOA PROPRIETARY AND
CONFIDENTIAL INFORMATION

B Phase 1 and 2 repairs

At the end of Phase 1 and Phase 2, a repair needed to be installed on each crack to continue to the next phase of testing. Both cracks were repaired using Boeing 727 structural repair manual 53–30–3 as guideline. This appendix provides some details of the procedure and material used for the installation of Structural Repair Manual (SRM) repairs.

Figure 39 shows the location of the two SRM repairs on Panel 1. Before the installation of the SRM repair, the surface of the skin was cleaned with acetone and dry air to remove any contaminants. Next, the eddy current system was used to mark the crack tips for both crack locations.

After marking the crack tips, further procedures were followed in accordance with the B727 SRM skin repair instructions. The basic requirement is that for a minimum of three rows of rivets beyond the damage cutout, the repair doubler should be one gage thicker than the skin material and it is acceptable to use button head rivets instead of countersunk rivets, as shown in Figure 40. Figure 41 and Figure 42 show the actual image of the SRM repairs after installation.

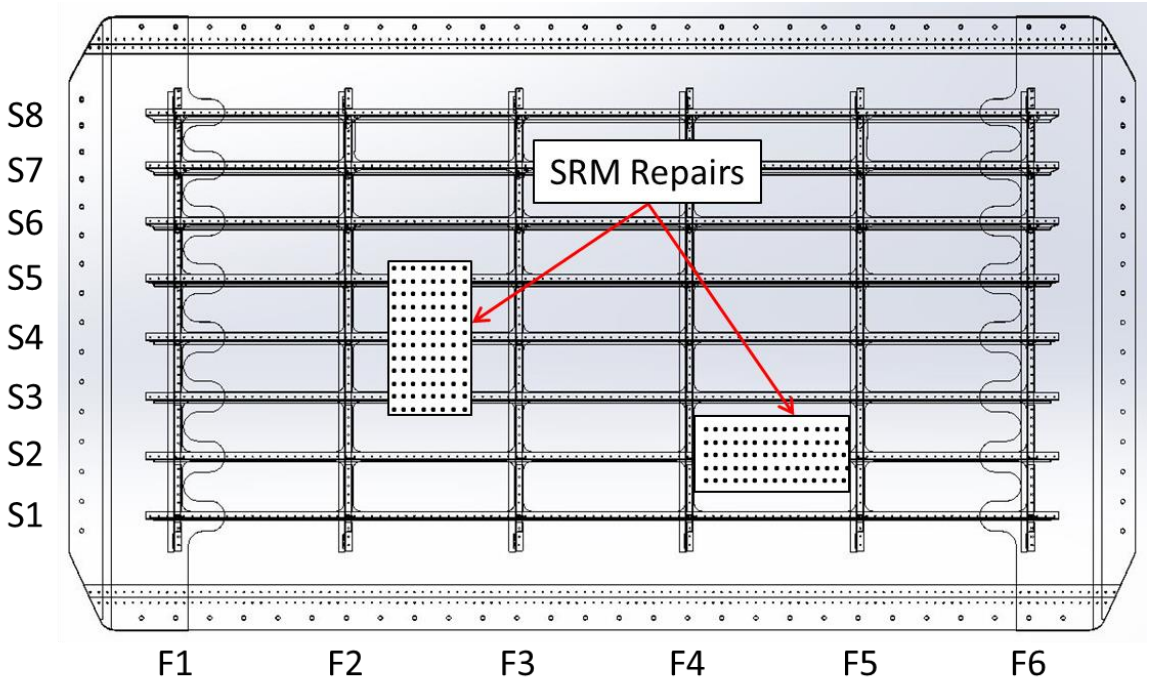

Figure 39. Location of Phase 1 and Phase 2 SRM repairs

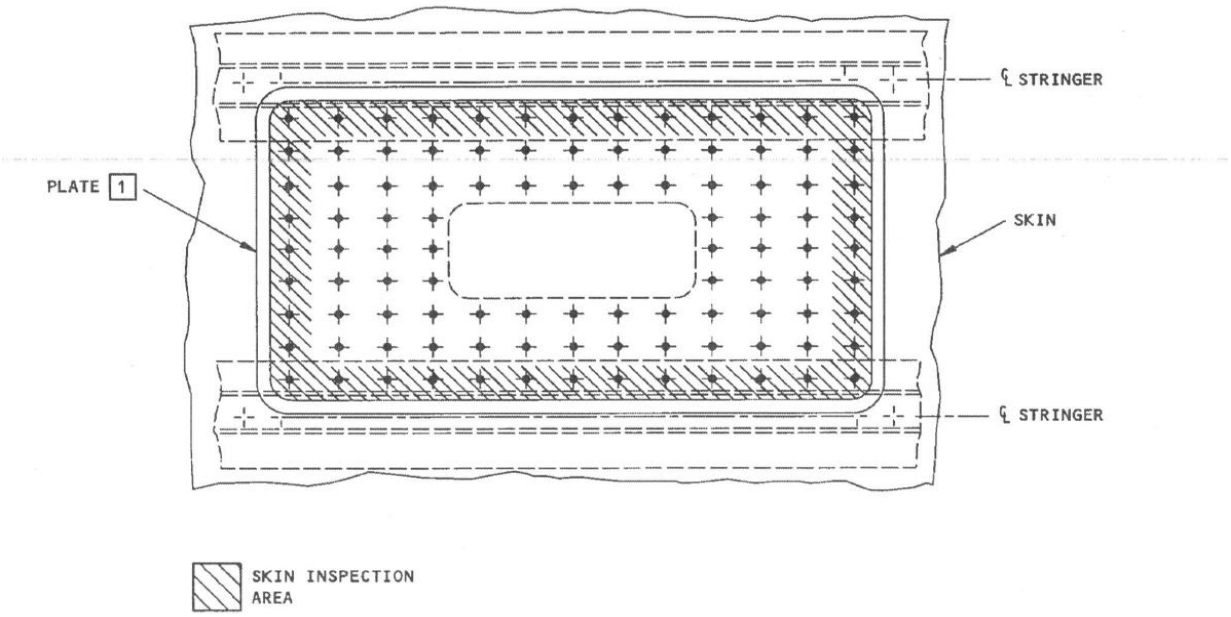

Figure 40. Typical SRM skin repair configuration

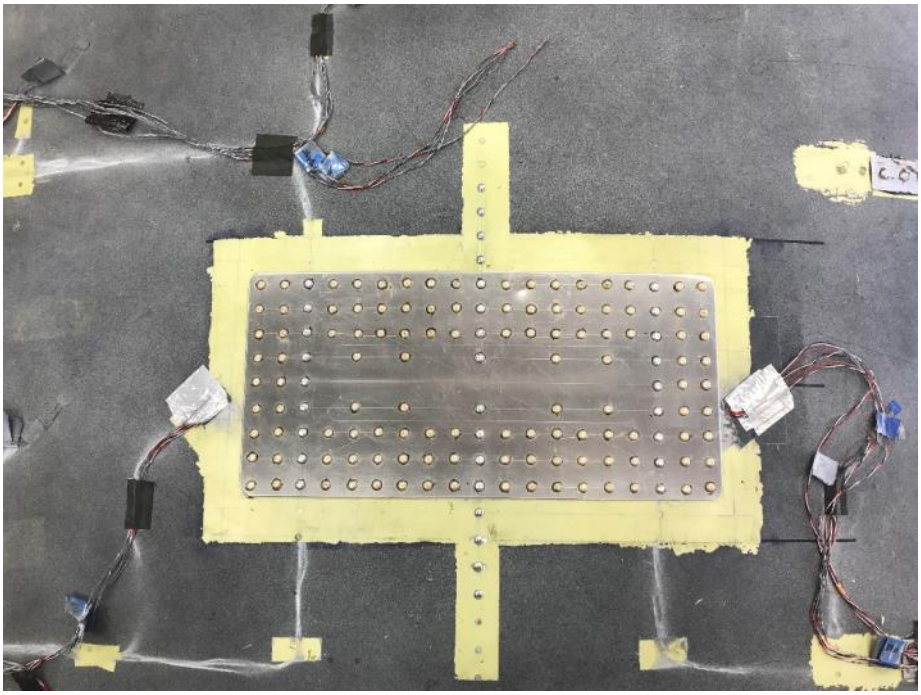

Figure 41. Phase 1 repair external view

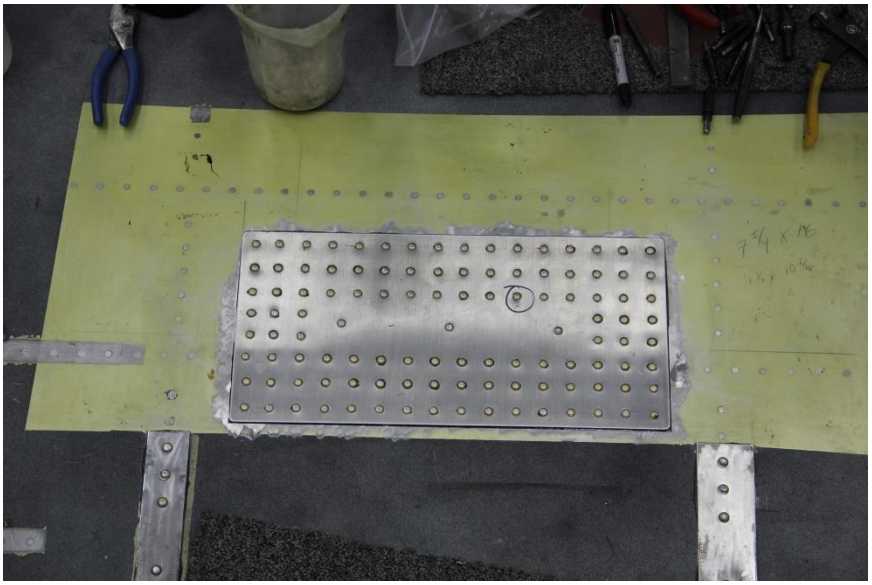

Figure 42. Phase 2 repair external view

C Strain gage instrumentation

The test panel was fully instrumented with strain gages within the test section to provide for real-time monitoring of the panel strain distributions. A total of 200 strain gage channels were used, including 22 external rosette gages, 18 internal rosette gages, 10 chain-gage arrays at phase one notch tip, 36 uniaxial gages on stringers, 32 uniaxial gages on frame flanges, and two uniaxial gages on a phase three stringer clip, as shown from Figure 43 to Figure 46. The locations of strain gages installed on the skin, frames, and stringers for each test phase are provided from Figure 43 to Figure 54.

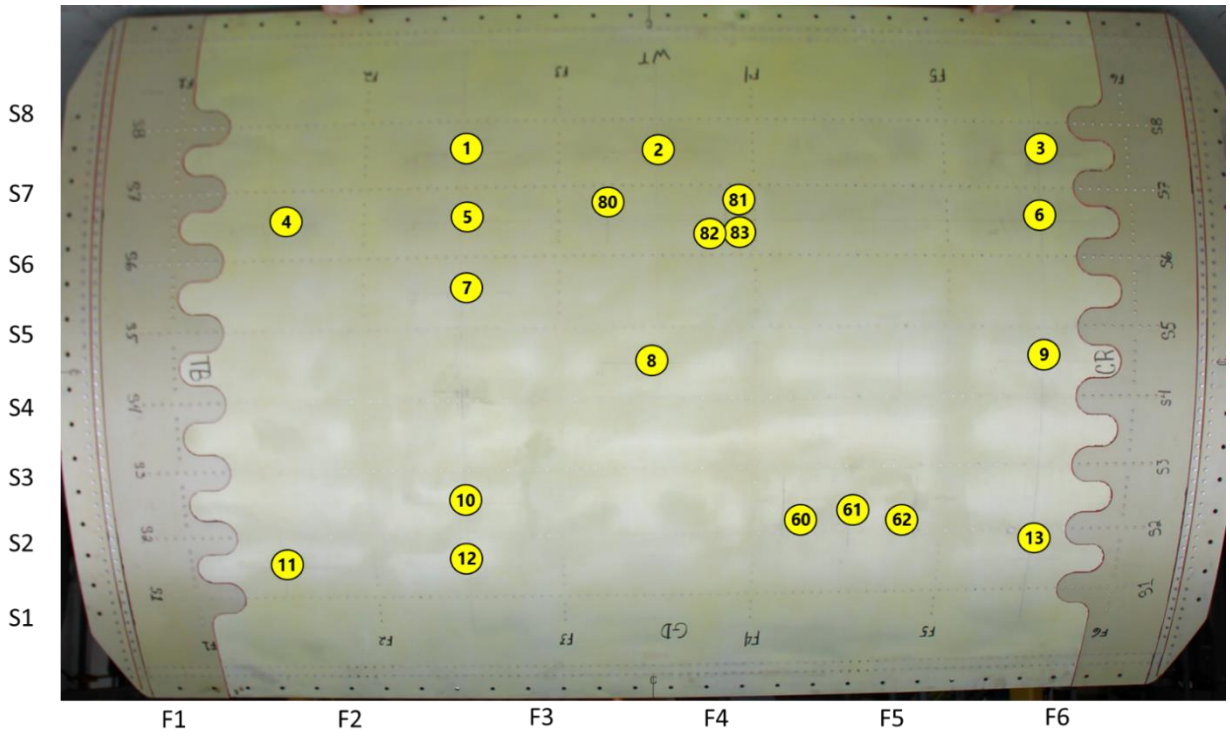

Figure 43. Picture of external rosette gages

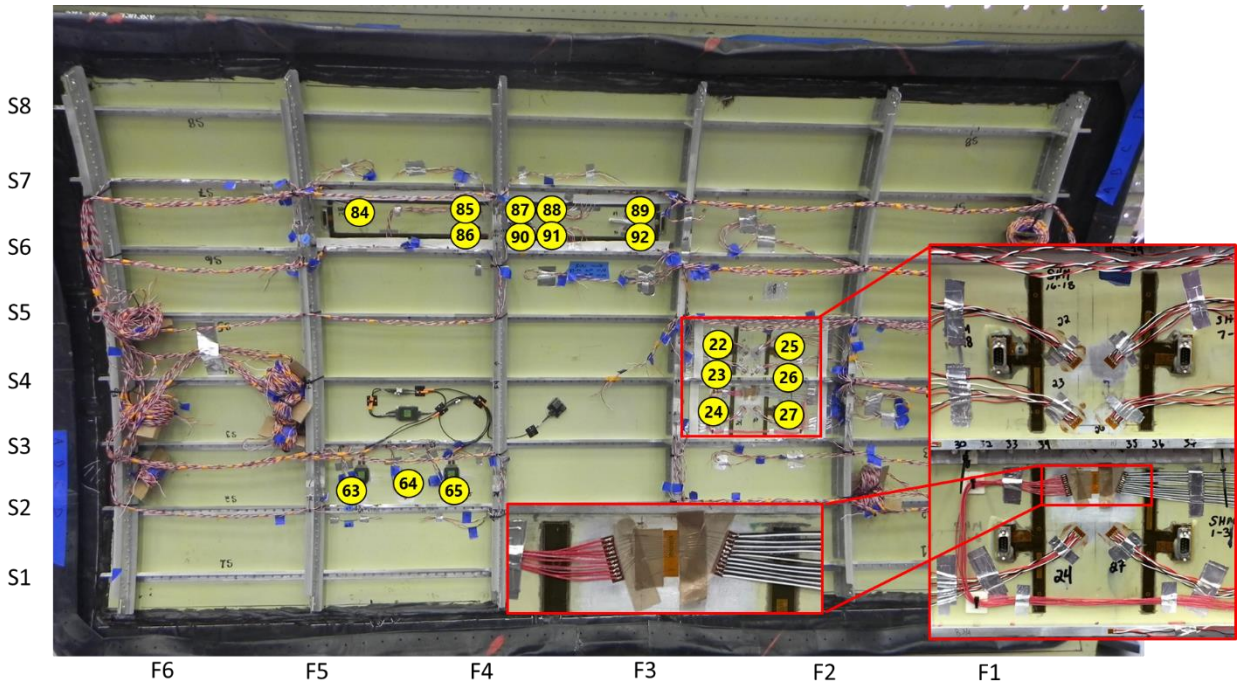

Figure 44. Picture of internal rosette gages and chain gage

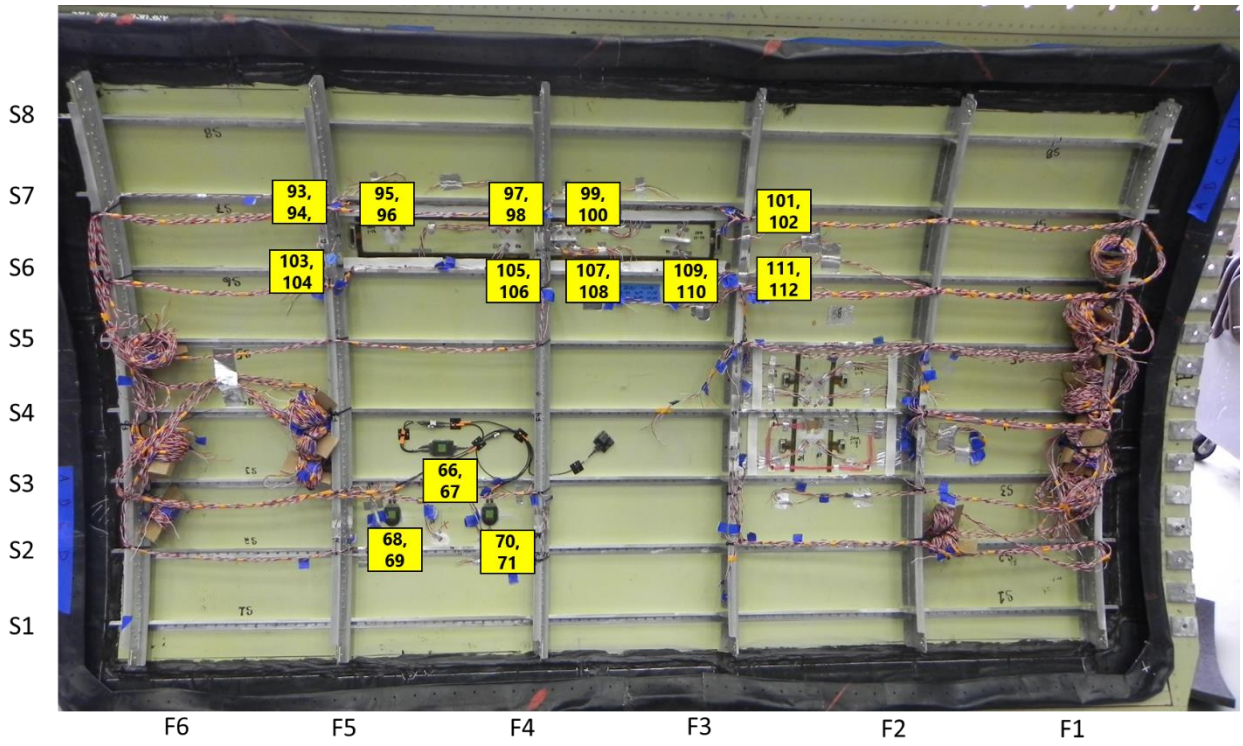

Figure 45. Picture of stringer gages

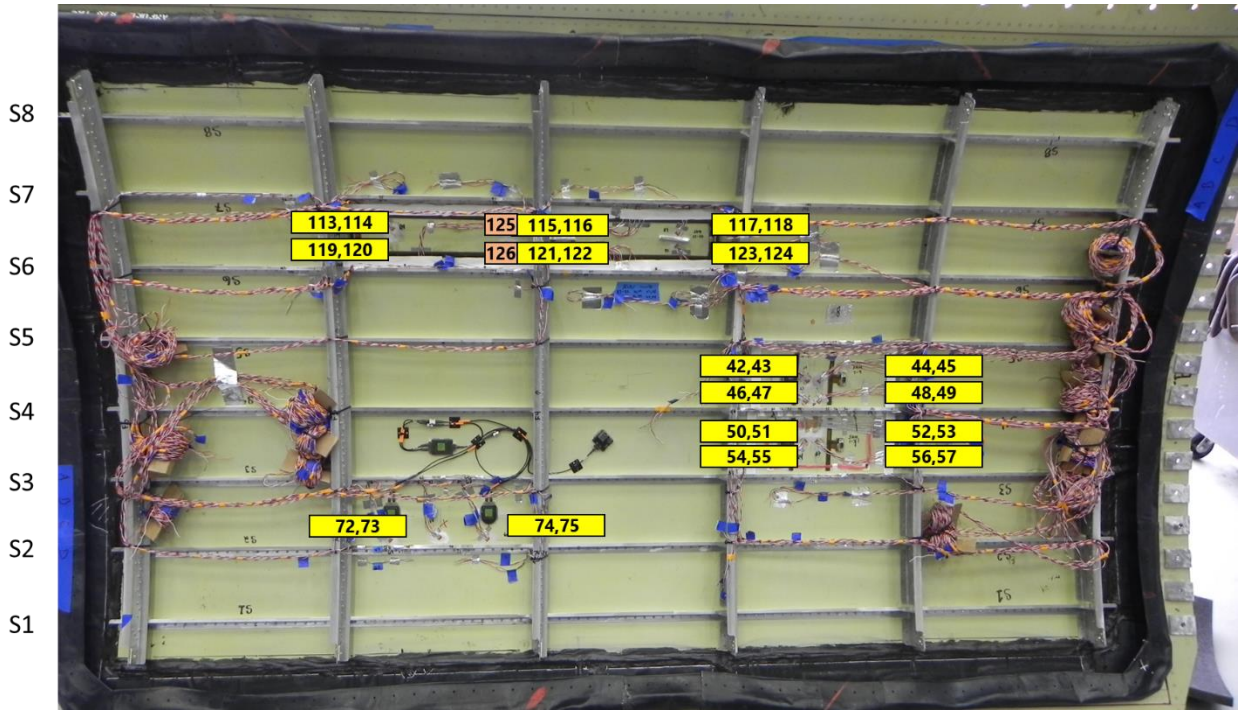

Figure 46. Picture of frame gages and stringer clip gages

Strain readings were recorded during holds occurring at equal load intervals up to the maximum applied loads during strain surveys. In addition, data was continuously recorded at a frequency of 1 Hz and at each endpoint to monitor the strains during the test. Strain gages at mid-bay locations that were monitored throughout all phases are shown in Figure 47.

The test panel was instrumented with strain gages to meet the following considerations:

1. Strain gages were strategically placed on the test panel to compare with the FEM analysis results. The gages were placed on the skins, stringers, and frames for the circumferential crack and longitudinal crack to confirm the variation in stress in these critical areas before cracks are inserted.

2. The gages were placed strategically close to the crack tip to confirm stresses once cracks start growing.

3. Strain gages were also placed at other strategic locations of the panel to compare with the FEM results based on prior experience the FAA has gained from testing panels.

The wires for strain gages that pass through the inside of the pressure box were Teflon-coated to prevent water damage. A lead wire minimum length of 15 feet extending outside the pressure box was soldered to each strain gage channel. Readouts for all strain gages were monitored

periodically and permanently recorded during the fatigue test and during strain survey under mechanical loading. Strain gages were self-compensated to minimize the temperature effects.

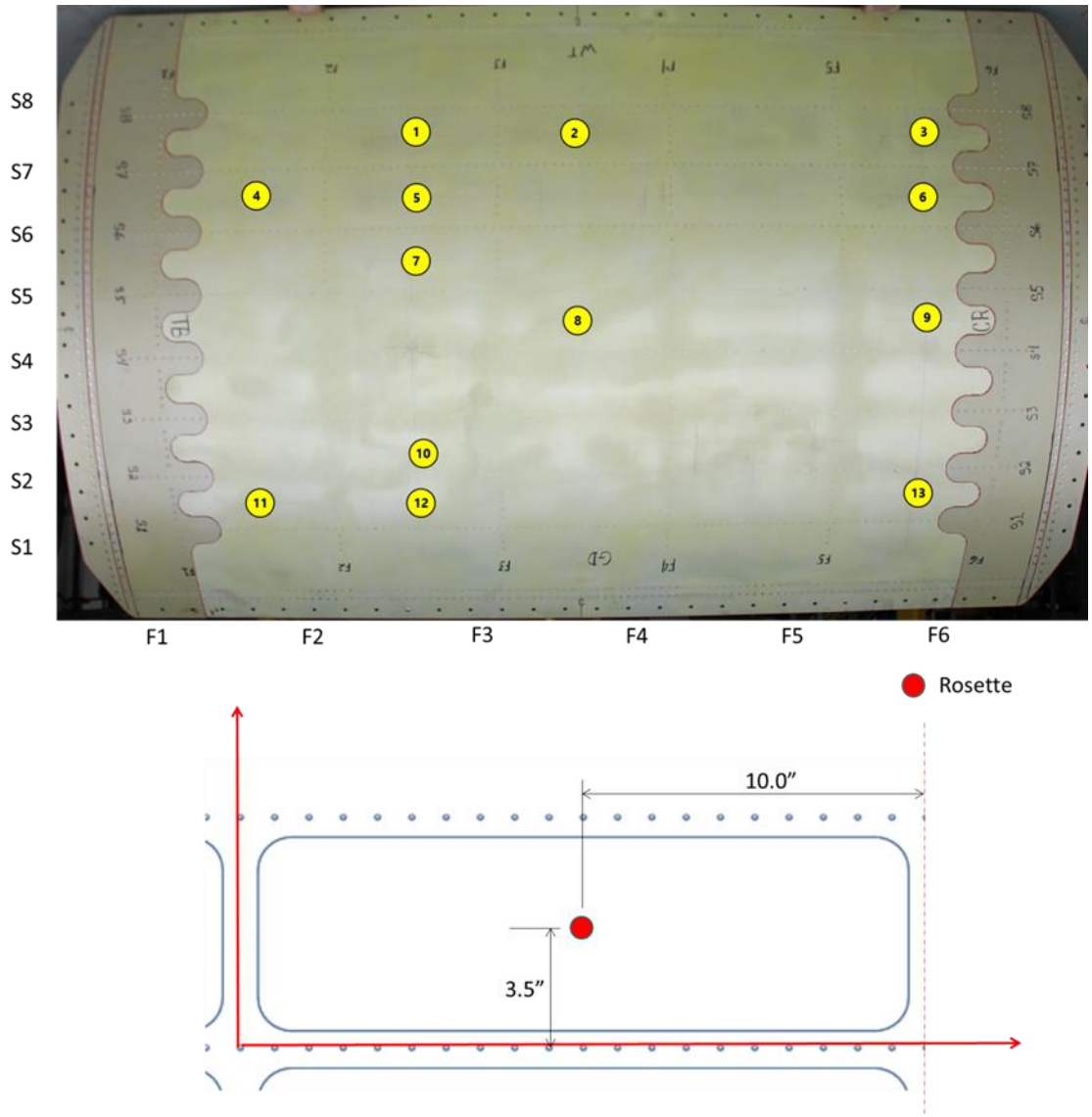

Figure 47. Mid-bay location strain gages

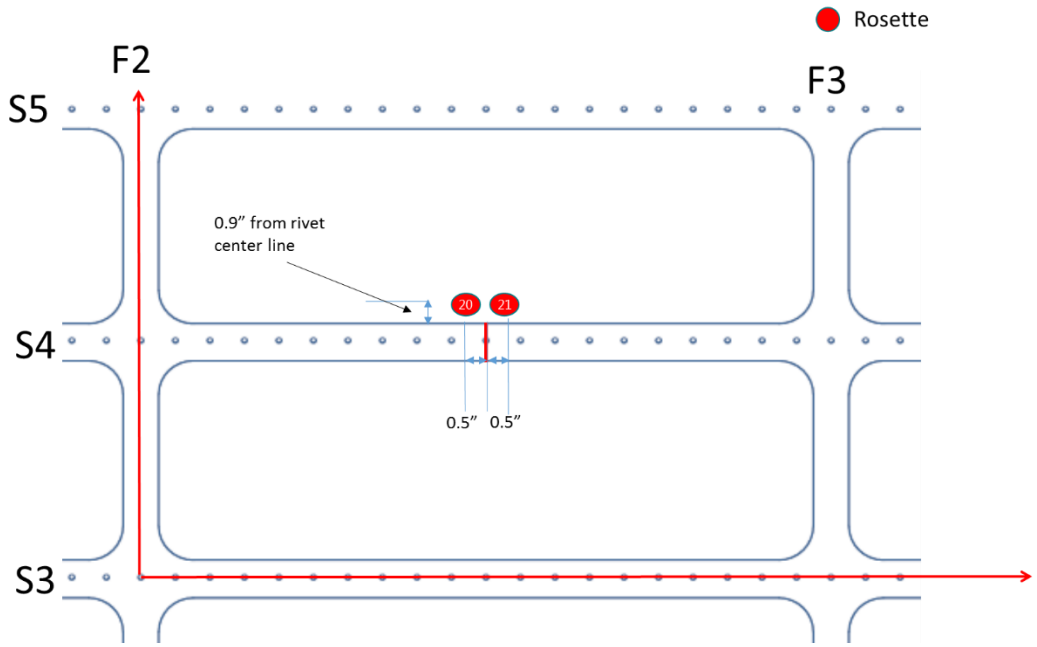

Figure 48. Phase 1 external skin gages

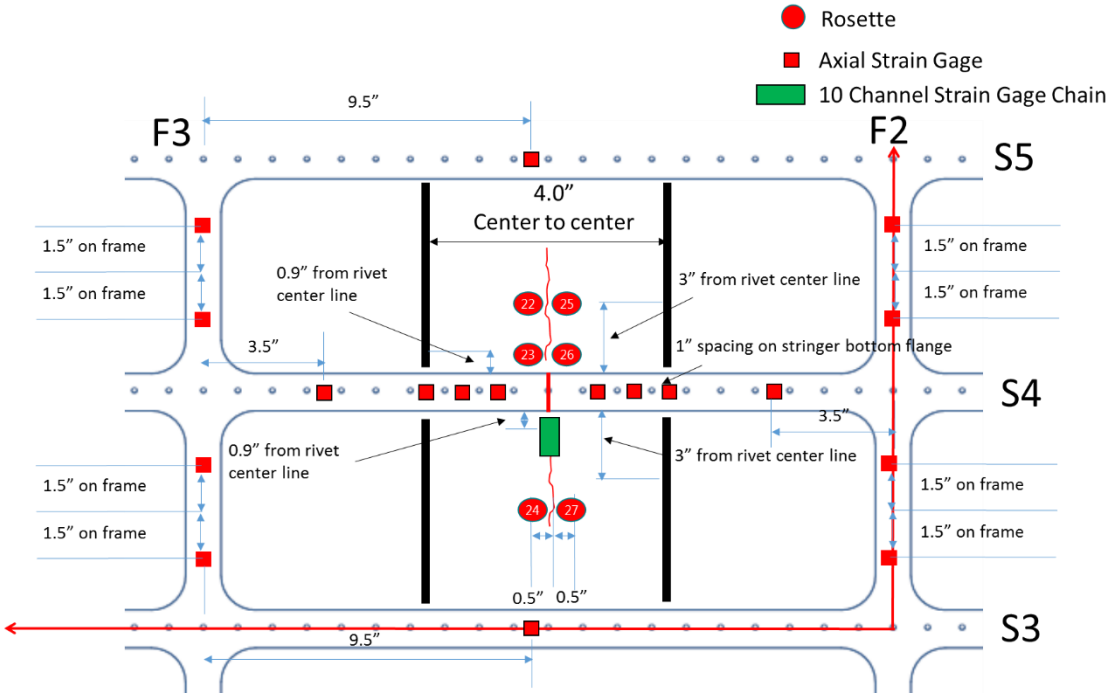

Figure 49. Phase 1 internal gages

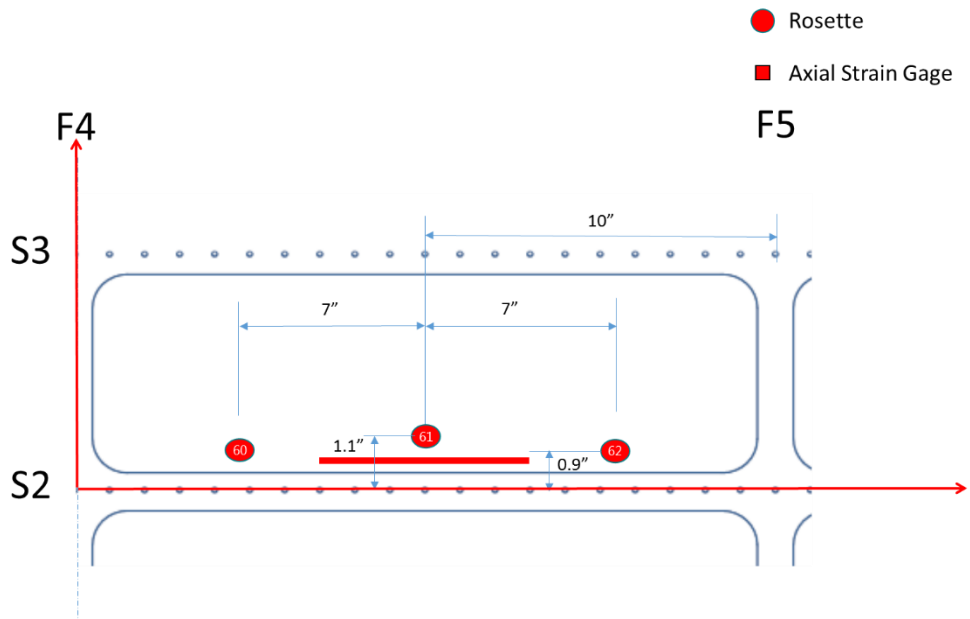

Figure 50. Phase 2 external gages

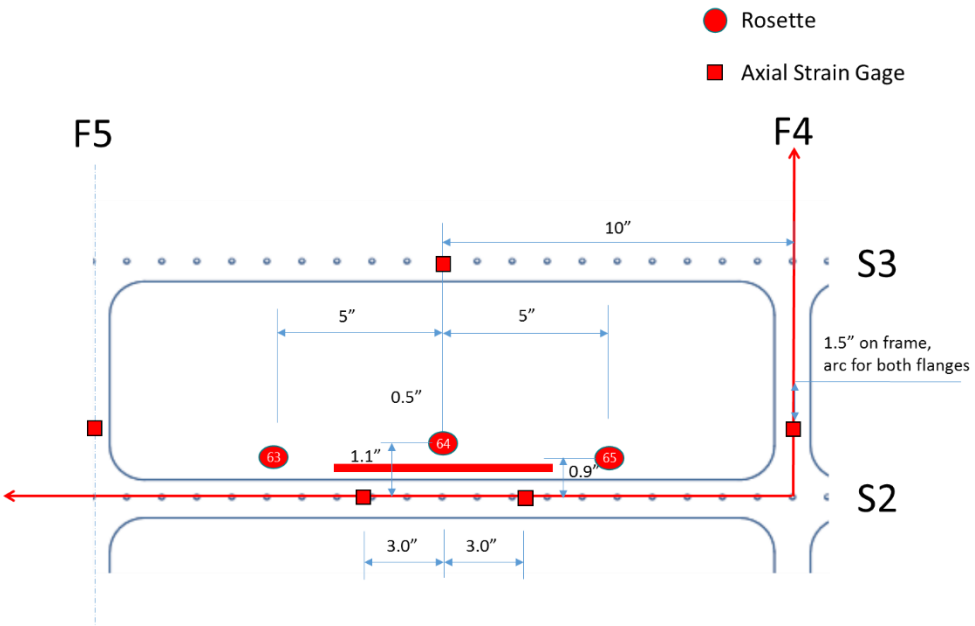

Figure 51. Phase 2 internal gages

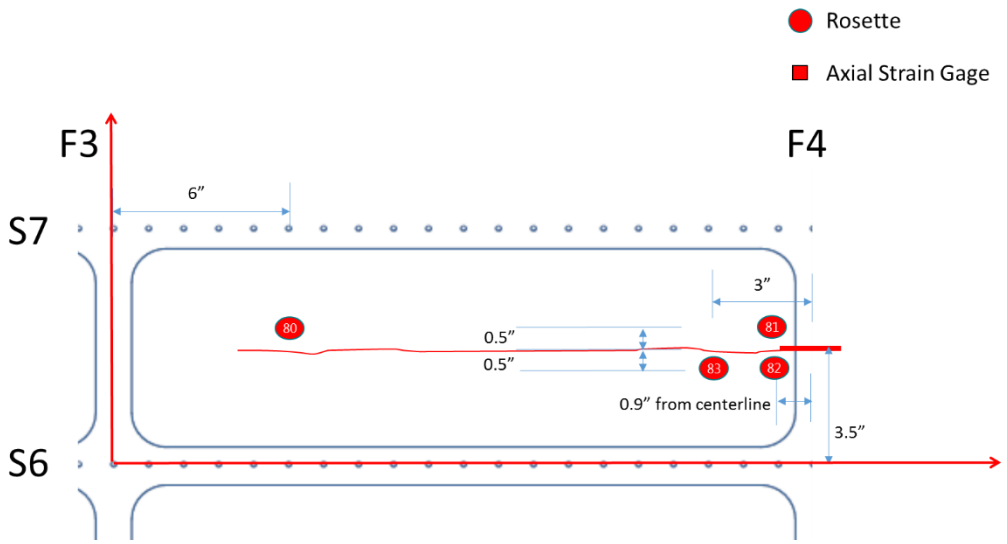

Figure 52. Phase 3 external gages

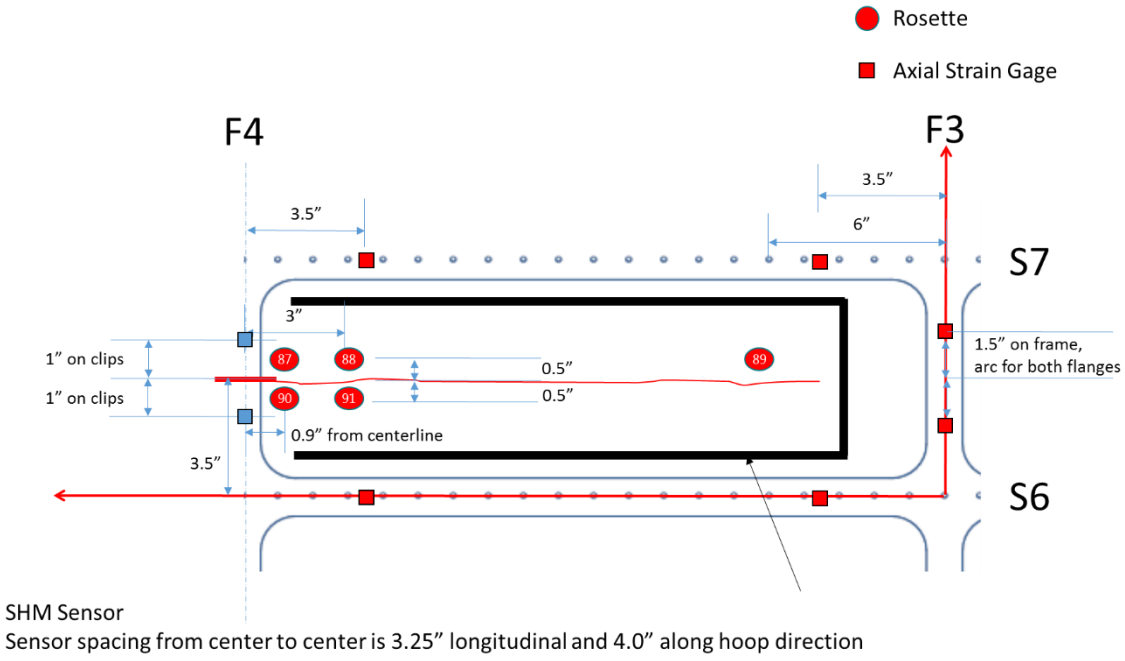

Figure 53. Phase 3 internal gages: left side

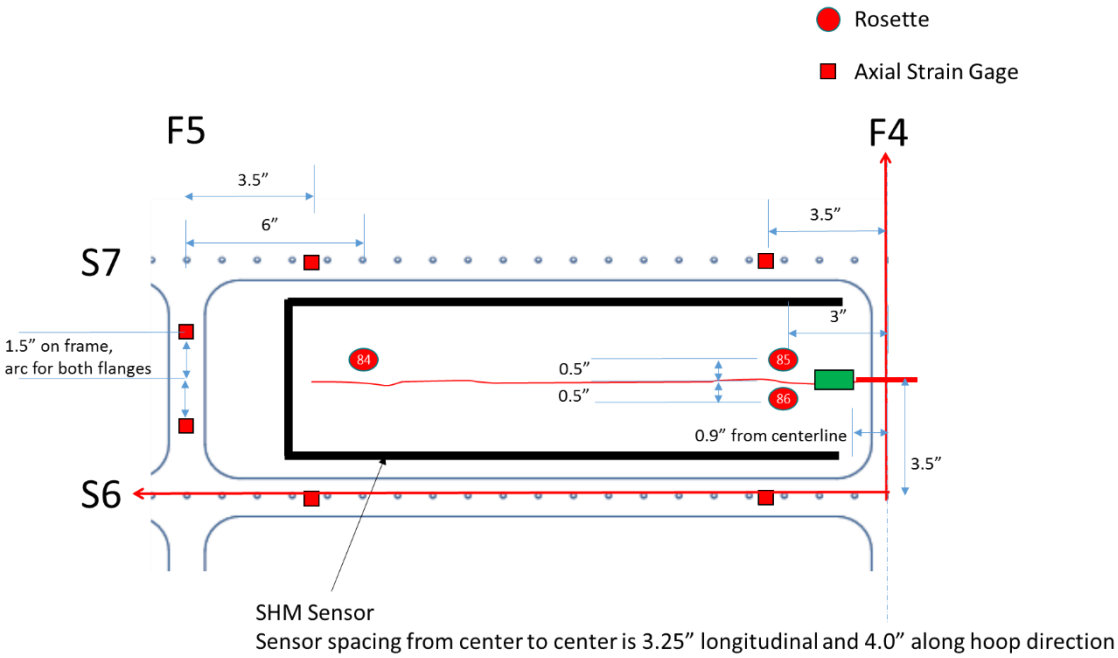

Figure 54. Phase 3 internal gages: right side

D ARAMIS digital image correlation system

Full-field deformation and strain data were recorded during the loading of the test panels using the ARAMIS™ three-dimensional digital image correlation (DIC) system. The system, which uses two 5-megapixel cameras, is capable of accurately measuring full-field strain within 50 με. The typical system setup and stochastic pattern used are shown in Figure 55.

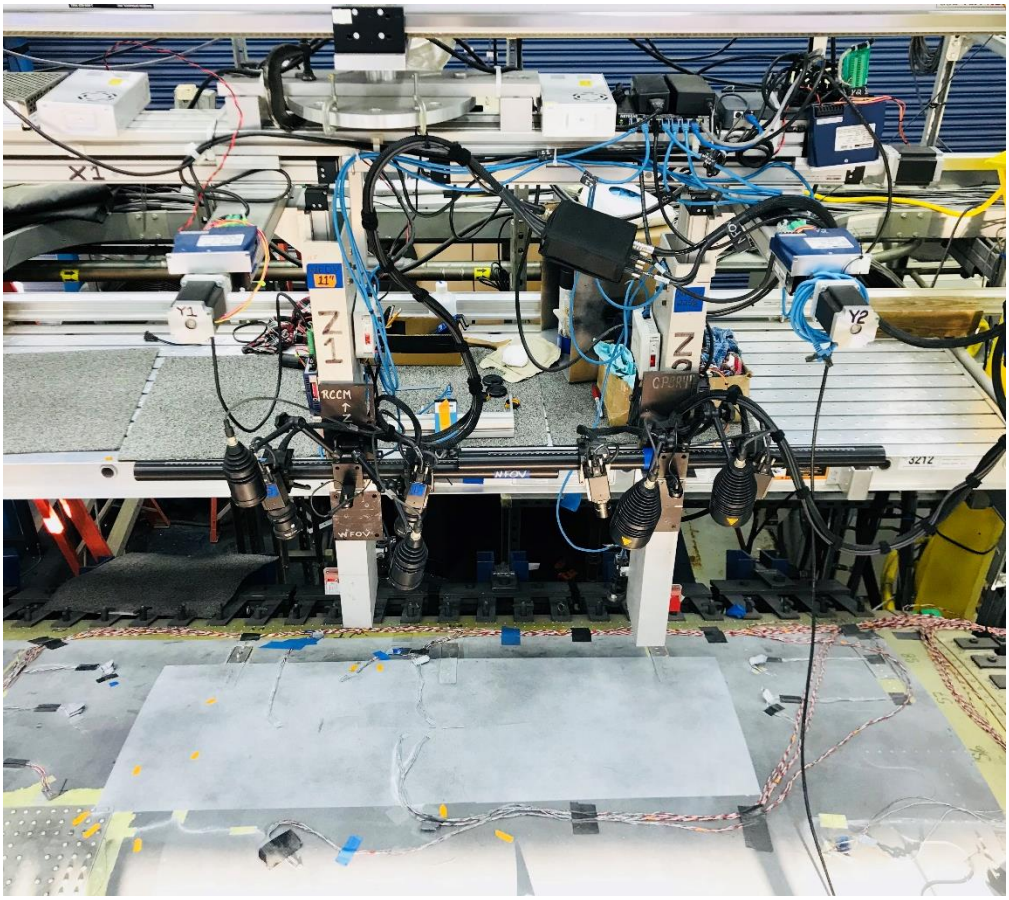

Figure 55. ARAMIS system setup and stochastic pattern on panel

E Structural health monitoring system

Structural Health Monitoring (SHM) systems will be used to monitor and record damage growth: an Acellent system for Phase 1 circumferential cracks and Phase 3 longitudinal cracks, and a Metis design system for Phase 2 mill line cracks, as shown in Figure 56. Both systems consist of three major components: piezoelectric sensors, hardware, and software. Both systems use piezoelectric sensors to create an ultrasonic wave to interrogate the part. Installation of sensors is similar to bonding a strain gage in terms of surface preparation and time required. Sensor locations and cables were routed—so as to not interfere with strain gages—and connected to a data acquisition unit. Data were recorded during periodic inspection of the test article.

Both Acellent and Metis Design traveled to the site to install and set up the SHM systems. When the testing was stopped periodically for inspection, in accordance with the test procedures, SHM data was collected by FAA Tech Center personnel. Acellent and Metis Design trained FAA personnel on how to collect the data and transmit that data back to both OEMs.

Acellent system

Acellent's structural health monitoring system is comprised of SMART Layer® sensors, the Scan Genie III data acquisition hardware, and a laptop with SHM Patch software. The predominant method of damage detection and damage localization in this system is the "pitch–catch" technique across multiple paths optimized by Acellent algorithms.

Two sensor configurations were used for two damage scenarios:

- The SMART Layer PCB (P/N: 407-000095-001), with a three-sensor pinout, was used for the Phase 1 circumferential crack, with two sensors placed on either side of the damage site, as shown in Figure 57. In total, four SMART Layer PCBs (i.e., a total of 12 sensors) were used, and one SMART Layer had an embedded temperature sensor.
- The SMART Layer PCB (P/N: 407-000096-001), with a 12-sensor pinout, was used for the Phase 3 longitudinal crack. The SMART Layers were manufactured in a horseshoe shape to capture damage from both sides, as shown in Figure 57. One SMART Layer had an embedded temperature sensor.

Acellent sensors were installed using vacuum bags for uniform clamping pressure to ensure the bonding quality.

Metis design system

The Metis Design system consists of two MD7P-ACQ-0011 sensors, a MD7P-ACC-0050 accumulation node (hard drive), and PuTTY software (the GUI was developed by UTS Aerospace System).

The locations of the sensors relative to the Phase 2 initial damage are described in Figure 58. Sensors were installed using a Metis Design installation kit. Metis Design uses two methods, "pitch–catch" and "pulse–echo", for damage detection and damage localization.

Note: During the preparation of Phase 2 testing, the Metis sensors were disbonded; therefore, there is no SHM data from the Phase 2 test.

Data analysis

The Tech Center used algorithms developed by Embraer, Boeing, and Sikorsky to assist in the analysis of the SHM systems, and the results will be published in a separate technical note.

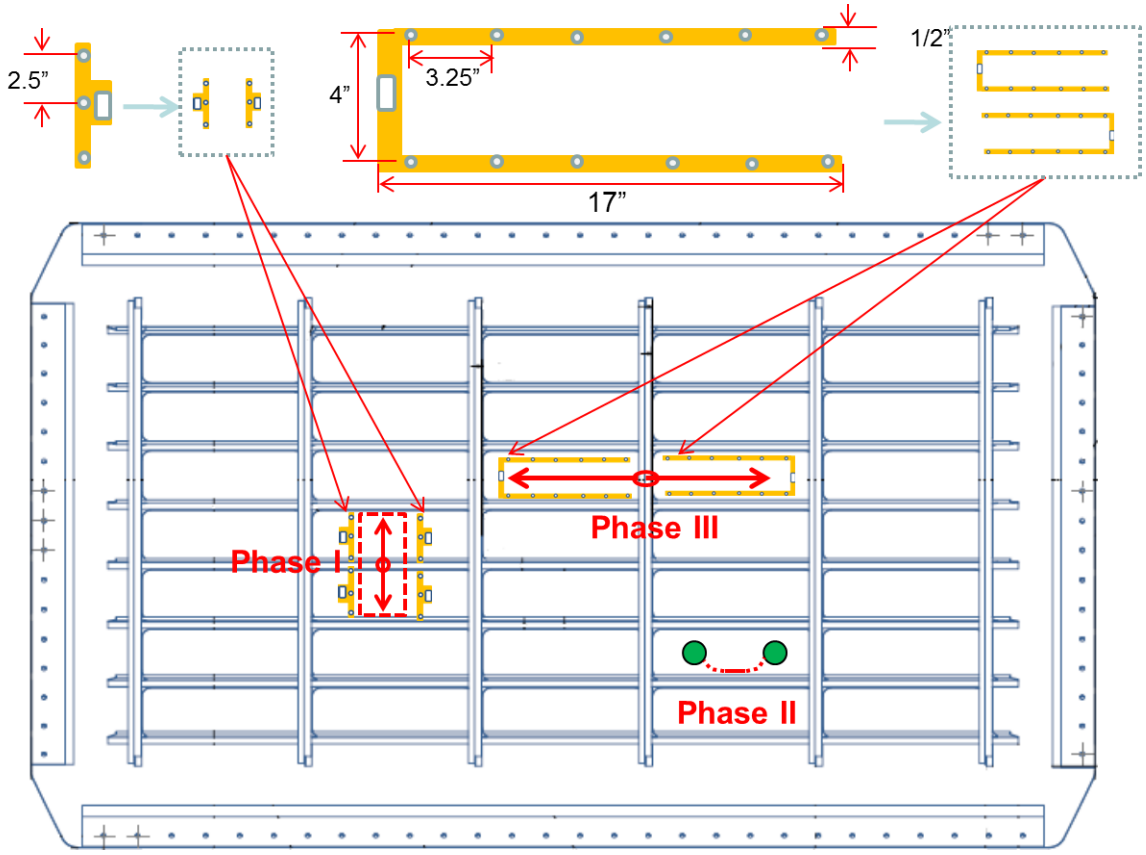

Figure 56. SHM sensor locations for panel #1

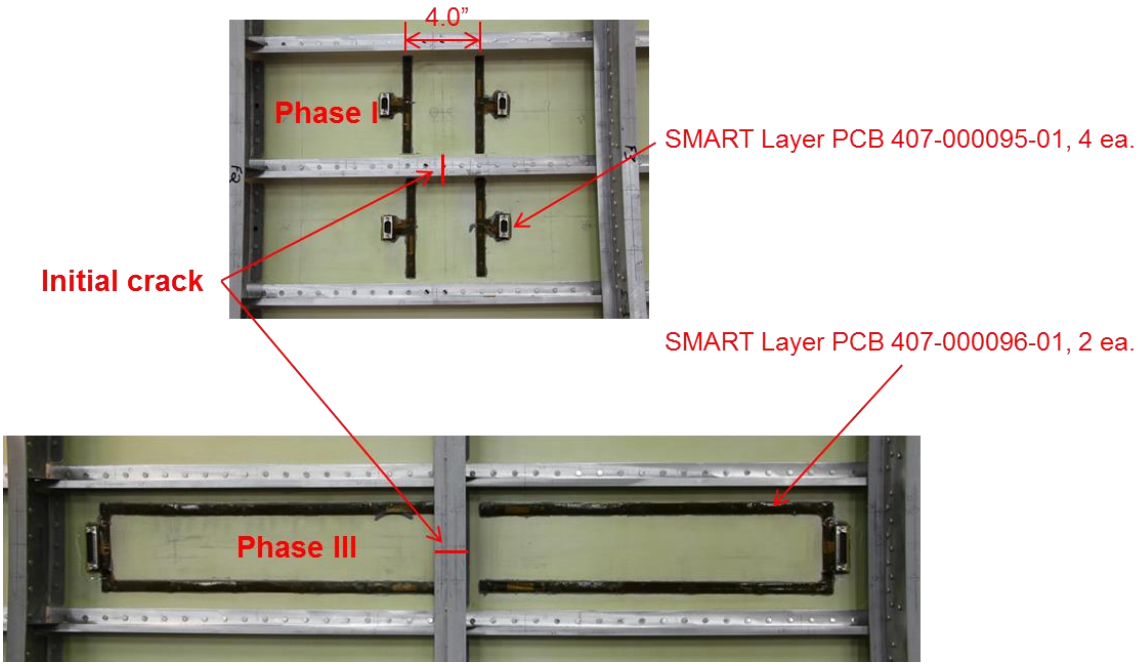

Figure 57. Acellent sensors for Phase 1 and Phase 3

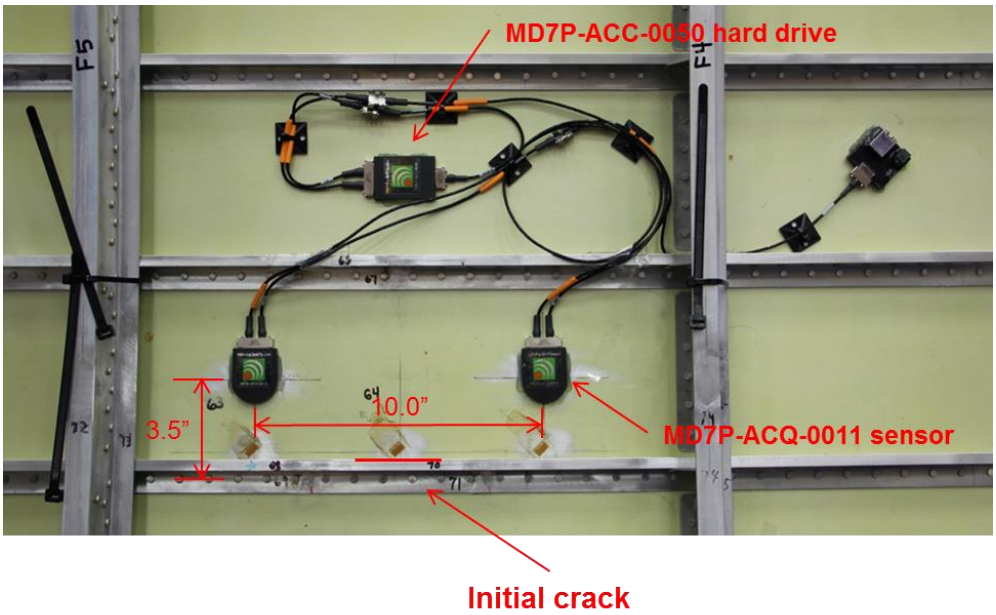

Figure 58. Metis design sensors for Phase 2

Prior to testing, the areas to be monitored by the photogrammetry system were coated with a high-contrast, stochastic speckle pattern. Flat-black spray paint was used to create a random pattern on top of a flat white layer. The coarseness of the pattern directly affects the resolution of the measured strain field. Baseline images were taken using both cameras at zero loads.

Deformed images were recorded using both cameras while under an applied load. The baseline and deformed images are then used to determine the full-field deformation and strain field.

F Frame repair

During the Phase 1 fatigue testing, the frame end of F5 was unexpectedly broken at 19,800 cycles due to the lack of a reinforcement doubler on frame ends, as shown in Figure 59. The frame end broke again during the Phase 2 fatigue test—at around 4,500 cycles—due to the use of general aluminum rivets and the absence of structural adhesive bonding. A thorough inspection was conducted, which found cracks in the majority of frame ends. The test panel was removed from the FASTER fixture due to the limitation of working space inside of the pressure box and the intensity of the repair work. The frame ends were reinforced on both ends as shown in Figure 60, Figure 61, and Figure 62. The extra frame end pieces from the previous 727 test panel were used to reinforce the frame ends. The new end stringer clips were fabricated based on the drawings in Appendix A. The panel was installed back on the FASTER fixture after the repair, and the strain survey was conducted to ensure the frame repair and reinforcements did not change load introduction, as shown in Figure 63.

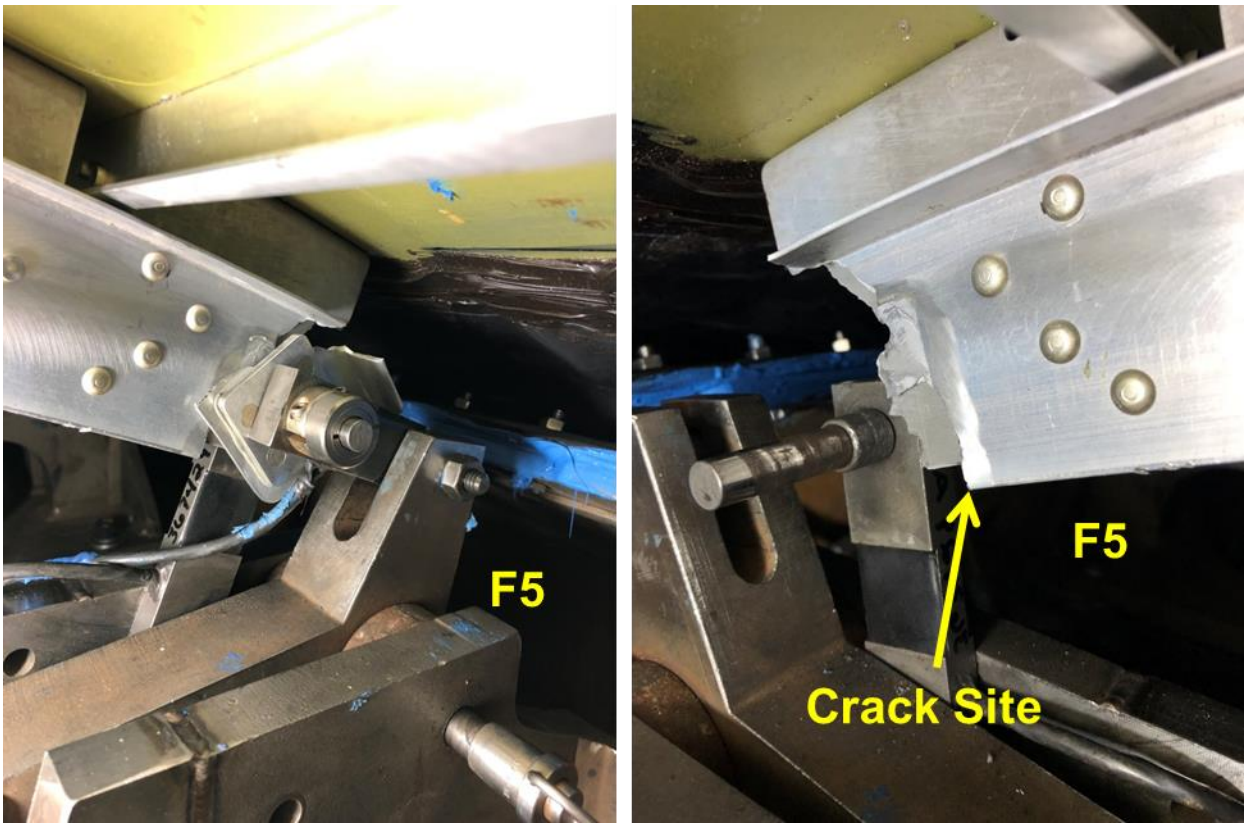

Figure 59. Location of crack at frame end

Figure 60. Picture of frame end repair at frame

Figure 61. Configuration of frame repair from both ends

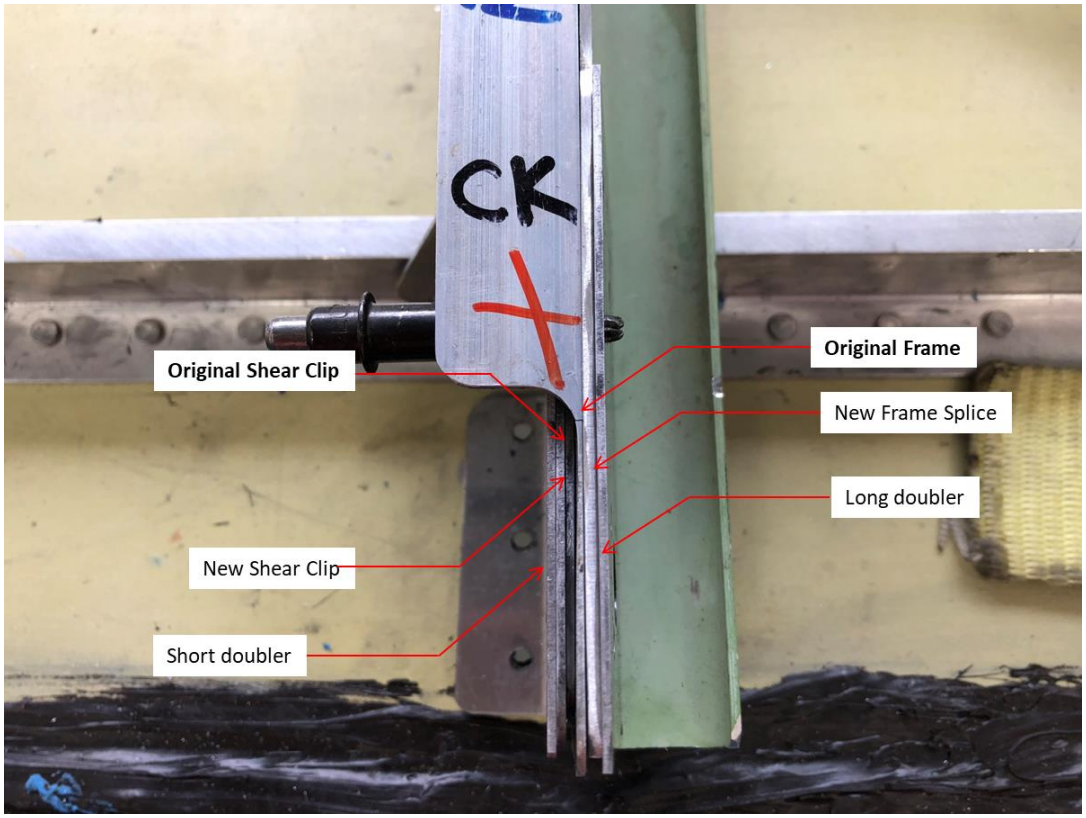

Figure 62. Frame end repair final layup

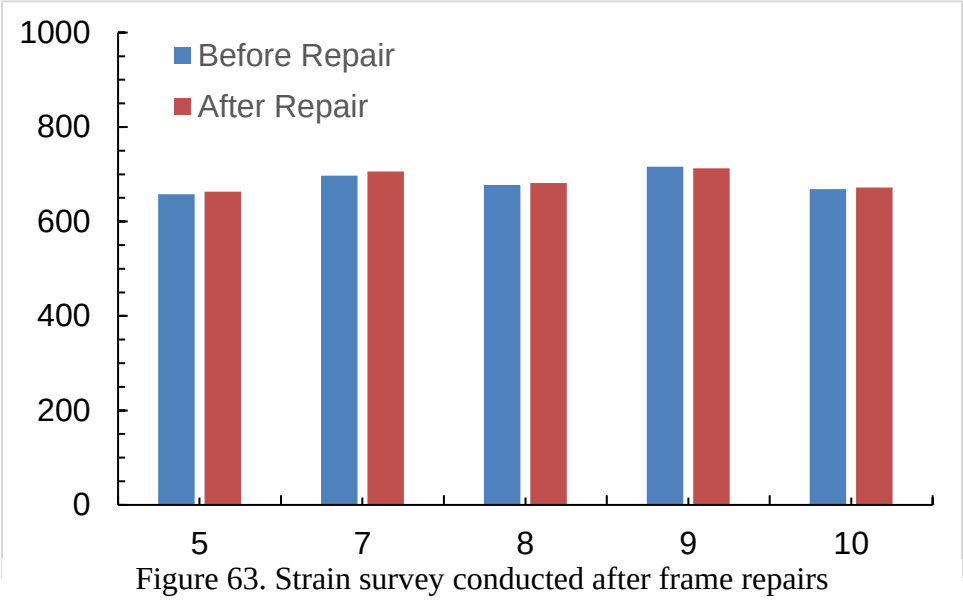

Figure 63. Strain survey conducted after frame repairs